FOREWORD

This report describes a program conducted by Dynatech Corporation, Cambridge, Massachusetts, under Contract No. AF 33(657)-9423. The work was sponsored by the 6570th Aerospace Medical Research Laboratories, Wright-Patterson Air Force Base, Ohio, under Project No. 6373, entitled "Respiratory Support Equipment," Task No. 637302, entitled "Design Study of a Liquid Oxygen Converter for Use in Weightless Environments." Mr. R. L. Mela, Manager, Advanced Systems Department, was the principal investigator. The work was performed for the Dynatech Corporation by Dr. John M. Reynolds, III, Dr. Harry Y. Choi, Mathew Hurwitz, Edgar H. Sibley, James O'Neil, and Joseph Gerstmann. Lt. W. Evon of the Respiratory Equipment Branch, Biotechnology Division, Biomedical Laboratory, 6570th Aerospace Medical Research Laboratories was contract monitor commencing on July 1962. He succeeded Mr. I. H. Lantz of the same laboratory. The contract ran from June 1962 to February 1963.

This report is cataloged by Dynatech Corporation as Report No. 391.

ABSTRACT

A basic investigation directed towards the development of the dielectrophoretic oxygen converter has been conducted. The work has covered dielectrophoretic theory, application to design, supporting experiments, preliminary design of a 25-liter converter, and construction of a small dielectrophoretic tank for flight test experiments. We find that the level of the dielectrophoretic forces can be predicted quantitatively. These force levels are limited in a practical converter design by dielectric breakdown of the medium, by stability of the fluid-vapor interface, and sometimes by force wells that trap fluids in the vicinity of the electrodes. Criteria for converter design in view of these limitations are developed, and it is shown that in a 25-liter converter "equivalent dielectrophoretic gravity fields" in the region from 10^{-3} to 10^{-1} g_o should be attainable on the fluid with a 20,000 volt potential. Provision is made for uninterrupted operation up to 25 g_o. Liquid-vapor separation occurs continuously in the converter. The entire converter, with auxiliaries, weighs 14.0 pounds dry.

PUBLICATION REVIEW

This technical documentary report has been reviewed and is approved.

Wayne H. McCandless

WAYNE H. McCANDLESS
Technical Director
Biomedical Laboratory

TABLE OF CONTENTS

TABLE OF CONTENTS
(Continued)

TABLE OF CONTENTS
(Continued)

LIST OF ILLUSTRATIONS

LIST OF ILLUSTRATIONS (cont)

LIST OF TABLES

LIST OF SYMBOLS

A	constant defined in Equation (2)
a	radius of a fluid sphere, cm
Bo	Bond Number
b	inner radius of outer electrode
C	capacitance per unit length, farad/cm
C_D	drag coefficient
D	tank diameter, cm
D_h	dimensionless hang-up parameter defined on Page 11
d_h	hang-up diameter, cm
E	electric field strength, statvolt/cm, or, $\sqrt{\text{dyne}}/\text{cm}$
E*	electrical breakdown strength, statvolt/cm
e	stage element diameter, cm
F	force, dynes
F_1, F_2	defined in Equations (10) and (11)
f	volume force, dyne/cm ^{3}
g	acceleration due to gravity, cm/sec^2
g_o	acceleration due to gravity on Earth's surface, 981 cm/sec^2
g_e	"equivalent gravity field" due to dielectrophoresis, $f/\rho_L g_o$
H	tension in a stage element, dyne
h	enthalpy, BTU/lb
I	current amps
j	$\sqrt{-1}$
K_1	design parameter defined in Equation (14), cm$^{3/2}$
K_2	design parameter defined in Equation (14)
K_p	constant defined in Equation (50)
K_s	safety factor
L	characteristic length cm, or tank length, cm

N_1, N_2, N_3	scaling parameters, dimensionless
N_e	number of stage elements
P	pressure, dyne-cm^2, or psia
P_{crit}	loading on stage spool core, lb
Q	heat rate, BTU/hr
q	charge, statcoulomb
Q_L	steady heat leakage, BTU/hr.
R, r	radial displacement from axis of cylindrical tank, cm
R_o, R_1, R_2	radii of cylindrical stages numbered from the outside to the inside, cm
R*	radius of cylindrical fluid interface, cm
Re	Reynolds Number
s	spacing between axes of stage elements, cm
T	vapor-liquid surface tension, dyne/cm
t	time
U	volume, cm^3
u	velocity, cm/sec
$\bar{u}_r$	unit vector in radial direction
$\bar{u}_\theta$	unit vector in tangential direction
V	applied voltage, statvolts (Note that 1 statvolt = 300 volts)
We	Weber Number
w	mass flow rate, lb/hr
x, y	linear displacement, cm
Z	electrical resistance, ohm
Δ	variation
Γ	defined as $\frac{\kappa_i - \kappa_o}{\kappa^*}$
δ	displacement or deflection
κ	dielectric constant (relative permittivity)
ϵ_o	capacitivity of free space, $\frac{1}{4\pi}$, esu

θ	angular displacement
μ	viscosity, gram/cm-sec
ν	Poisson's Ratio
π	circumference/diameter
ρ	density, gram/cm^3
σ	stress, psi
τ	thickness
Ω	ohms
ω	angular frequency, radian/sec

Subscripts

b	refers to fluid spheres or bubbles
E, e	refers to dielectrophoretic or electric
H	heater element
h	refers to hang-up parameters
i	inner
L	liquid
m	refers to matrix fluid
n	introduced in Equation (14) to number stages
o	ambient conditions
R	refers to some specific radial location

List of Abbreviations

Vol.	volume
crit.	critical
EFF	effective
min	minimum
max	maximum
grad, ∇	gradient
ℓn	logarithm to the base e

log	logarithm to the base 10
SF	factor of safety
VA	volt-ampere
wt.	weight
$\mu\mu$f, pf	picofarad = 10^{-12} farad

INTRODUCTION

An oxygen converter is essentially a device for storing liquid oxygen and converting it to vapor for use in vehicle life support systems. In the weightless environment encountered in orbiting or deep space vehicles, there is a severe problem in orienting the liquid-vapor agglomerate so that only vapor is withdrawn from the converter.

The approach on which this effort is based depends on a phenomenon called dielectrophoresis, which is the study of the forces and motions of dielectric media subjected to nonuniform electric fields. When a molecule of a dielectric material such as oxygen is subjected to such a field, a force is set up on the molecule whose magnitude is dependent on the relative permittivity of the oxygen and whose direction is dependent on the gradient of the field. Thus liquid oxygen can be separated from oxygen vapor, and it may be located in a manner dictated by a geometrical shaping of the field as determined by the designer. Once the liquid and vapor are separated and held in predetermined locations, venting of the vapor may be accomplished. By the dielectrophoretic approach, liquid and vapor are promptly and continuously separated.

The basic theory of dielectrophoresis has been understood for some time. The purpose of the present program was to extend the theory to the design of a practical device, with three specific objectives:

a. The generation of theoretical and design information which will enable the design of dielectrophoretic oxygen converters.

b. A preliminary design of a 25-liter oxygen converter to specifications provided by the Air Force.

c. The construction of a model of the tank portion of the converter, suitable for proof-of-principle testing in zero-gravity flight tests.

In terms of accomplishing these basic objectives, considerable advances in the theoretical aspects of dielectrophoresis were made under this program. A good understanding of problems related to fluid surface stabilities and to methods of producing optimum electric fields throughout the converter volume was achieved, and considerable progress toward the solution of these problems was made.

Safety characteristics were considered, and it was found that no unusual hazards exist if working voltages are kept well below breakdown voltages and current limiting features are included in the power supply. It was demonstrated in simulator experiments that the dielectrophoretic forces do exist as predicted, and that the basic mechanisms are available to design and build a dielectrophoretic oxygen converter.

A preliminary design layout of the 25-liter converter is shown in Figure 23. Analysis shows that dielectrophoresis may be used to control the fluid orientation to $10^{-3} g_o$, and a more conventional vapor delivery approach is used when the gravitational field exceeds $10^{-3} g_o$. The weight of the complete converter, including tankage, insulation, supports, pressure relief, pressure control, high voltage supply, electrodes for producing the desired field, and a valving system to control venting above $10^{-3} g_o$, is 14.0 pounds, dry. Of this total, components unique to the dielectrophoretic approach (power supply and electrodes, etc.) comprise 8.4 pounds. (This weight, of course, must be compared with weights of converter components in other approaches.) The electrodes and power supply are static, high reliability components. The time to achieve a separated equilibrium configuration from an initially dispersed liquid-vapor agglomerate is less than 4 seconds.

Considerable progress toward the development of the dielectrophoretic converter has been made under this program, and it is anticipated that confirmation of the basic approach in an actual flight test will take place within the next few months. This should give further insight to a variety of secondary problems, none of which is expected to be seriously limiting, but which have been difficult to study in laboratory analog experiments. These problems include retention of liquid drops on the electrodes, behavior of the LOX mass under oscillations, and behavior of liquid in corners of the converter where vapor outlet ports might be placed. Aside from flight tests, proof-of-reliability tests of certain components, including vent valves and power supply, will be required.

THEORY

The term "dielectrophoresis" refers to certain forces on dielectric media in nonuniform electric fields. A simple explanation of the phenomenon is offered here.

Charged particles in an electric field experience a force equal to the product of the charge and field strength. Although the molecules of a dielectric material have no inherent net charge, they do polarize under the influence of an electric field, forming a dipole. This means that charges orient in the direction of the field, as shown in Figure 1. If the field is uniform, the

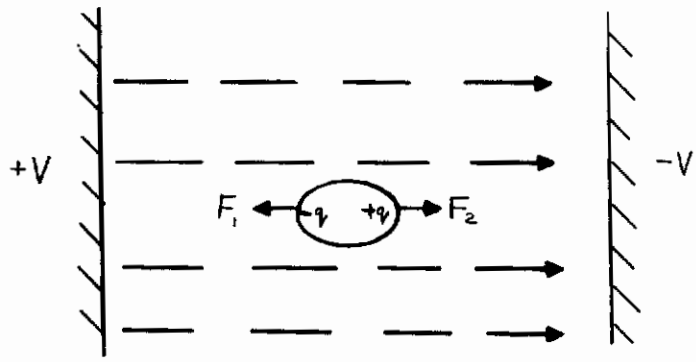

Figure 1. Molecule in a Uniform Electric Field
(Equal Forces, i.e., $F_1 = F_2$)

electric forces on the charged ends of the dipole are equal and opposite. But, in a nonuniform field the end of the dipole which is in the region of strongest field experiences a larger force than that felt by the other end. There is, therefore, a net force on the molecule, the direction of this force being towards the region of increasing field. The behavior of a dielectric particle in the nonuniform field existing between concentric cylindrical electrodes is shown in Figure 2. The net force is radially inwards. If the polarity of the source were reversed, the induced charge would

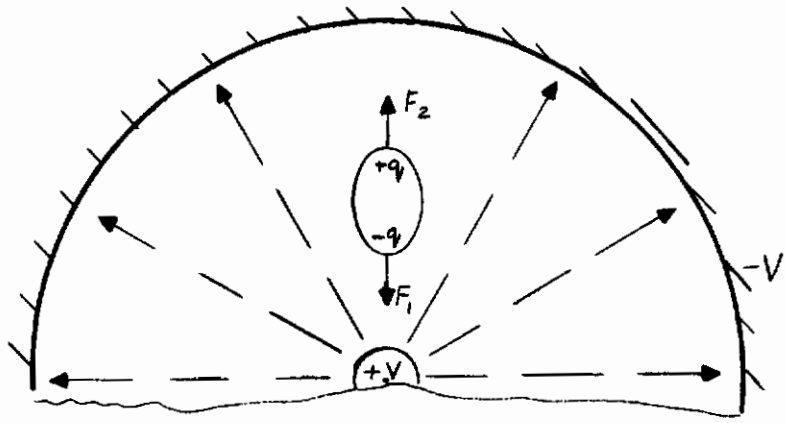

Figure 2. Molecule in a Radial Field
(Unequal Forces, $F_1 > F_2$)

be reversed and the net force would still be radially inwards. This suggests that the effect for ac is the same as for dc.

The Cylindrical Dielectrophoretic Cell

The cylindrical dielectrophoretic cell is perhaps the simplest of all separator configurations. It consists of two concentric cylinders. The dielectric medium occupies the annular cylinder bounded by the inner and outer electrode. Figure 3 is a section view of such a cell.

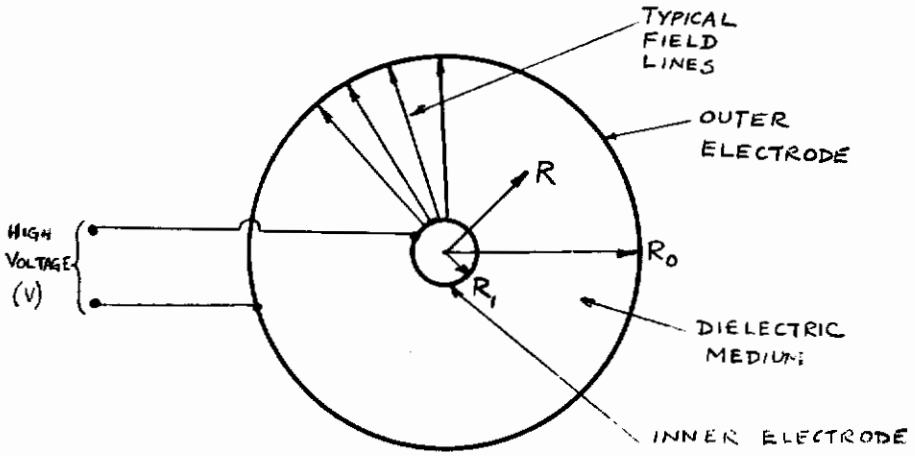

Figure 3. The Cylindrical Dielectrophoretic Cell

The derivation of the expression for the body force on a unit volume of a homogeneous dielectric medium is well established in the literature (Reference 1, 2, 3).

$$F = 1/2 \text{ grad } \left[E^2 \rho \left(\frac{\partial \kappa}{\partial \rho} \right)_{\substack{\text{const.} \\ \text{temp.}}} \right] \qquad (1)$$

where:

E is the electric field strength

ρ is the fluid density

κ is the dielectric constant

and where:

$\left(\frac{\partial \kappa}{\partial \rho} \right)_{\substack{\text{const.} \\ \text{temp.}}}$ denotes the partial derivative of κ with respect to ρ at constant temperature.

A commonly used expression relating dielectric constant and fluid density is the Clausius - Mossoti equation which provides a reasonable correlation of experimental observations on nonpolar fluids (Reference 4). That is:

$$\frac{\kappa - 1}{\kappa + 2} = A \rho \qquad (2)$$

where:

A is a constant depending on the particular fluid under consideration.

In deriving a one-dimensional equation for the body force experienced by a fluid in a cylindrical dielectrophoretic cell the following assumptions are made:

1. That the Clausius - Mossoti Law may be used to relate the fluid density and dielectric constant,
2. That end effects are negligible,
3. That extraneous charges are not present, and,
4. That the properties of the fluid are homogeneous and invarient with time.

Accordingly, the fluid density terms are eliminated from Equation (1) using Equation (2) and the result is,

$$\bar{F} = \frac{\epsilon_o}{6} (\kappa - 1)(\kappa + 2) \text{ grad } E^2 \quad * \tag{3}$$

A noteworthy characteristic of this force is that its direction is radially inward independent of the polarity of the field. It should further be noted that since the force is derivable from a potential, it cannot be used as the basis of pumps to drive fluids through external circuits.

Consider now the net dielectrophoretic force acting on a small unit sphere of fluid, of dielectric constant κ_L, surrounded by a matrix fluid of dielectric constant κ_v. The force on the sphere cannot be obtained from Equation (3) since the charge on the interface between the two fluids must be taken into consideration. Assuming that the electric field is not significantly perturbed by the presence of the sphere, the expression for the force on the unit sphere is:

$$\bar{F} = \epsilon_o \frac{3\kappa_v (\kappa_L - \kappa_v)}{2(\kappa_L + 2\kappa_v)} \text{ grad } E^2 \tag{4}$$

An account of the derivation of Equation (4) is given in Reference 5.

The electric field at some general point, R, in the simple system of Figure 3 is obtained from the Laplacian solution, $\bar{E} = - \nabla V$.

$$\bar{E} = - \frac{\bar{u}_r V}{R \ell n \frac{R_o}{R_1}} \tag{5}$$

where:

V is the applied voltage

$\bar{u}_r$ is the unit vector in the radial direction

R_o is the radius of the outer electrode

R_1 is the radius of the inner electrode

Thus grad E^2 is given by:

$$\text{grad } E^2 = - \frac{2\bar{u}_r V^1}{R^3 \left(\ell n \frac{R_o}{R_1}\right)^2} \tag{6}$$

*Electrostatic units (esu) are used except where the use of another system of units will aid the reader. In this unit system $\epsilon_o = \frac{1}{4\pi}$. Each departure from esu is clearly identified.

Substitution of Equation (6) into Equation (4) results in an expression for the force on a unit sphere of fluid in the simplest cylindrical system. That is,

$$\bar{F} = -3\epsilon_o \kappa_v \left(\frac{\kappa_L - \kappa_v}{\kappa_L + 2\kappa_v}\right) \frac{a_r V^2}{R^3 \left(\ell n \frac{R_o}{R_1}\right)^2} \tag{7}$$

In the system under discussion here, the normal equilibrium configuration (in the absence of a gravity field) is defined by the fluid with the higher dielectric constant forming a cylinder of radius R * around the central electrode. (See Figure 4.) In such a system, the electric field at a point is no longer given by Equation (5) since a discontinuity of field occurs at the fluid interface. However, neglecting the time varying surface charge, the assumption may be made that $\kappa_L E_L = \kappa_v E_v$. This boundary condition leads to the result,

$$\bar{E} = \frac{V}{R \kappa_R \left[\frac{1}{\kappa_L} \ell n \frac{R^*}{R_1} + \frac{1}{\kappa_v} \ell n \frac{R_o}{R^*}\right]} \tag{8}$$

where:

R is the point of interest

R* is the radius at the fluid interface

R_o is the tank radius

R_1 is the inner electrode radius

V is the voltage

κ_R is the dielectric constant at R (note κ_R changes discontinuously at R = R*)

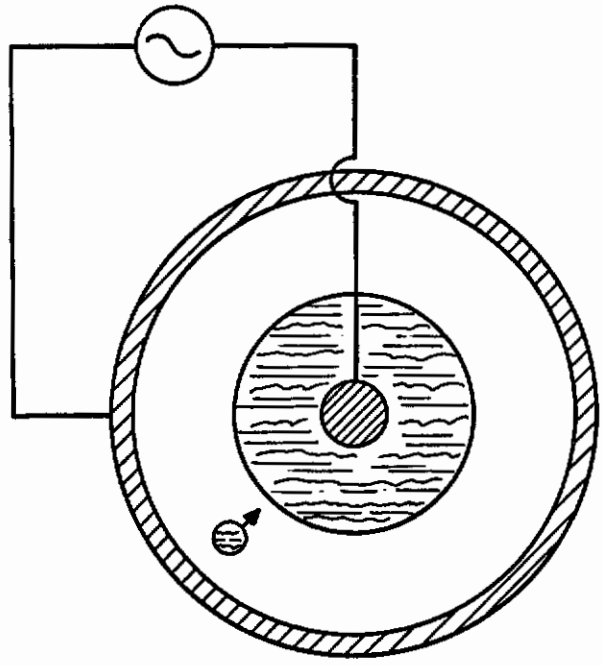

Figure 4: Equilibrium Configuration in the Simplest Cylindrical Dielectrophoretic Cell

The capacitance of the system is given by:

$$C = \frac{2\pi\epsilon_o}{\frac{1}{\kappa_L} \ell n \frac{R^*}{R_1} + \frac{1}{\kappa_v} \ell n \frac{R_o}{R^*}} \quad \text{farad/cm} \qquad (9)$$

where:

C is the capacitance per unit length of the system in farad/cm

ϵ is the capacitivity of free space, 8.85×10^{-14} in c.g.s system of units

c.g.s units are used in this equation to avoid unfamiliar units of capacitance

It is noted that C decreases as the volume of the oriented fluid decreases (this will occur when liquid oxygen is consumed in the converter system). Thus the volume of oriented fluid may be sensed by changes in the system capacitance.

Dynamic Analysis of a Spherical Fluid Element

When a spherical fluid element is in motion in a nonuniform electric field, there will be both mechanical and electrical forces acting. This is shown in Figure 5, with two mechanical forces acting:

1. Inertia--There is a force due to the acceleration of the body, equal to the product of mass and acceleration, i.e

$$F_1 = \left(\frac{4}{3} \pi a^3 \rho_b \right) \frac{d^2 r}{d t^2} \qquad (10)$$

where:

a is the sphere radius,

ρ_b the mass density of the body, and

$\frac{d^2 r}{d t^2}$ the instantaneous acceleration.

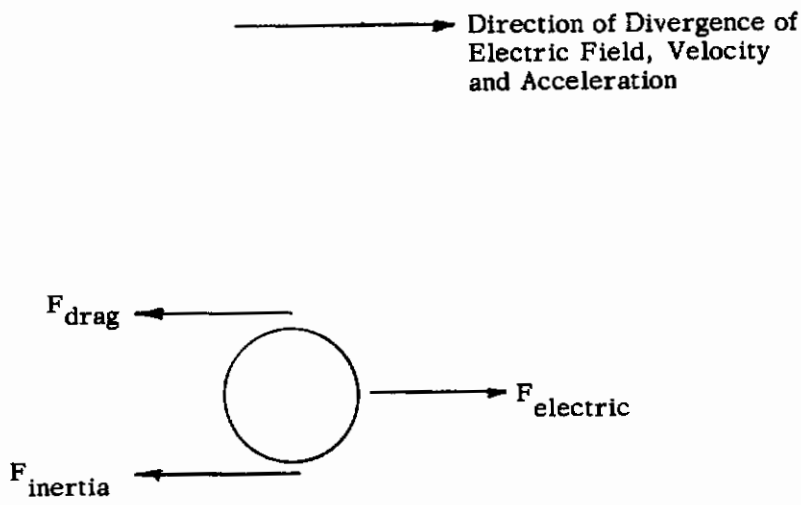

Figure 5: Force Balance on a Moving Element

2. Drag--There is a viscous force due to the velocity drag on the body. This depends on the projected area ($\pi \cdot a^2$), density of the matrix fluid (ρ_m), instantaneous velocity $\left(\frac{dr}{dt}\right)$, and a factor known as the drag coefficient (C_D). The relationship is:

$$F_2 = (\text{Area}) C_D \rho_m \frac{V^2}{2} = \pi a^2 C_D \rho_m \left(\frac{dr}{dt}\right)^2 \tag{11}$$

The drag coefficient of a sphere, C_D, is a function of Reynolds Number. Values of C_D have been experimentally determined. Typical values may be found in Reference 6. A further drag force may exist due to rotation of the fluid in the sphere itself. For reasons discussed elsewhere (Reference 7), this may be neglected.

The force balance may be written

$$F_1 + F_2 = F_E \tag{12}$$

where $F_1 + F_2$ are defined in Equations (10) and (11) and F_E is defined in Equation (4). Thus:

$$\frac{4}{3} \pi a^3 \rho_b \frac{d^2 r}{dt^2} + \pi a^2 C_D \rho_m \left(\frac{dr}{dt}\right)^2 =$$

$$\frac{3}{2} \epsilon_o \kappa_v \left(\frac{\kappa_L - \kappa_v}{\kappa_L + 2\kappa_v}\right) \text{grad } E^2 \tag{13}$$

where:

subscripts b and L refer to the liquid bubble, and
m and v refer to the vapor matrix

This equation is a second order nonlinear differential equation relating position and time. Experimental tests have been made to verify this expression. These are discussed later.

Since viscous terms are negligible in an actual oxygen converter, the expression simplifies and is directly integrable. Collection times may therefore be calculated. The results, as shown in Appendix B, give agglomeration times of order of 4 sec in practical converters.

Dimensionless Converter Parameters

The usual way of exploring the relative importance of the various physical forces which may be exerted in a hydrodynamic problem is to express ratios of those forces as dimensionless parameters. A partial list of those common to analyses of this kind is given:

1. Reynolds Number (Re), the ratio of inertial to viscous forces,
   $\text{Re} \equiv \frac{\rho u L}{\mu}$,
2. Weber Number (We), the ratio of inertial to surface forces,
   $\text{We} \equiv \frac{\rho u^2 L}{T}$,
3. Bond Number, (Bo), the ratio of gravity to surface forces,
   $\text{Bo} \equiv \frac{\rho g L^2}{T}$.

Due to the inclusion of a dielectrophoretic force field, the discussion of the oxygen converter system requires the definition of some additional parameters. These are listed below:

4. $\frac{\text{dielectrophoretic force}}{\text{surface force}} \equiv N_1 \equiv \frac{V^2}{LT}$

5. $\frac{\text{dielectrophoretic force}}{\text{inertial force}} \equiv N_2 \equiv \frac{V^2}{L^2 \rho u^2}$

6. $\frac{\text{dielectrophoretic force}}{\text{viscous force}} \equiv N_3 \equiv \frac{V^2}{L \mu u}$

where:

V is the applied voltage (which is considered to have the dimensions-- $\sqrt{\text{dyne}}$)*

L is a characteristic length, cm.

T is the vapor-liquid surface tension, dyne/cm

ρ is a mass density, gram/cm^3

μ is a viscosity, gram/cm -sec

u is a characteristic velocity, cm/sec

g is the acceleration due to gravity, cm/sec^2

The relative magnitudes of N_1, N_2, and N_3 are now inspected both for a laboratory simulator (peanut oil and silicone oil) and for the prototype. (Liquid oxygen and gaseous oxygen at 70 ± 20 psia and 110 ± 5°K.) The values of the dimensionless groups are tabulated below.

	Laboratory Analog		Prototype	
	Drop of peanut oil in silicone oil	Drop of silicone oil in peanut oil	Vapor Matrix	Liquid Matrix
N_1	10^{10}	10^{10}	10^9	10^9
N_2	10^{12}	10^{12}	10^{14}	10^{12}
N_3	10^{13}	10^{13}	10^{16}	10^{14}

The two columns for the prototype are necessary to account for the two distinct variations of the system:

1. The motion of liquid globules in a vapor matrix, and,
2. The motion of gaseous bubbles in a liquid matrix.

Since N_1, N_2, and N_3 are all large, it may be noted that the dielectrophoretic force dominates in in both simulator and prototype. Because N_2 and N_3 contain velocities which vanish in the equilibrium state, these parameters are only important in studying such time dependent phenomena as collection times or effects due to vibration. The remaining parameter N_1 is slightly smaller in the prototype than in the simulator. This parameter is important to steady state phenomena such as liquid "hang-up" and interfacial stability. Thus, stability design problems must be treated more carefully in the prototype than in the analog.

Systems with Staging

The Concept of Intermediate Stages

Operational tankage for a typical zero gravity vehicle usually requires a higher average force level (i.e. a higher energy density) than is obtainable with a single central electrode. Several

* For the purposes of this discussion, ϵ_o may be treated as a dimensionless quantity.

limiting factors prevent the achievement of this goal through the unlimited increase of system voltage. These are:

1. The finite electrical breakdown strength of the stored fluids,
2. The limitations imposed by the current state of the art in the area of high-voltage insulating materials, and,
3. The significant power supply weight penalties which occur for very high voltage requirements.

Fortunately, there is another way of increasing the minimum force level within the tank. It is noted that the dielectrophoretic forces do not depend upon polarity, therefore it is possible to construct a system of a number of concentric stages having alternate potentials. The force on a fluid element inside the concentric annular space between any two stages is still radially inward.

Ideally, the stage boundaries would consist of extremely thin, porous conductors, say, fine wire mesh screens. Practical limitations, however, are imposed by surface tension forces. A wetting liquid would be held up on such stages. The movement of liquid from the tank wall toward the axis of the system would be impeded to an intolerable degree and the outward flow of vapor would be blocked. A workable solution to this problem is seen in a rather coarse array of individual electrodes (stage elements). The stage elements are held parallel to the axis of the cylindrical tank and they are arrayed in concentric cylinders, the elements of each cylinder being maintained at the same potential.

Design of Stage Radii

Staging may be positioned according to various performance requirements. Three design methods will be discussed here.

(A) In the first method there is imposed a lower limit on the dielectrophoretic force on a unit sphere of liquid in a vapor matrix. The ideal force profile in a system designed with a specified minimum force level is sketched in Figure 6. A parameter g_e is defined

$$g_e \equiv \frac{f_{min}}{\rho_L g_o}$$

which may be thought of as describing the "equivalent gravity field"--in g_o's--due to dielectrophoresis. The staged system is specified when the following parameters are fixed:

1. The minimum acceptable dielectrophoretic force on a unit bubble of liquid, f_{min},
2. The voltage of the system, V,
3. The tank radius, R_o,
4. The dielectric constants of the liquid, κ_L, and of the vapor, κ_v.

Accordingly, the first general stage design equation may be written

$$\rho_n \frac{R_n}{R_{n+1}} = K_1 R_n^{-3/2} \qquad (14)$$

where:

$$K_1 \equiv \left(K_2 \; V^2 \; f_{min}^{-1} \right)^{1/2} \text{--- in cm.}^{3/2}$$

$$K_2 \equiv \frac{\epsilon_o \kappa_v \left(\kappa_L - \kappa_v \right)}{3 \times 10^4 \left(\kappa_L + 2\kappa_v \right)}$$

$$n \equiv 0, 1, 2, \text{--------}$$

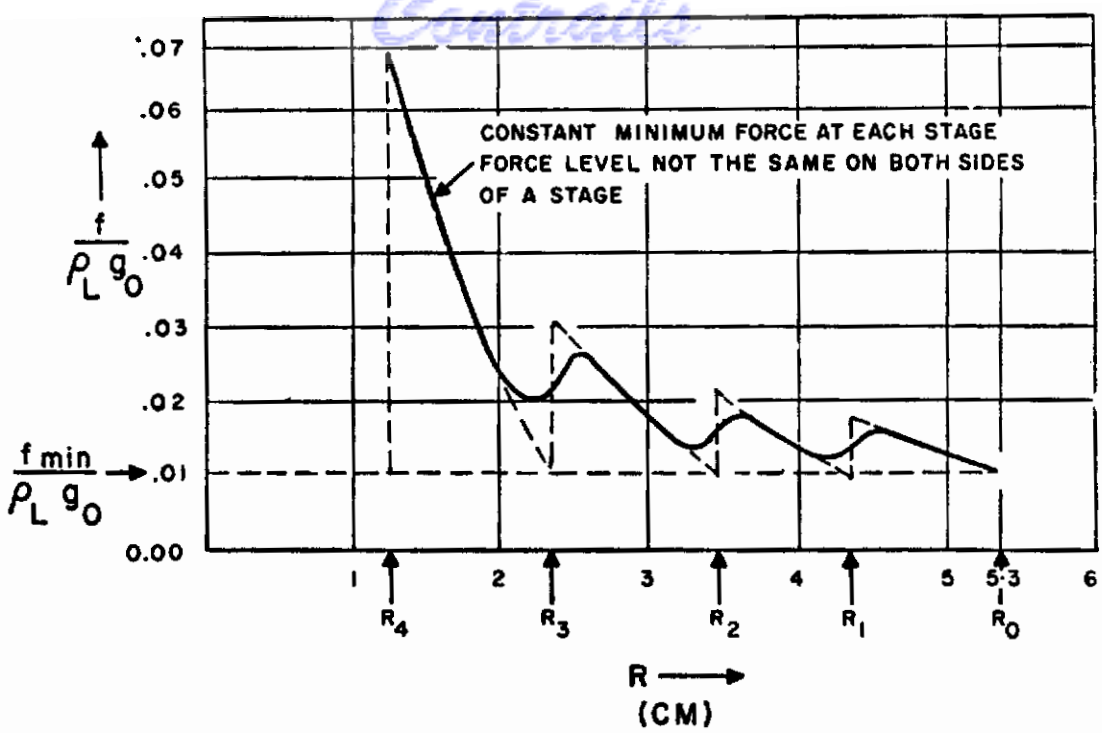

Figure 6: Idealized Force Profile in a Typical System Designed for Specified Minimum Volume Force

(R_o, R_1, R_2, etc. refer to the stage radii)

[Note that the convention for numbering stages will be subscript zero, R_o, for the radius of the tank wall, subscript one, R_1, for the radius of the next stage inward, and so on. The use of the stage numbering convention is illustrated in Figure 7.]

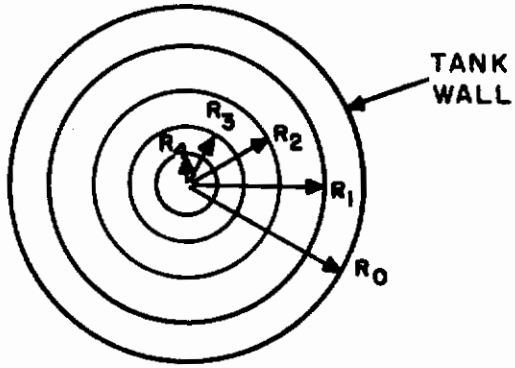

Figure 7: Stage Numbering Convention

(B) In the second design method there is placed a lower limit on the force on a unit sphere of liquid at the tank wall. In addition, there is a boundary condition that the field be continuous throughout the system. The force profile in such a system is sketched in Figure 8. For this method, the energy level in the tank is higher, resulting in some weight penalty. The general stage design equation for a system having a continuous force profile is

$$\frac{R_n}{R_{n+1}} = \text{constant} \qquad (15)$$

where the constant is given by evaluating the first stage radius using Equation (14).

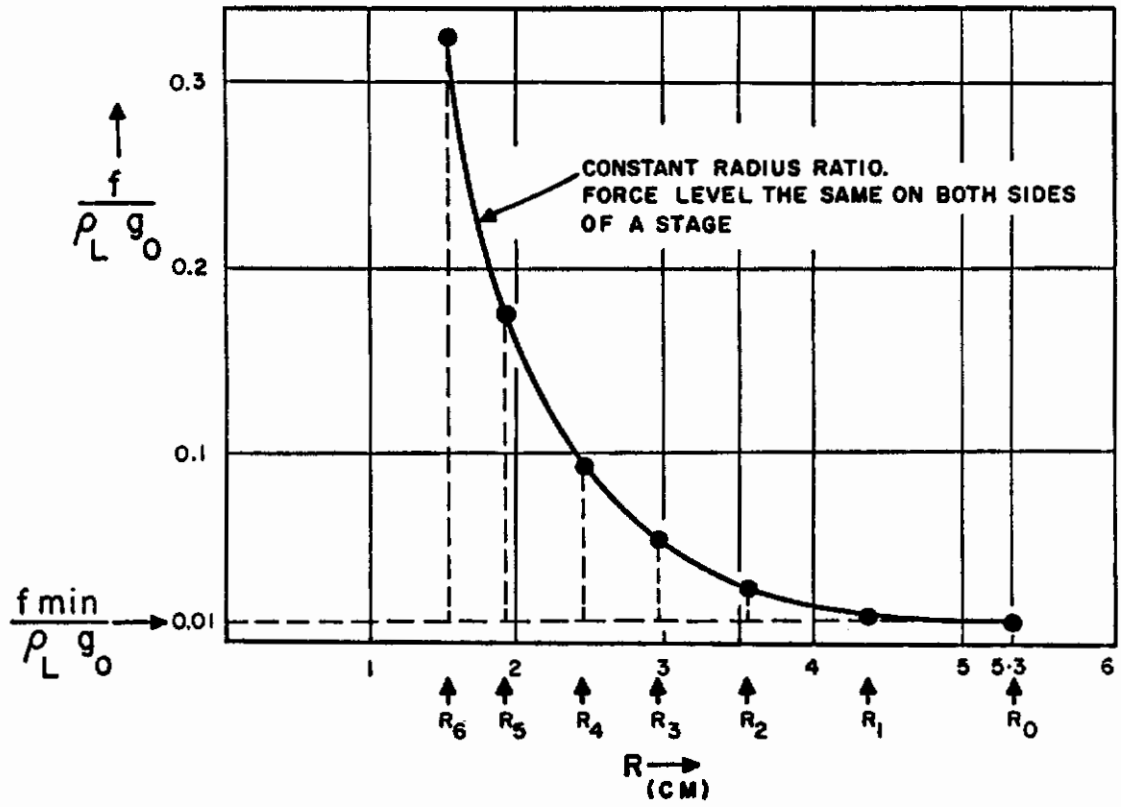

Figure 8: Idealized Force Profile in a Typical System Designed for Continuous Force Across Stages

(R_o, R_1, R_2, etc. refer to the stage radii)

(C) A third design method is based on the maximum electric field intensity in the system. The system is designed such that the maximum electrical stress is constant and lower by some safety factor than the breakdown strength of the media within the tank. The design equation for such a system may be expressed as follows:

$$\ell n \frac{R_n}{R_{n+1}} = \frac{V}{E_{max} R_{n+1}} \qquad (16)$$

where E_{max} is the maximum electric field existing in the annulus between stages.

Figure 9 shows the force profile for such a system. Equation (16) applies to ideal stages. Since real stage electrodes are not concentric cylinders but are rod-like elements arrayed in concentric cylinders, the maximum electric field intensity is somewhat larger than would be predicted on the basis of Equation (5). The general solution to the equation describing field intensity in a system having rod-like elements may be obtained only through a computer program (See Appendix A). This complication may be obviated by imposing a suitable factor of safety, K_s, upon Equation (16).

$$\ell n \frac{R_n}{R_{n+1}} = \frac{V K_s}{R_{n+1} E^*} \qquad (17)$$

where $K_s > 1$ and E^* is the dielectric strength of the media.

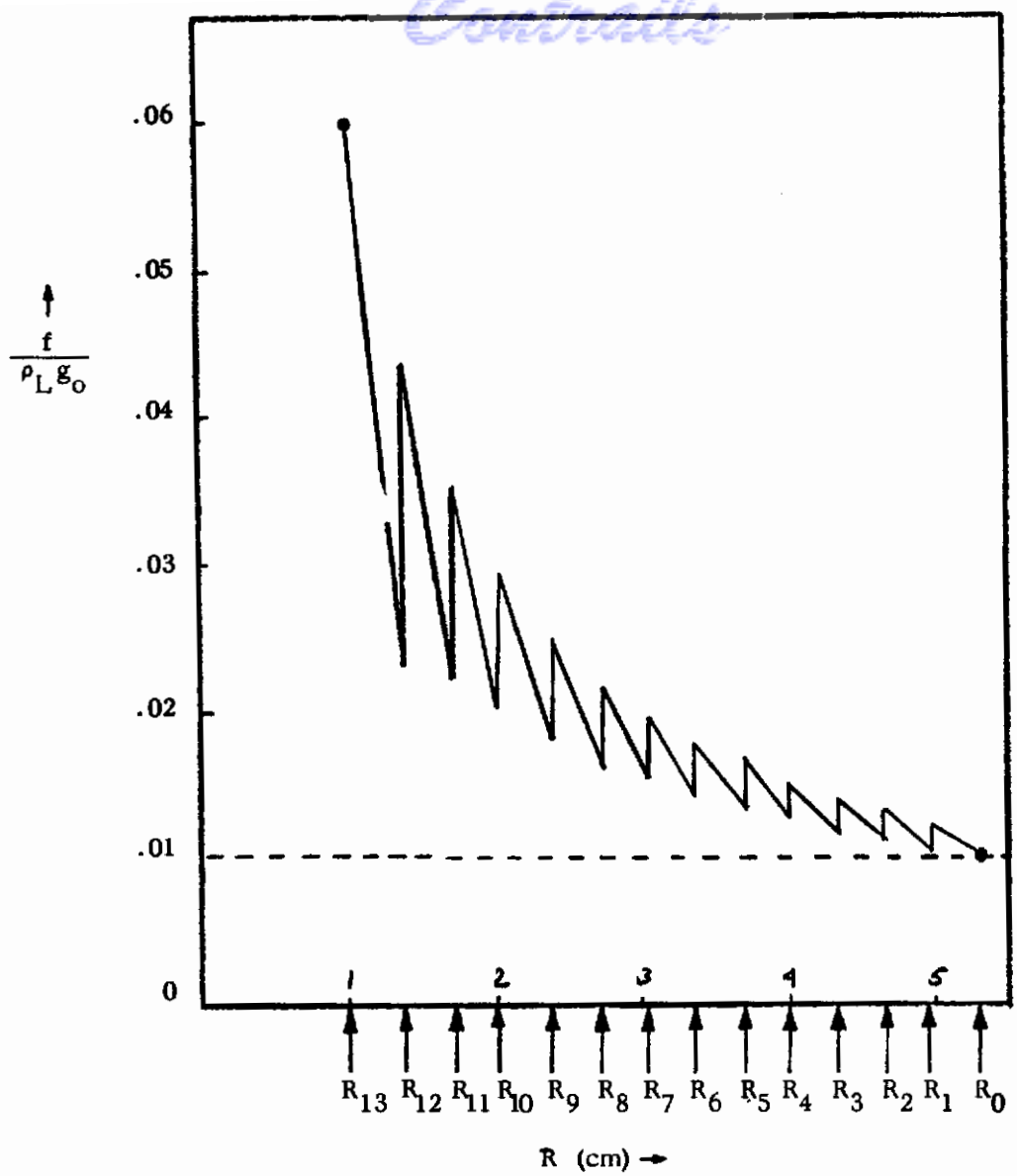

Figure 9: Idealized Force Profile in a Typical System Designed for Constant Maximum Electrical Field Throughout

Equation (17) may be restated as a design constraint. That is, that nowhere in the system shall the maximum field exceed the breakdown strength of the fluids (with some appropriate safety factor included).

$$E_{max} = \frac{V}{R_n \ln \frac{R_n}{R_{n+1}}} \leq \frac{E^*}{K_s} \qquad (18)$$

For the oxygen converter a suitable safety factor is $K_s \approx 10.$ Note that for oxygen vapor, under the conditions prevailing in the converter, $E^* \approx 500$ KV-cm^{-1}.#

At S.T.P., E_o^* for oxygen ≈ 30 KV-cm^{-1}. To predict E^* for the conditions prevailing in the converter, the approximation $\rho E^* \approx \rho_o E_o^*$ is used.

The ultimate choice of design method depends upon certain factors. The first factor is that of "hang-up". Although this is discussed further in the next section, some relevent statements are made here. The force profiles of Figures 6 and 9 show finite discontinuities at the stage. When stage elements are used, the electric field cannot be discontinuous, and will approach the dotted curve, AB, in Figure 10. The force profile is a derivative of the field (proportional to $-\nabla E^2$), and thus the slope reversal in Region AB means that the force reverses close to each electrode. This means that fluid is driven towards the electrode, and tends to "hang-up" there. Note that liquid adhering to the stage electrodes eventually vaporizes and is used. It is a problem only where it might impede the performance of the converter. If totally unchecked, liquid hang-up on the stages might conceivably interfere with the operation of vapor outlets at the tank wall and with level indicator performance. It is therefore concluded that if hang-up is minimized, stages must be designed with constant radius ratios.

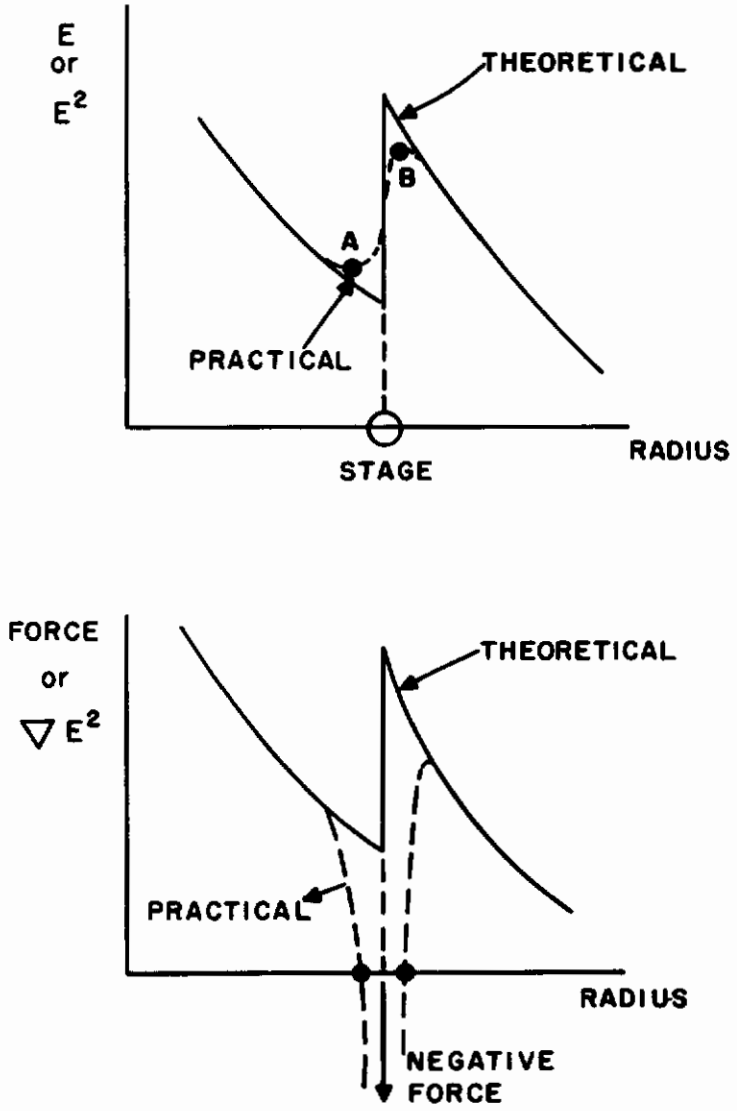

Figure 10: Force Field and Hang-up

There is yet another factor to be considered due to the stability limits of the liquid-vapor interface. The term stability is used in reference to the behavior of the cylindrical interface following a small disturbance. A stable surface will return to its original configuration following a disturbance. An unstable surface will depart radically from a cylindrical geometry and will break up. It may be shown that for real dielectric fluids, having finite electrical

conductivity, unstable behavior of the interface is predictable. This means that a system operating with given fluid properties (σ_L, σ_V, κ_L, κ_V, T) and having a power supply of fixed angular frequency (ω) has:

1. A minimum value of stage radius ratio, $\frac{R_n}{R_{n+1}}$, below which unstable operation is predicted,

2. A minimum voltage, V, below which the fluid interface collapses, and,

3. A maximum voltage above which the interface breaks up.

The constraints imposed by the stability analysis are discussed in some detail in Appendix C. It suffices here to state that reasonable dielectrophoretic force levels may be maintained in a 25-liter oxygen converter system without violating the criteria imposed by stability considerations.

According to hang-up considerations, it was shown that it is desirable to design stages with constant radius ratio. Utilizing stability criteria, the minimum constant radius ratio may be found. The designer must not exceed this ratio because that would decrease the force level within his system, nor may he go below this or the system will be unstable.

Hang-Up on Stage Elements

In any dielectrophoretic cell the fluid with the highest dielectric constant is attracted to regions of strongly divergent field. In the simple single electrode system, there is only one such region. In a system comprised of an array of stage elements, there will be small regions of diverging field around each element. In these regions the net body force is directed toward that element.

The detailed analysis required to predict the degree of "hang-up" even in a relatively simple system having a single intermediate stage involves equations requiring computerized solution. Fortunately, however, simple experiments may be performed to evaluate staging geometries on a comparative basis.

In Figure 11 a system with a single intermediate stage is shown; the equilibrium position of the fluid is indicated.

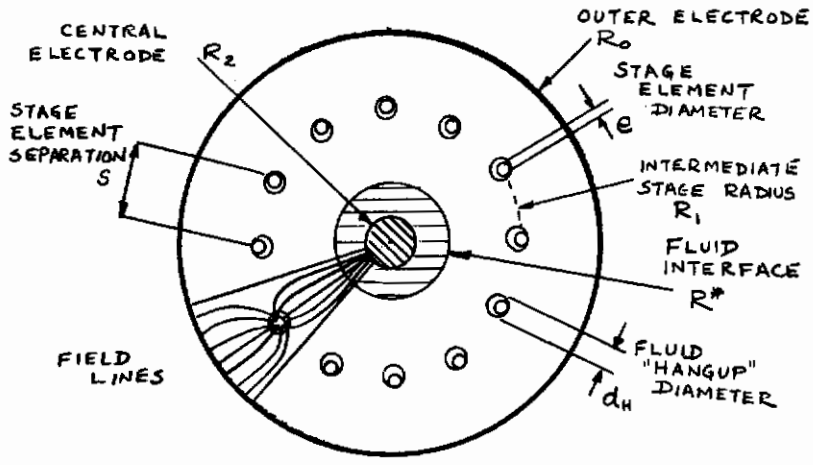

Figure 11: The Elementary Single Stage System Showing "Hang-Up"

In addition to the effect of local field disturbances due to the finite number of stage elements, there is an effect due to a discontinuity of field across the stage radius. That effect was discussed in the previous section (see Figure 10).

A single parameter may describe liquid "hang-up" in a system. This parameter is defined

$$D_h \equiv \frac{d_h}{e}$$

where d_h is the diameter of the fluid hang-up region and e is the diameter of a stage element.

It is expected that there be a functional dependence of D_h upon N_1 (where $N_1 \equiv \frac{V^2}{LT}$). The characteristic length governing the hang-up phenomenon may be taken to be the stage element diameter, e. The parameter, N_1, is greater in the laboratory analog than in the prototype (i.e., surface forces are more dominant in the prototype). Due to practical limitations imposed by a lack of variety in laboratory working fluids, the surface tension may not readily be changed. The dimensionless number (N_1) may be varied over a wide range, however, by adjusting (V) and (e). This suggests a simple method of investigating the hang-up problem in the laboratory and relating the results to the prototype system.

The efforts to reduce or eliminate "hang-up" on stage elements in a small (25 liter) system must be restricted to making geometrical adjustments. Other schemes for minimizing the problem involve the addition of components which tend to add to the system's weight and detract from its simplicity and reliability. Such possible schemes are:

1. Mechanical removal of fluid hang-up by vibration of the stage elements.

2. The use of a special electrical-mechanical switching network which permits periodic grounding of the stages in a radially inward sequence.

This last scheme has been shown to work in the laboratory. Fluid hang-up on the first outer stage is stripped off quite rapidly and completely by momentarily holding that stage at the same potential as the outer electrode. The process is continued by holding the next inner stage at the same potential as the tank wall and the outer stage, and so on.

A dimensional analysis indicates that

$$D_h = D_h \left[\frac{V^2}{eT}, \frac{R_o}{R_1}, \frac{R_1}{R_2}, \frac{S}{e}, \frac{R_o}{S} \right]$$

The effect of these parameters upon the hang-up volume may be determined experimentally.

The influence upon hang-up of distorted stage elements can only be studied experimentally. The idea to be tested using off-shape element designs is that the transfer of fluid between stages may be enhanced by allowing the distance between stages to vary along the length of the converter. This last concept is illustrated in Figure 12. The arrows indicate the expected direction of fluid flow. Coating the inside of the converter with a non-wetting substance such as Teflon may provide an additional means for keeping liquid away from the regions of the vapor outlets while reducing neither the simplicity nor reliability of the converter nor increasing its weight appreciably.

Electric Field and Force Equations for a General Converter

In previous sections it was indicated that it is necessary to have intermediate stages with a finite number of elements. Strictly speaking, an exact field solution is essential for precise determination of the force profile within the system. The analytical solution to the field and force profiles could be used to:

1. Optimize the electrode design using comparative force field mappings
2. Predict the best location of vapor outlets

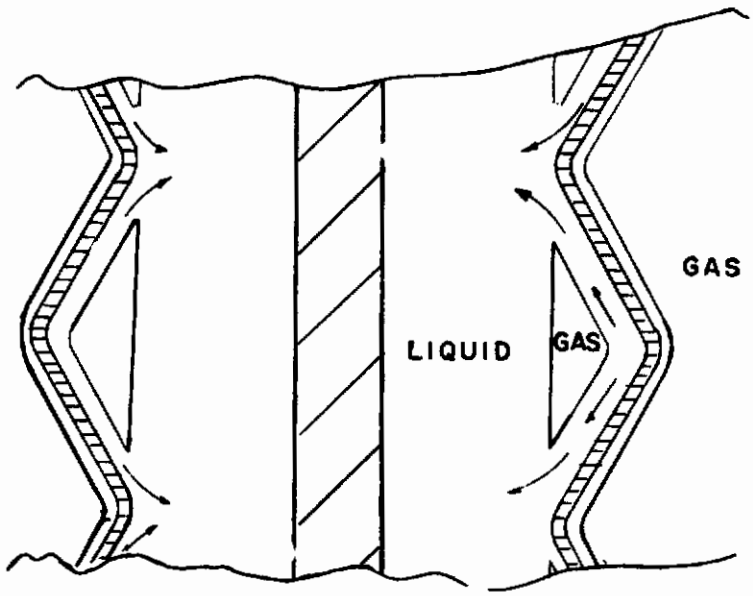

Figure 12: A Proposed Off-Shape Design of Stage Elements

3. Determine collection times
4. Provide the designer with a closed form theory on the hang-up phenomenon
5. Determine maximum electric field

Appendix A presents the basis for the derivation of the electric field $\bar{E}$ and grad E^2 for a general system. Equations for $\bar{E}$ and grad E^2 for the elementary system of Figure 11 have been developed. For the general axisymmetric system, $\bar{E}$ is of the form.

$$\bar{E} = -\nabla V = -\left(\bar{u}_r \frac{\partial v}{\partial r} + \bar{u}_\theta \frac{1}{r} \frac{\partial v}{\partial \theta}\right) \tag{19}$$

where:

$\bar{u}_r$ is the radial unit vector

$\bar{u}_\theta$ is the circumferential unit vector

$\frac{\partial v}{\partial r}$ is the radial voltage gradient

$\frac{\partial v}{\partial \theta}$ is the circumferential voltage gradient.

The expression for $\bar{E}$, even for an elementary system, is complex, and that of grad E^2 contains twenty-three terms. To avoid the need for a computerized solution, it was necessary to approximate the electric and force fields by ignoring the effects of the finite number of electrodes. However, adequate factors of safety may be used to compensate for this simplification.

Stability of a Cylindrical Fluid Interface

The stability of cylindrical fluid interfaces under the influence of electric fields must be assured if operational devices of the type under consideration are to become a reality. The following discussion summarizes the essential results of an analysis presented in greater detail in Appendix C.

The basis of any unstable behavior of the interface lies in the electrical conductivity of the fluids. However small, a finite conductivity results in the appearance of free charge at the interface. This is because Ohm's law requires that the normal components of current density must be continuous across the interfacial boundary while the change of the normal component of the displacement current is equal to the free surface charge. The Ohm's law condition cannot, in general, be satisfied without yielding a discontinuity in displacement current. There are two modes of unstable behavior. The conditions which must be satisfied in order to prevent these modes will be discussed.

The first condition may be thought of as one which indicates how closely a system may approach a parallel plate geometry and still retain a stable interface. A parallel plate geometry ($R_o/R_1 = 1$) is always unstable for an interface parallel to the electrodes. Equation (20) below states the condition which must be met to prevent the first mode of unstable behavior, i.e., the collapse of the interface.

$$\frac{V^2}{T R^*} \geq \frac{\epsilon^{*2}}{\epsilon_L \epsilon_v \Gamma^2 (1-\Gamma)} \tag{20}$$

where:

V is the system voltage in statvolts

T is the interfacial surface tension in dyne/cm

R* is the radius of the cylindrical interface in cm

κ_L and κ_v are the dielectric constants of the liquid and vapor phases respectively

and where:

$$\kappa^* \equiv \kappa_L \ell n \frac{R_o}{R^*} + \kappa_v \ell n \frac{R^*}{R_1}$$

$$\Gamma \equiv \frac{\kappa_L - \kappa_v}{\kappa^*}$$

It has been determined‡ that a rational design point for the particular system under consideration is $\Gamma \leq 0.9$. To assure peak system performance, the system should be operated at $\Gamma = 0.9$. Equation (20) may be rearranged to yield a criterion for the lower limit on applied voltage.

$$V \geq \sqrt{\frac{(\kappa_L - \kappa_v) T}{\epsilon_o \kappa_L \kappa_v \Gamma^2 (1-\Gamma)} \cdot R^*} \tag{21}$$

In the oxygen converter, under the conditions of pressure and temperature which exist there, $\kappa_L = 1.45$, $\kappa_v = 1.0$, and $T \approx 8$ dyne/cm. Thus $V \geq 10\sqrt{\pi R^*}$. For example, this last result may be used to find the maximum allowable tank radius which can be used in conjunction with a power supply of known voltage. The minimum allowable staging radius ratio (R_o/R_1) which may be tolerated is simply determined from the condition that $\Gamma \leq 0.9$. This condition will be met when $\kappa^* \geq (\kappa_L - \kappa_v)/0.9$. Since $\kappa_L > \kappa_v$, therefore κ^* is smallest when $R^* = R_o$ (i.e., when $\kappa^* \rightarrow \kappa_v \ell n R_o/R_1$). This represents the worst (and limiting) case.‡‡

‡ See Appendix C

‡‡ Note that since

$$\kappa^* = \kappa_L \ell n \frac{R_o}{R^*} + \kappa_v \ell n \frac{R^*}{R_1}$$

thus when $R^* = R_1$

then $\kappa^*)_{max} = \kappa_L \ell n \frac{R_o}{R_1} + \kappa_v \ell n (1) = \kappa_L \ell n \frac{R_o}{R_1}$

and when $R^* = R_o$

then $\kappa^*)_{min} = \kappa_v \ell n (1) + \kappa_v \ell n \frac{R_o}{R_1} = \kappa_v \ell n \frac{R_o}{R_1}$

Thus a condition for stability is:

$$\kappa_v \ell n \frac{R_o}{R_1} \geq \frac{\kappa_L - \kappa_v}{\Gamma} \qquad (22)$$

$$\text{or} \qquad \frac{R_o}{R_1} \geq 1.6$$

for LOX under the conditions of operation.

This result may be used to monitor the design of stages. It places an upper limit on the force levels attainable.

The second mode of unstable behavior can best be described as a fountain effect. Peaks and dimples form on the interface. Where there are sharp peaks, tiny liquid droplets will be sprayed out into the vapor phase. This instability which has been observed in the laboratory may be prevented when the condition of Equation (23) is met.

$$\frac{V^2}{TR^*} \leq \left[\frac{4}{\Gamma^2} \frac{\kappa_1 + \kappa_o}{\kappa_1 - \kappa_o}\right]^2 \left[\frac{\kappa_1 - \kappa_o}{\kappa_1 \quad \kappa_o}\right] \qquad (23)$$

Recapitulating, a stable cylindrical fluid interface may be supported if

1. The tank radius does not exceed that implied by Equation (21),
2. The radius ratio of adjacent stages exceeds the value implied by Equation (22),
3. The system voltage exceeds that implied by Equation (21), and,
4. The voltage is less than that implied by Equation (23).

Level Indicator

The design of the converter requires a concentric cylinder geometry with ac voltage applied between adjacent cylinders. Since these cylinders have a (small) capacitance, they will draw a small powerless current from the supply. The current (I) is related to the capacitance (C), frequency (ω) and voltage (V) by:

$$I = \omega V C \qquad (24)$$

Consider the simplest cylindrical separator, such as is shown in Figure 4. The capacitance has already been given (Equation 9) as:

$$C = \frac{2\pi\epsilon_o}{\frac{1}{\kappa_L} \ell n \frac{R^*}{R_1} + \frac{1}{\kappa_v} \ell n \frac{R_o}{R^*}}$$

In normal operation, the liquid of dielectric constant (κ_L) is on the inside, and the vapor (κ_v) on the outside. The ratio of full to empty capacitances will be equal to the ratio of the dielectric constants*, or 1.45 for LOX/Oxygen vapor. The curve of Figure 13-A will be typical of the variation of capacitance (and hence current) with percentage full. There are three factors which could lead to inaccurate readings:

* This neglects end effects which will be small if length is large compared with radius.

1. The non-ideal orientation of fluid, i.e., hang-up etc.,
2. The effect of acceleration forces causing sloshing,
3. The effect of multistaging.

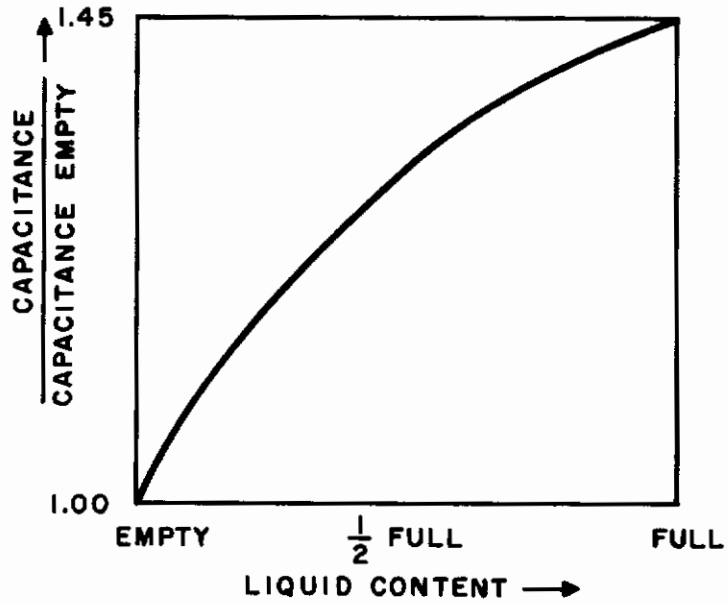

Figure 13-A: Variation of Capacitance with Volume of LOX (Ideal Simple Separator)

The final flight testing will evaluate this technique; however, preliminary tests and calculations have shown that level indication to within ± 10% is possible using this capacitance technique. A typical recording of tank capacitance versus time (or percent full) is shown in Figure 13-B. Even though the variations of capacitance due to liquid reorientation will cause error, the recording will show a definite trend.

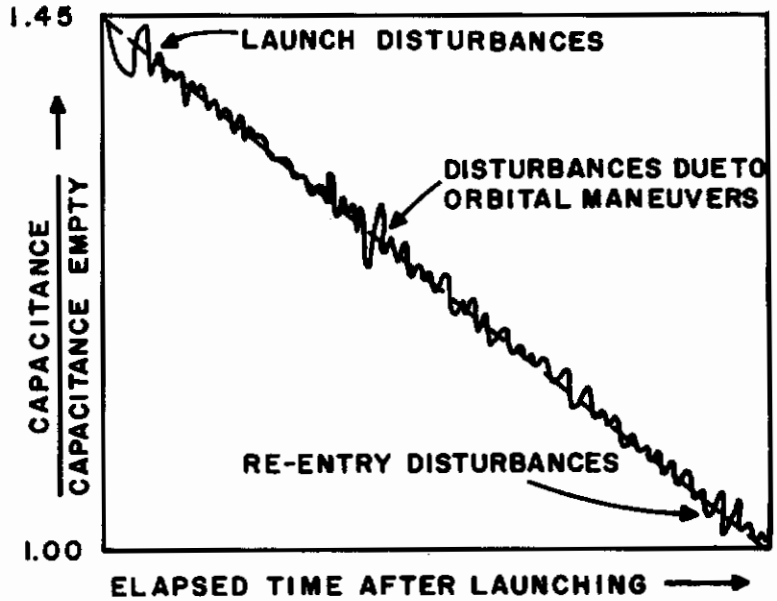

Figure 13-B: Expected Performance of a Level Indicator Over The Course of a Mission

The magnitude of dielectrophoretic forces involved in typical converter tank systems is such that the performance of these devices can be measured only when the effects of normal gravity forces are absent. To permit laboratory testing of converter design concepts, a two fluid analog was devised using a pair of immiscible, dielectric oils of equal density. The tests performed on the laboratory analog served four main purposes:

1. To provide experimental verification of the dielectrophoretic force equations,
2. To evaluate the merits of various electrode configurations on the basis of a comparison of their performance,
3. To provide some insight as to the best location of vapor withdrawal outlets, and,
4. To evaluate a capacitive level indicator.

In addition to tests carried out with the analog, certain other experiments were performed to study the safety of the dielectrophoretic oxygen converter. These were:

1. Investigation of the breakdown voltages in real configurations, and,
2. Tests to determine the nature of the explosion hazards due to ordinary hydrocarbon contaminants.

The Laboratory Analog

A zero-gravity simulator is necessary for evaluation of model devices in the laboratory. The simulator used in this work consists of two equal-density but immiscible dielectric fluids. The behavior of the fluids is observed through the glass walls of a model converter. The glass is coated on the inside surface by a transparent, electrically conducting film. Typical analog models are shown in Figure 14.

The requirements on a pair of analog fluids are as follows:

1. The fluids must be mutually immiscible,
2. They must have low (and unequal) dielectric constants,
3. They must be transparent,
4. The specific gravity of one of the fluids must be adjustable to permit the preparation of an equal density pair,
5. The electrical conductivity must be very low,
6. Should have interfacial surface tension equal to LOX-vapor,
7. Viscosity should match that of LOX.

Several pairs of fluids have been found which satisfied a majority of the requirements. A good many, though immiscible, exhibit the undesirable trait of forming filaments rather than rounded bubbles in one another. This is a manifestation of fluids having very low interfacial surface tension.

The search for suitable simulator fluids was ended when it was found that silicone oils are immiscible with most vegetable base oils. The silicone oils chosen were the Dow Corning 200 series which are available in a range of densities. The four vegetable base oils which best satisfy the laboratory requirements are peanut oil, corn oil, castor oil, and soybean oil. The

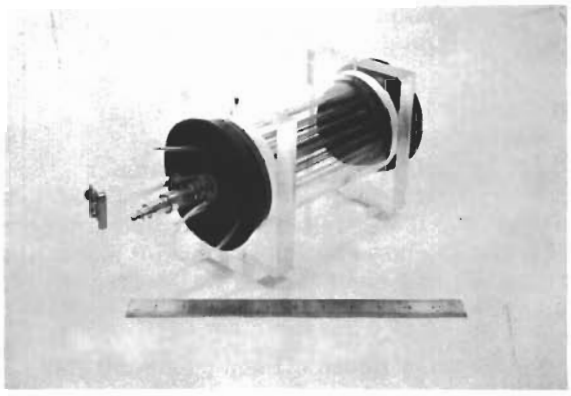

A Multi-staged System in a 4-inch Cylinder, 8 inches Long. Capacity Approximately 1 Liter

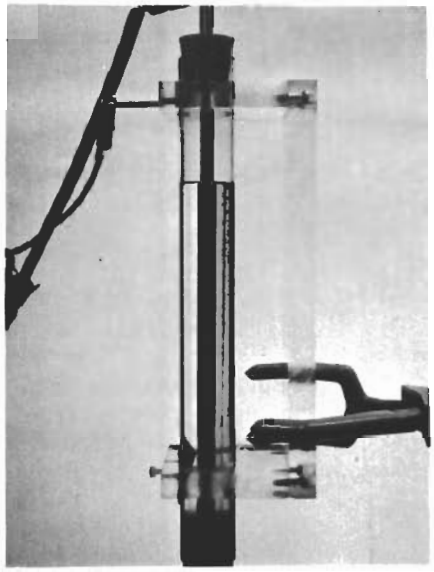

A Basic System in a 1-inch Cylinder, 10 inches Long

Figure 14. Two Laboratory Analog Models

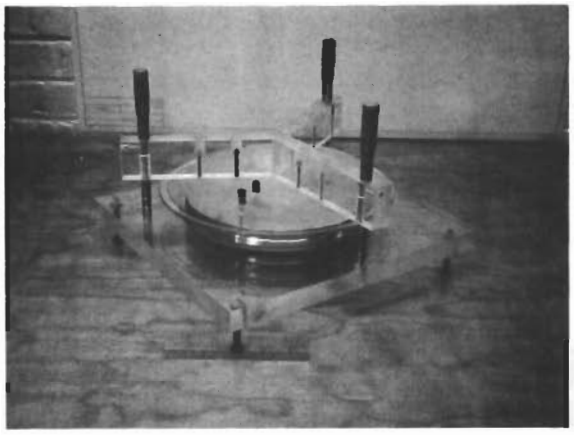

a) Assembled

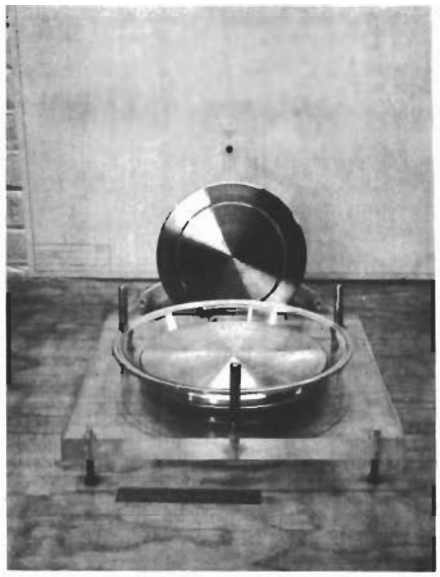

b) Disassembled

Figure 15. Parallel Plate Capacitor for Dielectric Constant Measurement

best combination from all points of view is silicone oil and peanut oil. The silicone oil used is a blend of 3 centistoke and 5 centistoke Dow Corning 200 oil.

Some properties of an equal density combination of silicone oil and peanut oil are summarized below.

	Dielectric Constant	Specific Gravity	Volume Resistivity (ohm-cm)	Color
Silicone Oil	2.5	0.91	10^{15}	Clear
Peanut Oil	3.0	0.91	10^{12}-10^{14}	Amber

Because the oils used were commercial grade, it was felt that their dielectric constants should be checked from time to time. Figure 15 shows a simple parallel plate capacitor constructed for this purpose. The dielectric constant of a fluid sample was determined from a measurement of the current when a known voltage was applied across the system.

The interfacial surface tension existing between silicone oil and peanut oil was found using a ring-type tensiometer. This apparatus finds surface tension by measuring the force required to pull a calibrated wire ring through an interface. For the purposes of this experiment, the densities of the fluids are not held equal. This assures a flat, horizontal interface through which the ring could be pulled.

There are certain disadvantages to the particular simulator system chosen. The surface tension between silicone oil and peanut oil is of the order of 1.3 dyne/cm, whereas for oxygen liquid-vapor at 70 psia the value is 7 to 8 dyne/cm. Thus, hang-up phenomena in the prototype are not exactly duplicated by the laboratory analog. Also, as might be anticipated in any choice of fluids, the viscosity of the oil which acts as the analog to liquid oxygen is about 10 times too great; and the viscosity of the oil analogous to gaseous oxygen is about 1000 times too great. Thus, collection time is far slower in the model than in the prototype. Furthermore, since the analog relies upon the use of equal density fluids, laboratory studies may not be made of the effects of external shocks and vibrations. For these reasons, not all testing may be done with the laboratory analog. Certain investigations must be done in actual zero-g tests of a scale-model oxygen converter. One purpose of laboratory ground testing is to aid in the design of the scale model. The scale model will have, as its working fluids, a liquid and vapor closely approximating oxygen liquid and vapor. This model must be tested in an environment of simulated weightlessness such as may be attained for short times in drop towers or in special aircraft traveling in parabolic trajectories.

Dynamic Behavior of a Spherical Fluid Element

The dynamic behavior of a spherical fluid element in a simple cylindrical dielectrophoretic cell may be studied with the laboratory analog. Experimental verification of the force balance equation is useful on at least two accounts:

1. To provide evidence that the dielectrophoretic force is the important electric force acting, and that its magnitude may accurately be predicted from Equation (7),

2. To verify Equation (13), which may then be used as the basis for predicting collection times.

The experiment was conducted in a cylindrical glass canister having a metal screen for its outer electrode and a metal rod as its center electrode. The canister was filled with silicone oil and a droplet of peanut oil was injected. A 60 cps, a c voltage was applied across this cell and the motion of the droplet was observed and recorded with a motion picture camera. The basic elements of the apparatus are seen in Figure 16. The filmed record of droplet position versus time provides the necessary data.

Reduction of the data was accomplished by projecting the motion picture film one frame at a time on a sheet of paper, and marking the progress of the drop as its image moved

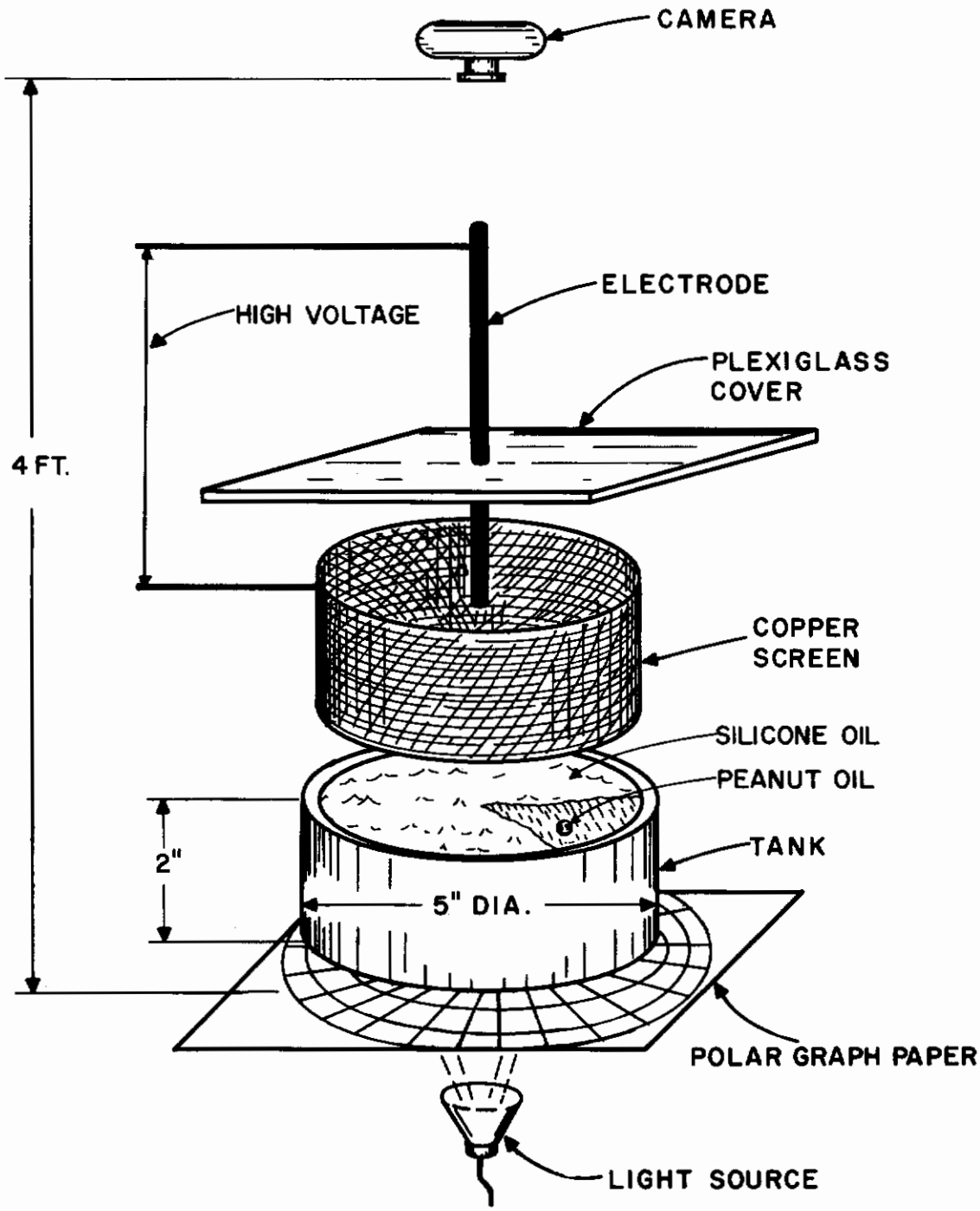

Figure 16. Bubble Dynamics Test Apparatus

across the screen. Scaling was made simple by a polar grid photographed through the transparent fluids. The velocity versus time and acceleration versus time of the droplet were obtained by graphical differentiation of the data. This procedure, though somewhat sensitive to truncation errors, yielded the results summarized in Figure 17. The important result is the verification of the simple force balance of Equation (12) to within experimental error. This makes possible the use of the dielectrophoretic force relations with a high level of confidence. Collection times may be calculated by integration of Equation (13).

Evaluation of Staging Systems

The laboratory analog is especially useful in the study of staging. An analytical approach to predicting the behavior of a real system has been shown to be impractical. The two-fluid analog provides a flexible means for obtaining much qualitative and some quantitative information useful to the design of real converter systems.

Early in the program, stages made with thin wire meshes were tried in the simulator. The effects of surface tension and of intense local electric field gradients around the wires of the mesh prevent any fluid flow through such stages. Even in the case of relatively coarse grids (1/4 inch squares), these stages were found totally unsatisfactory.

Another possible stage design consisted of sheet metal cylinders having evenly spaced holes. This method was also found unworkable for the same reasons which prevented wire meshes from performing properly.

The stage design consisting of rod elements disposed in a cylindrical array was subjected to intensive study in the laboratory analog. The simplified case of a single intermediate stage* was studied in some detail. On this model, the effects of variations of geometry are tested readily. The design information gained by study of this elementary system may be projected to the real converter since a complex multi-staged system may be thought of as a cascade of these single-stage components.

Two criteria serve as the basis for comparing the performance of various staging geometries:

1. The relative time required to separate phases from a thoroughly premixed state, and,

2. The relative quantity of fluid hang-up on staging.

The number of independent variables is large due to the rather complex geometry. The geometry of the elementary single stage system is specified by no fewer than five parameters:

R_o - the outer electrode radius

R_1 - the radius of the intermediate stage

R_2 - the inner electrode radius

e - the stage element diameter

s - the spacing between stage element axes.

Specification of two non-geometric parameters is necessary:

V - the impressed voltage

T - the liquid to vapor surface tension

The dimensionless parameters (see Page 15), found useful for describing performance of staging, are as follows:

*Much of the nomenclature and terminology in this discussion is defined in the section entitled "Hang-up on Stage Elements." The elementary single stage system is shown in Figure 11.

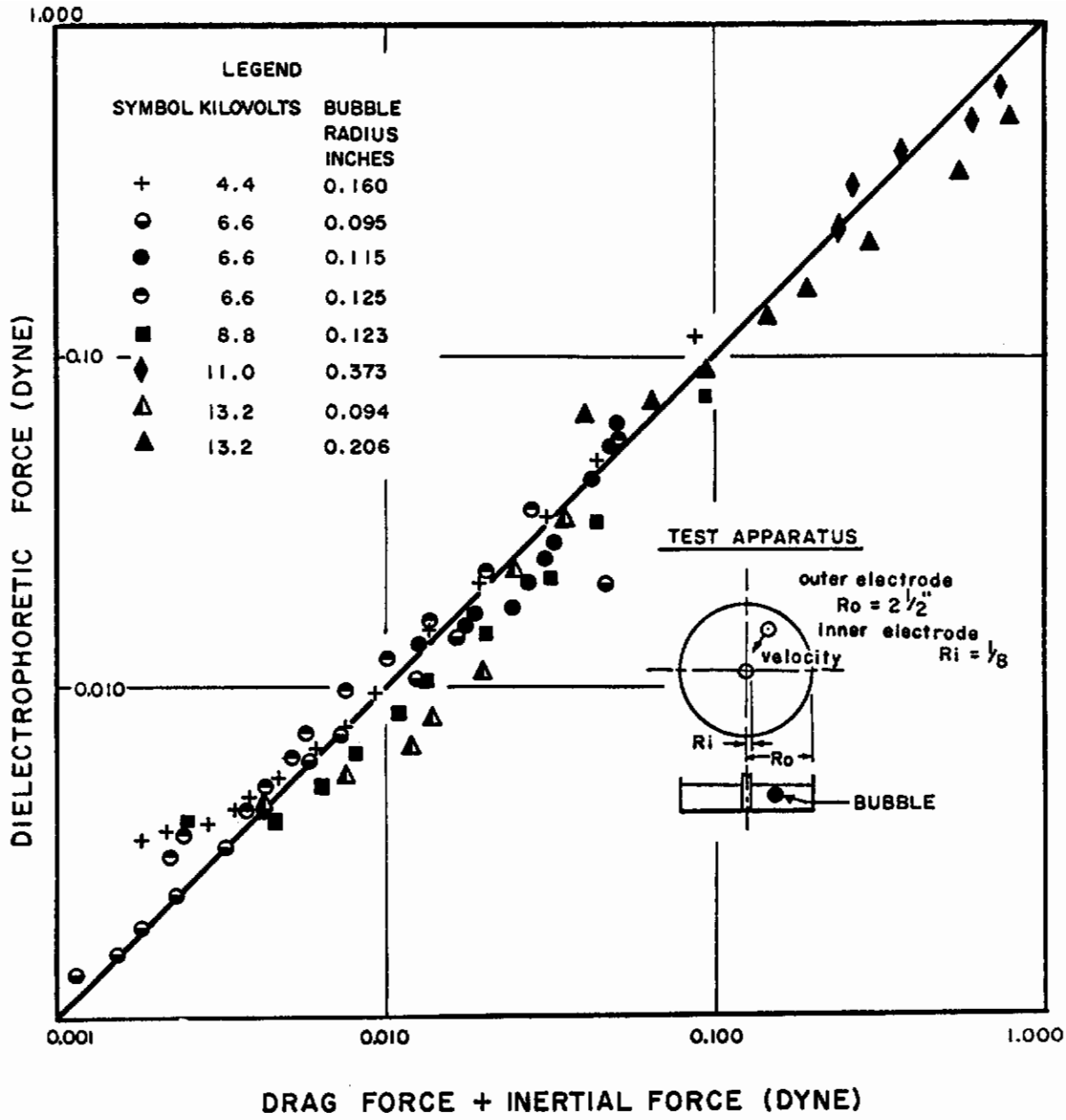

Figure 17. Bubble Dynamics Results

$$\frac{R_o}{R_1}, \frac{R_1}{R_2}, \frac{s}{e}, \frac{R_o}{s}, \text{ and also } \frac{V^2}{eT}$$

The performance of the device is specified in terms of the relative hang-up volume per unit length,

$$\frac{\pi}{4} e^2 \left(D_H^2 - 1 \right), \text{ where } D_H \equiv d_H/e.$$

This is measured from a photograph of the equilibrium fluid orientation. The separation time is measured with an ordinary wall clock. The experiments consist of varying, one at a time, the five dimensionless scaling parameters.

The effect of decreasing R_o/R_1 is, in general, as theory would predict. Equation (7) suggests that the body force on the liquid phase increases with decreasing R_o/R_1, thus, collection time is expected to decrease. This, in fact, is the case The effect of varying R_o/R_1 upon hang-up is almost negligible. However, when $R_o/R_1 = R_1/R_2$, hang-up is indeed diminished. This is the prediction of design Equation (15).

Since the theory dealing with the effects of varying s/e and R_o/s is mathematically intractable, the experimental results will be discussed in some detail. These parameters have a weak influence upon collection time but they exert a powerful effect upon hang-up. In general, the steady-state hang-up volume per electrode is decreased when s/e is increased. Representative data on this effect is tabulated below.

TABLE 1

THE INFLUENCE OF s/e ON
HANG-UP VOLUME

e (in)	$\frac{s}{e}$	Hang-up Volume per Unit Length (in^2)
0.125	4.5	$4.7\ 10^{-2}$
0.063	9.0	$3.2\ 10^{-2}$
0.030	19	$1.4\ 10^{-2}$
0.020	28	$1.4\ 10^{-2}$

It is seen from the table that there is a noticeable decrease in hang-up with increasing s/e. Note, too, that above a certain value of s/e, the hang-up seems to tend to a constant value. In systems where the electrode weight is an appreciable fraction of the total system weight, this fact might be put to good advantage. But in the system under study, stage electrode weights are typically small, i.e., on the order of 10^{-1} lbs., so it is not worthwhile to optimize s/e from a weight standpoint. For the design of a small separator (e.g., a 25-liter oxygen converter), s/e is made as large as is practicable from construction considerations.

The effects upon hang-up of varying R_o/s are minor. In very small analog models there is a small but noticeable influence of R_o/s upon hang-up, but in larger systems the influence seems to vanish. This apparent size effect may be attributed to the fact that the analog fluids involved are rather viscous; thus, in small systems, the flow of hang-up fluid from stage to stage is impeded more than in large systems.

The influence of V^2/eT, i.e., N_1, upon performance is observed in the analog. Both collection time and hang-up are reduced when N_1 is increased. The designer will want to make this quantity as large as possible. There is another reason for making N_1 large, and this lies in

the stability considerations. Since the designer may not exert any control over the surface tension, T, (within the framework of this discussion), and since he will naturally use the highest possible voltage consistent with weight, break-down strength, and stability considerations, he may increase N_1 mainly through decreasing e.

The influence of N_1 upon hang-up is shown in Table 2.

TABLE 2

DEPENDENCE OF HANG-UP ON N_1

$\frac{V^2}{eT} \equiv N_1$	Hang-up volume per unit length $(in)^2$
$1.2\ 10^9$	$5.3\ 10^{-2}$
$1.5\ 10^{10}$	$2.0\ 10^{-3}$

Recapitulating, the influence of the dimensionless converter parameters upon the performance of the device is summarized in Table 3.

TABLE 3

DESIGN PARAMETER INFLUENCE ON COLLECTION TIME AND HANG-UP

To Achieve:	The Designer Should:	
	Maximize	Minimize
Minimum Collection Time	$\frac{V^2}{eT}$, $\frac{s}{e}$	$\frac{R_o}{R_1}$, $\frac{R_1}{R_2}$
Minimum Fluid Hang-Up on Stages	$\frac{V^2}{eT}$ $\frac{s}{e}$	- - -

Electrical Break-Down Between Stages

In the design of the multi-stage dielectrophoretic oxygen converter, the electric field intensity between adjacent stages is approximated by Equation (5). To ensure against electrical break-downs stemming from excessively high field intensity, a factor of safety is used in Equation (18). In this way, the designer allows for the high local fields around stage elements.

Experiments were made to test the statement that the break-down voltage of the system remains essentially the same when only the stage element diameter is varied. This statement is based on the theory that break-down voltage is a function not only of the electric field intensity but also of the planar area over which it acts.*

*See Reference 8 on corona formation.

Tests were conducted on one of the multi-staged laboratory analogs. Two extreme values of stage element diameter were used (60 mil and 5 mil). The dielectric medium in the system was dry air. Testing consisted of increasing the voltage applied across two adjacent stages until a break-down was observed. First, the break-down voltages were recorded for stage elements of 60 mil diameter; then the stage elements were replaced by wires with 5 mil diameter and the tests were repeated. The break-down voltage was found to decrease by less than 3% for a ten-fold decrease in stage element diameter. It is, therefore, demonstrated that the dependence of break-down voltage upon stage element diameter is very weak indeed. The observed break-down voltages were compared with those predicted on the idealized basis of Equation (5). The ratio of actual to ideal break-down voltages is less than 2 which means that the factor of safety of 5 to 10 in Equation (18) should prove more than adequate.

Location of Vapor Withdrawal Outlets

A series of qualitative tests was made using the analog with different peanut-to-silicone oil volume ratios. These tests were designed to show the effect of volume ratio on the positioning of the liquid in both zero-g and non-zero-g conditions. The ultimate use of this information is in the design of the withdrawal outlets in a practical tank. Results of typical tests (shown in Figures 18 and 19) seem to be essentially independent of volume ratio. It will be seen from these that there are usually regions either at the top or bottom of the cylinder in which liquid is prohibited. Thus, if six equally-spaced vents are allowed at both top and bottom, it will always be possible to find one vent, under both zero-g and non-zero-g conditions, which is capable of venting gas rather than liquid.

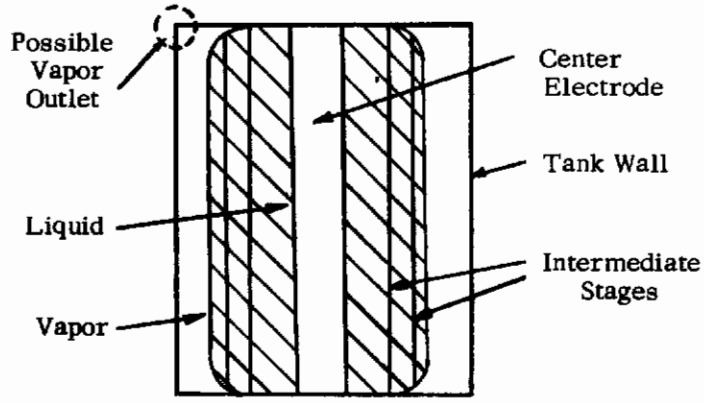

Figure 18. Fluid Orientation Due to Dielectrophoresis at Zero-g

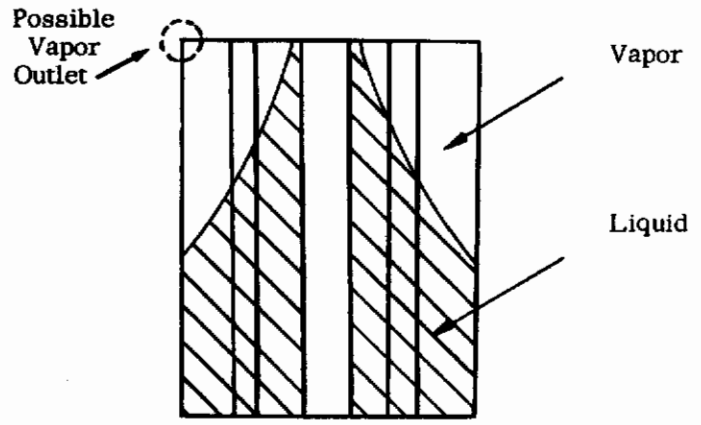

Figure 19. Fluid Orientation Due to Dielectrophoresis in Non-Zero-g

Commercial oxygen contains contaminants which can be ignited under certain conditions. It was necessary to demonstrate that such potential hazards would be unlikely in the converter due to electrical break-down.

The tests were performed within a steel tube imbedded in a sand-filled steel drum. Liquid oxygen was contained in a 1/2 liter Dewar which was placed in the drum. The Dewar was capped with a loose-fitting Teflon plug (see Figure 20) drilled to accommodate a pair of electrodes. Visual observation of arcing within the system was made through a vent hole in the Dewar plug. A variable resistance was wired in series with the test section. An increase in series resistance will decrease the spark intensity. (See Reference 9)

Attempts were made to ignite the natural contaminants of commercial grade LOX by repeated arcing through the LOX and oxygen vapor. Other tests were run in LOX deliberately saturated with acetylene or with benzene. In these tests, the series resistance was varied from 0 to 440 megohms, the voltage from 14 to 22 kv, and the electrode separation from 1/8" to 1/2". The electrodes used had hemispherical surfaces with radius curvature ranging from 0.005" to 0.030". In all of these tests, no evidence of explosion or ignition was observed though many arcs were passed.

It may be concluded that under the conditions encountered in these tests, it is possible to have electrical break-downs in commercial liquid oxygen without igniting the contaminants. Conditions in the oxygen converter and in the ignition test apparatus are the same in many respects. The LOX converter should be comparatively safe.

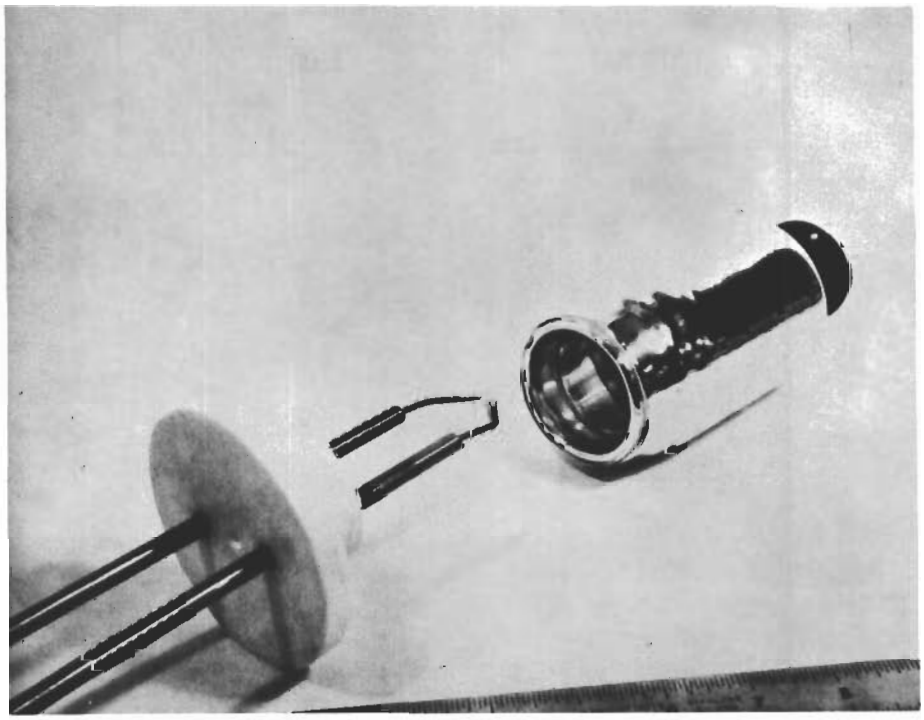

Figure 20. Safety Test Apparatus

As has been shown, the variation of the current drawn by the apparatus from the constant high voltage supply depends on the amount of liquid present.

Limited experiments have been made, using a laboratory analog having three intermediate stages and L/D ratio of approximately two. The results of these tests are shown in Table 4.

It is seen that the ratio of capacitance over the whole range, empty to full, is 0.84. This compares favorably with the ratio of dielectric constants of the analog fluids used (i.e., 2.5/3.0 = 0.833). It was found that the discrimination was not so good as anticipated in the whole range. This, apparently, is due mostly to hang-up in the analog. This trouble will be corrected in the final design model which, because it has thinner electrode wires, is less likely to exhibit severe hang-up problems (see Table 2). Calculations in Appendix F suggest that gross misorientation of fluid in a 25-liter converter may be tolerated without severe level indicator errors.

TABLE 4

LEVEL GAGE TESTS

% Full	$\frac{\text{Capacitance}}{\text{Capacitance Full}}$
0 empty	0.84
50%	0.95
100% full	1.00

Due to certain limitations of the laboratory analog, a scale model of an oxygen converter is supplied for testing in a flying laboratory. Such an aircraft, by flying through a parabolic arc, simulates a weightless environment for a period on the order of 25 seconds. The electrode design of this flight-test model is based upon experiments performed on the laboratory simulator. The purpose of the apparatus is to:

1. Verify the positions of vapor outlets,
2. Evaluate the level indicator,
3. Investigate staging performance with regard to collection time and equilibrium orientation and, finally,
4. Investigate the behavior of the system when under the influence of short-term accelerations.

The apparatus is designed to be compatible with LOX and other cryogenics. It is intended to be operated initially with liquids other than LOX in a glass enclosure to provide visual access, and later with LOX in an all-steel enclosure having no viewing ports.

The use of liquid oxygen in the initial flight-test model is neither advisable nor necessary. Fortunately, there are many fluids having properties very closely approximating those of LOX. Table 5 compares three such fluids. It may be noted that liquid nitrogen at 20 psia closely simulates liquid oxygen at 70 psia in all important respects. Its surface and dielectric properties are practically identical with those of the prototype fluid. This means that the hang-up and stability phenomena in an operational LOX prototype are simulated exactly by a flight-test model using nitrogen liquid-vapor at 20 psia.

TABLE 5

PROPERTIES OF FLUIDS USED TO SIMULATE OXYGEN IN FLIGHT-TEST MODEL

	Pressure (psia)	Boiling Temperature ($^{\circ}$C)	Surface Tension (dyne/cm)	Dielectric Constant of Liquid	Liquid Density ($gram/cm^3$)
Oxygen	15	-183	18.2	1.48	1.18
Oxygen under avg. conditions of convertor prototype	70	-163	8.0	1.45	1.00
Nitrogen	20	-193	8.27	1.43	0.795
Argon	20	-183	10.5	1.50	1.385
Carbon Tetrachloride	15	20	26.95	2.238	1.595

Design of the Flight-Test Model

The model oxygen converter is shown in Figure 21. It consists of a 1.4 liter glass cylinder having a transparent, electrically-conducting coating on its inner surface. Staging is made of thin wire elements supported by a spool having a steel core and plastic webs. The glass cylinder is sealed tightly by plastic end-caps which are held in position by a central bolt. This model is suspended in a glass Dewar by six thin-walled stainless steel tubes.

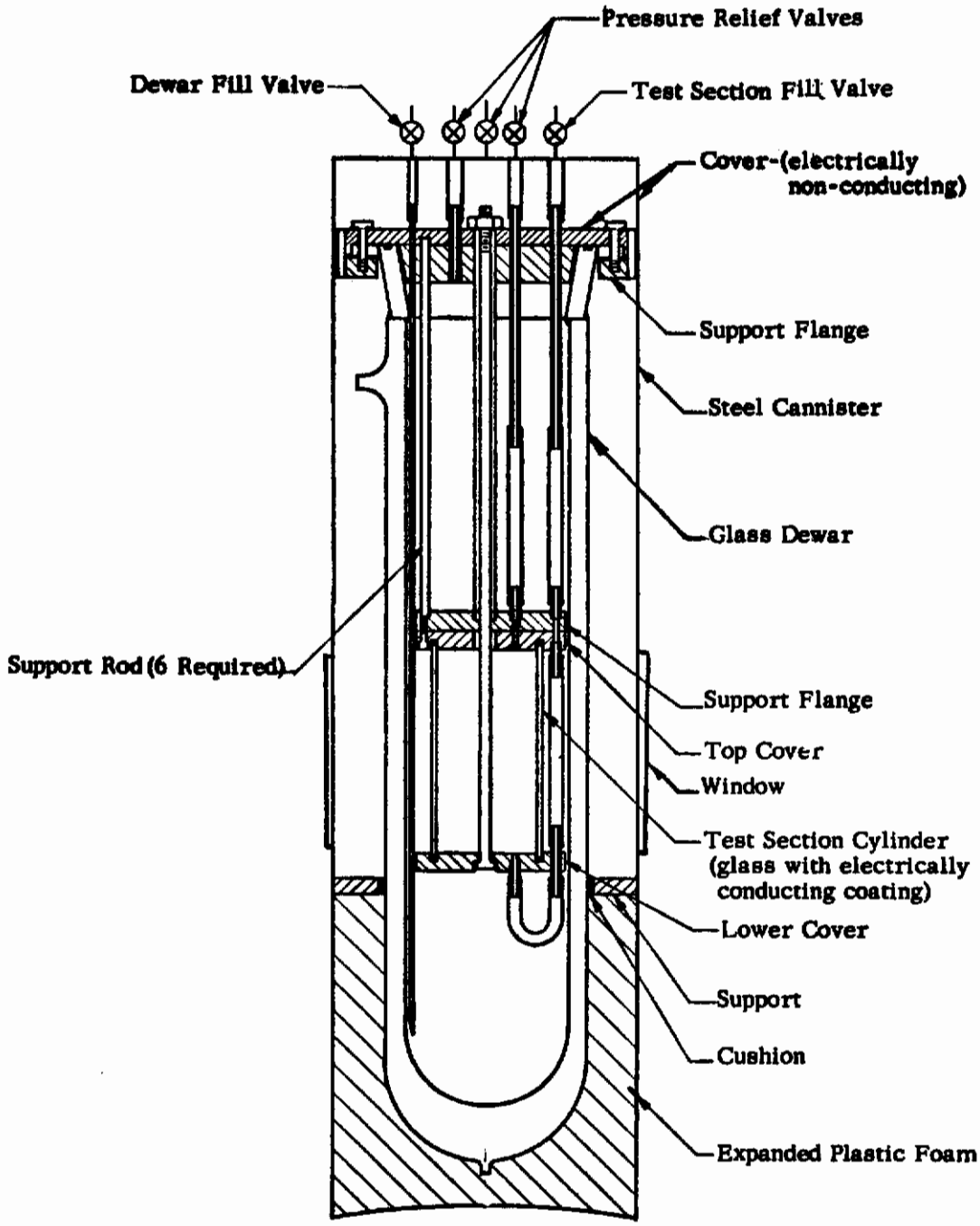

Figure 21. Flight-Test Apparatus

The test section may be filled or drained independently of the Dewar; thus, the system may be operated at any preset liquid volume ratio. The boil-off rate in the test section is kept to a minimum by immersion of the model in a cryogenic bath. Pressure within the system is maintained slightly higher than atmospheric--20 psia when liquid nitrogen is the working fluid. The active volume of the model is observed through an unsilvered window on the Dewar. For safety, the glass Dewar is contained in a steel canister having shatterproof windows. This protects personnel against flying glass and cryogenic fluid in the event of Dewar breakage. The Dewar is shock mounted within the canister by a form-fitting cushion of expanded plastic foam. A fixture of aluminum angle beams serves to support the canister, the instrumentation, and a pan head for a motion picture camera for recording the system's performance. The instrumentation consists of a control console for the high voltage supply, a milliammeter for the level indicator, and an elapsed timer. In addition, backlighting is provided for motion picture filming.

The apparatus is supplied with two stage ensembles: 1) Spool A, designed according to a radius ratio of 1.6, and, 2) Spool B, designed according to minimum force considerations. Both stage spools incorporate the best available laboratory information applied toward minimizing both hang-up and collection time.

The vital dimensions of the test section are summarized in Figure 22.

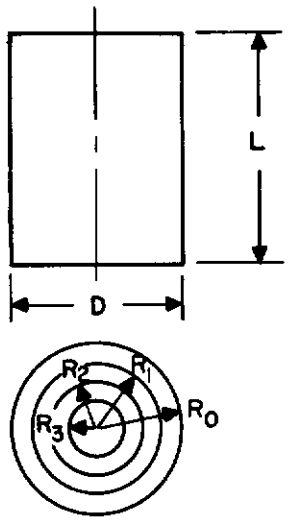

L = 18
D = $2R_0$ = 10.6

	Spool A	Spool B
R_1	3.3	4.4
R_2	2.1	3.4
R_3	1.3	2.3
R_4	--	1.3

Figure 22. Summary of the Vital Dimensions of the Flight-Test Model (All Lengths in Centimeters)

Operation of the Apparatus and Experimental Procedures

The mechanics of operating the apparatus are not involved. The test section, or active volume, may be filled independently of the Dewar. The boil-off rate in the active volume is held to a negligible level by immersing the test section in a bath of the working fluid. Thus, the experimenter may adjust the liquid-to-tank-volume ratio and may be confident that the ratio will hold constant over the course of a test run. With the liquid level controlled, the level indicator may readily be evaluated.

Staging may be interchanged or altered without difficulty. Two stage ensembles are provided so that the experimenter may investigate the relative merits of a design having the same minimum force level at each stage and one having a continuous force profile at each stage. The former is designed with radius ratios less than those indicated by stability considerations. The latter is designed for stability. Both have been designed to provide a minimum "equivalent g field" at the tank wall of $\sim 10^{-3} g_o$ at 10 KV. The experimenter may vary the magnitude of dielectrophoretic forces by varying the voltage over the working range of the included power supply (0 to 20 KV), giving minimum equivalent g-fields of 0 to $.004 g_o$. The average equivalent g-fields are somewhat higher. (see Figures 6 and 8).

A program to test the dielectrophoretic oxygen converter should include the following:

1. Degree of liquid orientation,
2. Evaluation of level indicator,
3. A study of optimum vapor outlet locations, and,
4. Comparison of the two stage ensembles with regard to collection time, hang-up, and interfacial stability.

The experimental procedures are in three parts--Before, During, and After the zero-g maneuver.

Before the Maneuver.

1. Open both fill-valves.
2. Flush Dewar and test section with dry nitrogen gas. This prevents frost formation.
3. Fill Dewar.
4. Allow boiling to subside.
5. Close Dewar fill-valve.
6. Check for correct operation of Dewar pressure-relief valve.
7. Fill test section to desired level.
8. Allow boiling to subside.
9. Close test-section fill-valve.
10. Check for correct operation of test-section pressure-relief valve.
11. Set voltage control on power supply console.
12. Turn on "LINE" switch on power supply console.
13. Press "H. V. ON" button on power supply console.
14. Check level indicator meter--when voltage is on it should be registering.
15. Press "LIGHTS" button.
16. Press "TIMER" button.
17. Aim camera and check settings.

During the Maneuver:

1. Trigger camera--use cable release.

After the Maneuver:

1. Turn off "LINE" switch on power supply console.
2. Open both fill-valves.

3. Turn off "LIGHTS."

4. Turn off "TIMER."

Ground Tests and Calibrations

Certain tests and calibrations have been performed on the zero-g flight-test apparatus. Both static and dynamic endurance tests have been performed. The static tests consisted of filling the Dewar with liquid nitrogen and then subjecting the system to a 20% overpressure. The dynamic endurance tests consisted of simulating a $2.5g_o$ acceleration of the system by filling it with a very dense fluid. The system survived these tests and it is felt that it will survive the g-loads and vibrations of flight-test maneuvers. The system has been checked for leaks.

The operation of the various subcomponents (light, timer, etc.) has been checked out. The apparatus is satisfactory in this respect.

The level indicator has been calibrated at its two extremes--full and empty. The full reading is 0.41 ma. and the empty reading is 0.28 ma. A 1.0 ma. scale is used so that resolution of a volume change of 90 cm^3 (i.e., 7%) should be possible.

The operating procedure of the previous section has been carried out without difficulty. There is no problem encountered in filling the apparatus with a cryogenic liquid. Filling with liquid nitrogen resulted in no damage due to thermal shock.

On the basis of control films taken with a Bolex Reflex 16 mm. camera, having a 75 mm. telephoto lens, the following advice is offered to insure good motion pictures using the backlighting provided:

1. Use Kodak Tri-X Film, ASA #160 Tungsten

2. Use f 11 for film speed of 16 f.p.s.
   f 6.8 for film speed of 24 f.p.s.
   f 4 for film speed of 64 f.p.s.

A major portion of the program consists of the preliminary design of a 25-liter oxygen converter. This design is considered in some detail in the section which follows. The purpose of the preliminary design is to establish operating characteristics such as weight and size, and to indicate possible problem areas. However, it will be evident from the discussions which follow that the design cannot be divorced from the vehicle environment, so it is necessary to make a number of quite arbitrary assumptions in order to outline any design.

A preliminary layout drawing of a typical 25-liter converter is shown in Figure 23. The converter consists of the following components:

1. The electrode assembly including the inner spool, outer shell, and intermediate stages, as well as the end discs or webs which support the stage electrodes and spool.

2. The inner tank, which contains the LOX and the electrode ensemble.

3. The outer tank.

4. The evacuated thermal insulation, which lies between the inner and outer tank.

5. The high voltage supply, consisting of an inverter and a transformer.

6. The vapor delivery system which consists of six carefully located ports which conduct oxygen vapor from the tank, automatic solenoid valves to close off those ports at which there is the possibility of liquid ingestion, the automatic pressurizer, to maintain the tank pressure between 50 and 90 psia for all values of vapor withdrawal between the specified limits of 0.5 to 5.0 liters per hour, and finally the automatic vapor flow control.

Each of these components is discussed below. Indicated schematically in the drawing is a manifold to collect vapor from the six vent lines; the design of this manifold will depend on the cabin layout.

In designing the tank and its auxiliaries, the length-to-diameter ratio was varied, while holding the volume constant, in an effort to relate the weight of the complete unit and the effective electrostatic force on the fluid to the tank dimensions. These relationships are shown in Figure 24. The weight is seen to pass through a minimum at L/D, of about 4. This is because tankage weight increases with L/D, while electrode weight decreases. Other components remain relatively constant as will be evident in the descriptions of them which follow. It is evident that although minimum weight is achieved at an L/D of about 4, little weight penalty is incurred in going to higher L/D whereas the effective g forces due to dielectrophoresis increase with L/D continuously. Furthermore, the number of electrode stages decreases with increased L/D thereby simplifying the construction. For these reasons, and in the absence of specified restraints on tank length, a high value of L/D is arbitrarily chosen (8.0 for purposes of this preliminary design).

The design parameters are given in Table 6, and the component weights and heat leaks are summarized in Table 7.

Stage Design

The Design of Electrode Stages for a Full-Sized Prototype

The design of electrode stages for the cylindrical dielectrophoretic oxygen converter is formalized below. The methods for specifying the ground rules are given first, then the calculation method. A worked example for a 25-liter converter is included.

First, the designer specifies total tank volume, i.e., payload volume plus ullage. The payload volume is presumed specified and the ullage volume is computed. To maximize reliability,

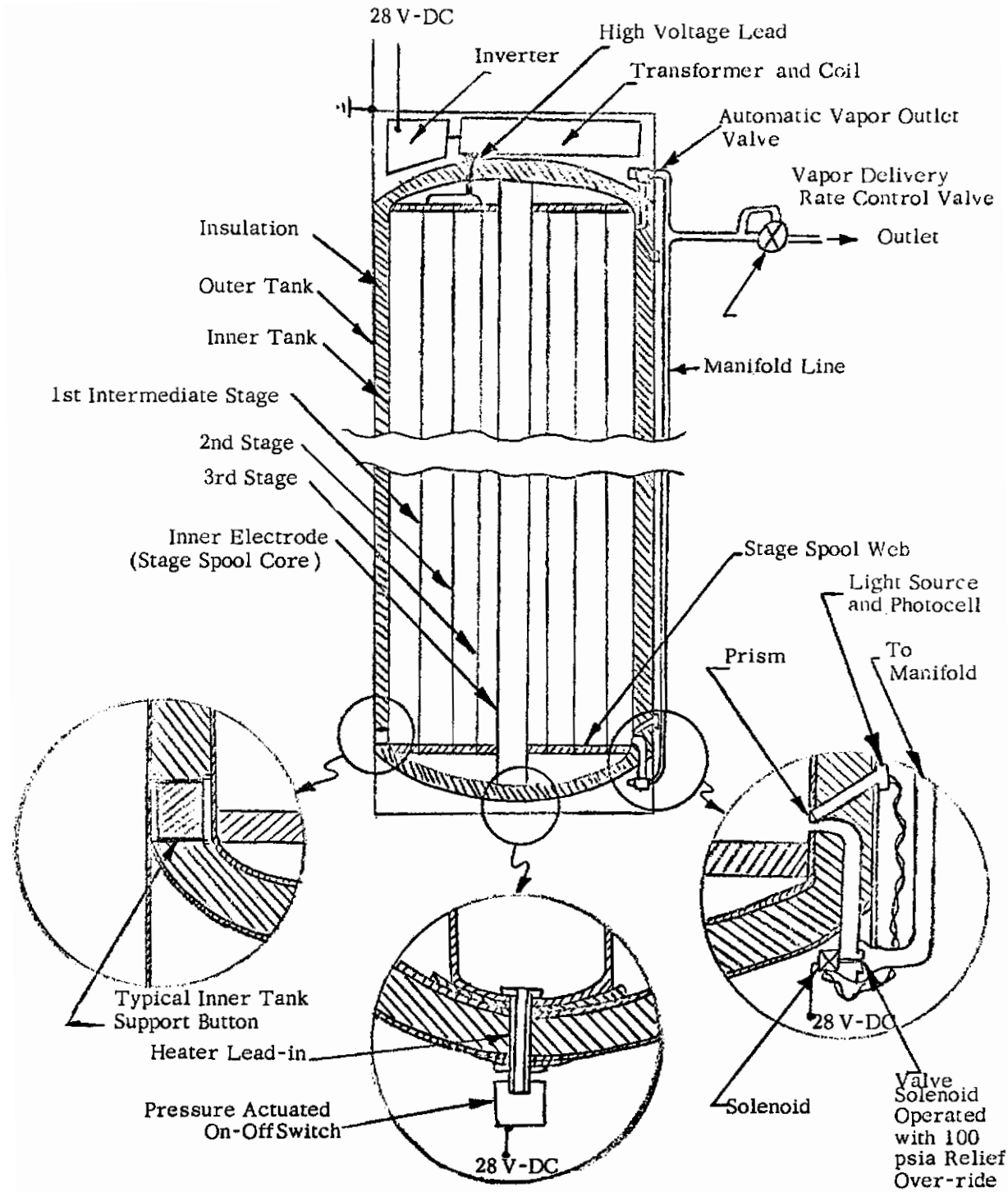

Figure 23: Preliminary Layout of a 25 Liter Converter

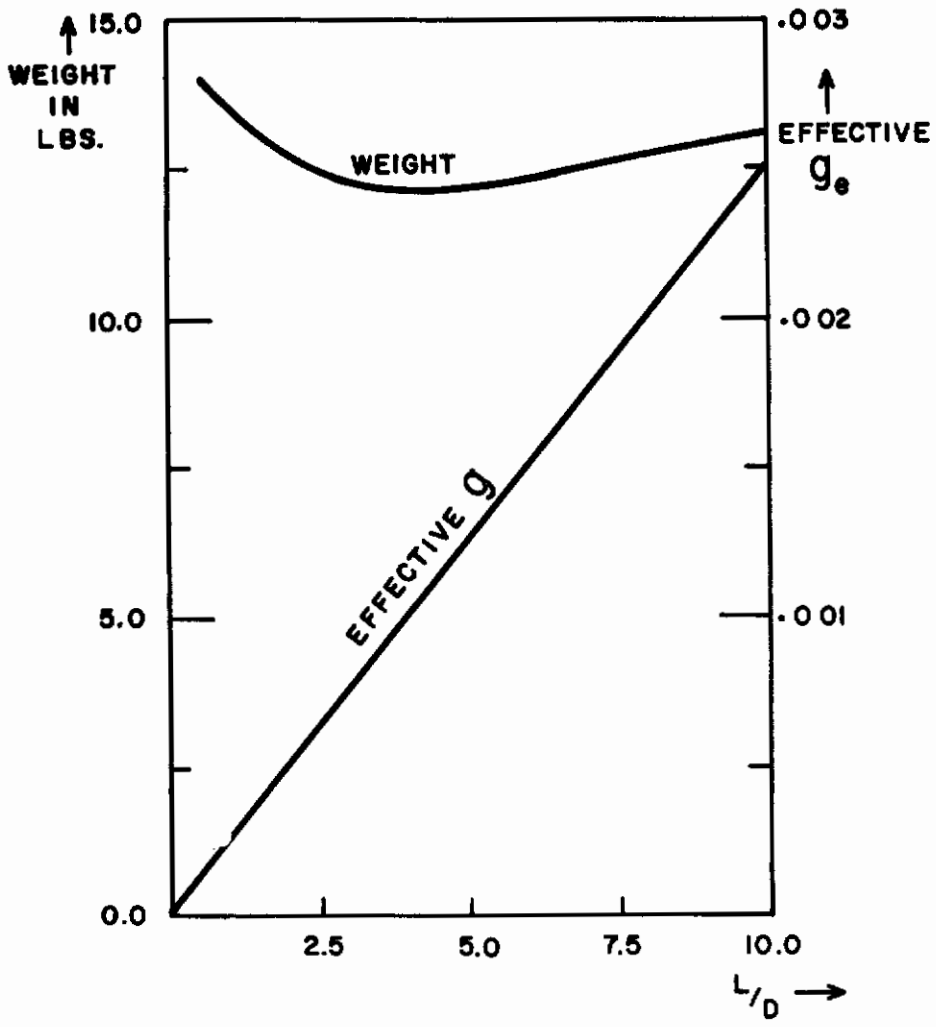

Figure 24: Total System Weight vs. L/D
"Effective Dielectrophoretic Gravity Field" vs. L/D

TABLE 6

DESIGN PARAMETERS OF THE
25-LITER OXYGEN CONVERTER

Operable range "g's"	
Dielectrophoretic Positioning	0 to $10^{-3} g_o$
Inertial Positioning	$10^{-3} g_o$ to $25 g_o$
Effective Minimum Force Level on LOX "g's"	$10^{-3} g_o$
Time to Equilibrium	~ 4 seconds or less
Tank Length, Overall	55 inches
Tank Diameter, Overall	8 inches
Gross Tank Volume	30 liters
Maximum Vapor Rate	5.0 liters/minute
Minimum Vapor Rate	0.5 liters/minute

TABLE 7

COMPONENT WEIGHTS AND HEAT LEAKS FOR
25-LITER OXYGEN CONVERTER (L/D = 8)

Component Description	Total Number Required	Contribution to Total Weight (lbs)	Contribution to Total Heat Leakage (BTU/hr)
Inner Tank	1	2.0	---
Outer Tank	1	2.9	---
NRC-2 Insulation	---	0.6	1.3
Internal Supports	25	0.6	3.8
Support Skirts	2	0.1	---
Power Supply and Inverter	1	4.0	---
High Voltage Lead	1	---	0.5
Stage Electrodes	~200	0.5	---
Stage Spool Core	1	0.2	---
Stage Spool Webs	2	1.0	---
Vapor Delivery Rate Control Valve	1	0.3	---
Vapor Outlet Ports	6	---	0.9
Vapor Outlet Valves	6	1.1	---
Manifolding	1	0.2	---
LOX Sensors and Sensor Tubes	6	0.4	0.2
Heater Sensor and Control	1	0.1	---
Heater Lead-In	1	---	0.5

the number of valves should be minimized with regard to any penalty paid for increased ullage. For small tanks, the over-all percent weight penalty attributed to a percent increase in ullage is modest; in large systems, where the tank comprises most of the total weight, the penalty of increasing the ullage is considerable.

The next step is to choose the length-to-diameter ratio of the converter's active volume. First the designer sets a range of possible L/D from allowable space and fabrication considerations. This range may be made wide or narrow depending on the vehicle application; however, the lower limit of L/D is somewhat dependent upon power supply factors and force field requirements. The lower limit on L/D may be determined after the designer specifies two things:

1. The voltage and frequency of the supply consistent with the design procedures and the stability requirements of Equations (21) and (23),

2. The minimum acceptable "equivalent dielectrophoretic gravity field," $f_{min}/\rho_L g_o$. Figure 24 relates $f_{min}/\rho_L g_o$ to L/D for a system containing oxygen and having a 20 kv power supply. It is noted that L/D must exceed 4 in order that the minimum equivalent gravity field exceed $10^{-3} g_o$.

The upper limit on L/D may be set by the available space within the vehicle or by the fact that L/D may not be made arbitrarily large without eventual weight sacrifices and increased valve requirements.*

Having formulated values for the total tank volume, power supply voltage and frequency, and L/D ratio, the designer must consider one remaining ground rule, the stage radius ratio, defined by Equation (22). He is now in a position to make the stage design calculations.

Certain constraints on electrode design should be determined from the start. The tank wall must be at ground potential to insure safety to personnel. Since the central electrode comprises the core of the spool which supports all other stage elements, that electrode should be anchored to the inner tank. This imposes the constraint that the central electrode also be of ground potential and, therefore, that there be an odd number of intermediate stages. The central electrode must support a buckling load and so may not be too small in diameter, yet it may not be so large as to exceed a reasonable ullage, say 5% of the total tank volume.

The stage radius design procedure is quite simple. Since the total volume and length to diameter ratio are specified, the tank radius, R_o, is known. The radius ratio R_n/R_{n+1} is specified so the first stage radius may be found: $R_1 = R_o/(R_n/R_{n+1})$; this process is continued until an inner stage is specified which occupies 5% or less of the tank volume.

The designer now checks the criterion of maximum field. He calculates E_{max} for each stage on the basis of Equation (18) and compares the value with E^*/K_s, where it will be recalled that E^* is the electrical breakdown strength of the fluid and K_s is a safety factor of the order of 5 to 10. If the maximum field criterion is satisfied, the design continues, if not, the voltage and/or tank diameter must be changed.

The force profile and "equivalent gravity field" is determined next. The minimum equivalent gravity field is compared with the specifications of the ground rules. If it equals or exceeds specifications, the design is completed, if not, the design is reiterated with appropriate changes in voltage and/or tank diameter.

*For the case at hand it may be shown that the total system weight varies by only ± 2-1/2% over the range $2 < L/D < 8$. This is for a 6 valve system having 20% ullage.

A worked example is offered here. The working fluids are saturated oxygen liquid and vapor at 70 ± 20 psia. The dielectric constants are $\kappa_L = 1.45$ and $\kappa_v = 1.00$. The mass density of the liquid is:

$$\rho_L = 1.0 \text{ gram/cm}^3$$

The payload volume is 25 liters, the total volume is 30 liters, the ullage is 20%. The power supply voltage and angular frequency are:

$$V = 20 \text{ kv}$$

$$\omega = 2\pi \cdot 60 = 120\pi \text{ radian/sec}$$

The length to diameter ratio is:

$$\frac{L}{D} = 8$$

Therefore, the tank radius is

$$R_o = 8.4 \text{ cm}$$

The radius ratio according to Equation (22) is

$$R_n/R_{n+1} = 1.6$$

Now, by Equation (14), K_1 for each stage is given by:

$$K_1 = \left(\frac{K_2 V^2}{f_{min}}\right)^{1/2} = R_n^{3/2} \ln \frac{R_n}{R_{n+1}} = 0.47 R_n^{3/2} \tag{25}$$

and f_{min} may be found according to

$$f_{min} = \frac{K_2 V^2}{K_1^2} = \frac{1740}{K_1^2} \text{ dyne-cm}^{-3} \tag{26}$$

Also, E_{max} may be found according to

$$E = \frac{V}{R_{n+1} \ln \frac{R_n}{R_{n+1}}} = \frac{4.25 \times 10^4}{R_{n+1}} \text{ volt-cm}^{-1} \tag{27}$$

The design is summarized in Table 8. E* exceeds E_{max} at R_4 by a safety factor of 6. The central electrode, R_4, occupies 2.4% ullage.

TABLE 8

SUMMARY OF STAGE DESIGN
FOR 25-LITER CONVERTER

	R_n	$R_n^{3/2}$	K_1	K_1^2	f_{min}	$\frac{f_{min}}{\rho_L g_o}$	E_{max}		Stage Potential
R_o	8.4	24.5	11.5	133.00	1.04	0.0010	5050	12800	Ground
R_1	5.2	11.9	5.6	31.5	4.36	0.0044	8200	20800	20 kv
R_2	3.3	6.0	2.8	7.9	17.5	0.0178	12900	32800	Ground
R_3	2.1	3.0	1.4	2.0	69.0	0.0707	20000	50800	20 kv
R_4	1.3	1.5	0.7	0.49	282.0	0.2870	32600	83000	Ground
	cm	$cm^{3/2}$	$cm^{2/2}$	cm^3	$\frac{dyne}{cm^3}$	g_o's	$\frac{volt}{cm}$	$\frac{volt}{inch}$	

The Design of the Stage Support Spool

Stage electrode elements are supported by a spool having the central electrode as its core, and having electrically non-conducting webs. (See Figure 25.)

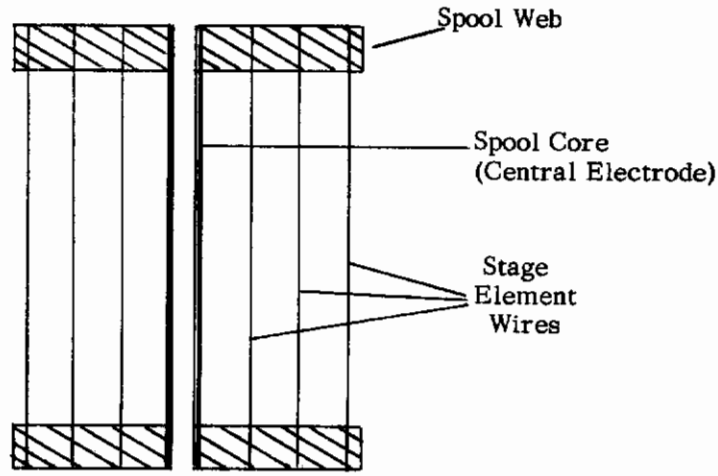

Figure 25. Stage Ensemble

The total weight of the stage ensemble is the sum of the weights of three components: the elements, the spool core, and the spool webs.

1. The stage elements are of thin wire and are closely spaced to minimize hang-up volume (according to results of experiments performed on analog systems). For mechanical reliability and ease of manufacture, a stage element diameter of 20 mils is chosen and the ratio of element spacing to diameter, s/e, is taken to be 20. This leads to a separation, s, of 0.4 inch. Thus, the total number of elements, N_e, is specified by the stage radius design according to,

$$N_e = \frac{2\pi}{s} (R_o + R_1 + \ldots + R_n) \quad (28)$$

The total element weight is the product of their number, N_e, their length, L, the cross-sectional area of each one, a, and their density, ρ_e,

$$W_e = N_e \rho_e L a \quad (29)$$

Strictly speaking, N_e is a decreasing function of L/D (e.g. for low L/D a system has more stages than for high L/D). Consequently, element weight is essentially independent of L/D. For a 25-liter converter the total element weight is not large compared with total system weight; for the design of Table 7, the total electrode element weight is of the order of 0.5 lb.

2. The spool core must support a load in compression due to the sum of the tensions of the stage elements. The tension in each wire must be sufficient to prevent excessive deflections due to lateral accelerations. For the 25-liter prototype, a maximum deflection, δ, of 0.1 inch is tolerable under the 10 g_o maximum lateral acceleration load. The tension per wire, H, is the total load on the spool core divided by the number of wires.

$$H = \frac{P_{crit}}{N_e} \quad (30)$$

The deflection relationship for a wire in tension subjected to a 10 g lateral acceleration is

$$H = \frac{10 \rho_e a L^2}{8 \delta} \quad (31)$$

Eliminating H from Equations (30) and (31) the result is

$$\frac{P_{crit}}{N_e} = \frac{10 \rho_e a}{8 \delta} L^2 \quad (32)$$

Thus for a specified wire size, a, and density, ρ_e, and for an assumed maximum deflection δ, P_{crit}/N_e is a function of L^2.

Since N_e is a function of L/D, then the compressive load on the spool core, P_{crit}, will vary with L/D also. Assuming the central electrode to occupy about 5% of the total tank volume, its radius, R_e, is uniquely specified by L/D of the tank. The mode of failure of the spool core is given by the classical buckling relationship for cylinders

$$P_{crit} = \frac{\pi E t_c^2}{\sqrt{(1 - \nu^2)}} \quad (33)$$

The designer is now in a position to calculate the thickness, t_c, of the spool core as a function of the tank L/D. This is accomplished by finding P_{crit} from Equation (32) putting the value thus obtained into Equation (33), and solving for t_c. The weight of the spool core is simply:

$$W_c = 2\pi \rho_c R_c t_c L \quad (34)$$

and since $\pi R_c^2 L$ = 5% of the total tank volume, then:

$$R_c^2 = \frac{(0.05)(\text{vol.})}{\pi L} \quad (35)$$

For the 25 liter converter, the total tank volume is 30 liters, thus:

$$W_c = 55\, K_3^{1/2}\, t_c \tag{36}$$

where:

K_s is a stress factor of safety = 4,

t_c is in inches.

For the range of $1 < \frac{L}{D} < 10$, the spool core weight varies from 0.14 lbs. to 0.25 lbs.

3. The spool webs are flat circular plates perforated with as many holes as there are stage elements. The stress in such a plate may be computed using Grashof's formula (Reference 1) with an appropriate correction factor due to Bynum (Reference 15). That is, the maximum principal stress, σ_{max}, is:

$$\sigma_{max} = \frac{3\, P_{crit}}{4\, \pi\, t_w^2}\, K_\sigma \tag{37}$$

where:

K_σ is the stress correction factor

t_w is the plate thickness

Equation (37) may be solved for t_w. Note that for the case at hand $K_\sigma \approx 4$.

$$t_w = \sqrt{\frac{3\, P_{crit.}}{\pi\, \sigma_{max}}} \tag{38}$$

The weight of the two spool webs is:

$$2\, W_w = 2\, \pi\, R_o^2\, t_w\, \rho \tag{39}$$

or

$$2\, W_w = 2\, \pi\, R_o^2\, \rho_w \sqrt{\frac{3\, P_{crit}}{\pi\, \sigma_{max}}} \tag{40}$$

Now, R_o is a function of L/D and the tank volume,

$$R_o = \sqrt[3]{\frac{Vol.}{L/D}} \tag{41}$$

The total spool web weight is then a function of L/D.

$$2\, W_w = 2\, \pi\, \rho_w \left(\frac{Vol.}{L/D}\right)^{2/3} \left(\frac{3\, P\, crit}{\pi\, \sigma_{max}}\right)^{1/2} \tag{42}$$

For the 25 liter oxygen converter, the web material chosen was alumina ceramic for its excellent dielectric properties and high fluxural strength. The spool web weight, $2\, W_w$, ranges from 4 lbs. at L/D = 1 to 0.9 lbs. at L/D = 10.

A table summarizing the weight of the electrode ensemble versus L/D is given.

TABLE 9

WEIGHT OF ELECTRODE ENSEMBLE
VERSUS L/D OF TANK

L/D	$2 W_w$	W_c	W_e	Total
1	3.9	0.14	0.5	4.5
3	1.9	0.18	0.5	2.6
5	1.9	0.20	0.5	2.1
7	1.05	0.22	0.5	1.8
10	0.85	0.24	0.5	1.6

Note: All values in lbs.

Vapor Delivery System

The vapor delivery system consists of six carefully located outlet ports, each having its own liquid sensor and solenoid actuated valve, a manifold or collector which takes gas from the outlet ports, a flow-delivery control system at the manifold outlet, and a tank-pressure control system.

Outlet Ports and LOX Sensors

The six outlet ports are located three at each end of the tank, (see Figure 26). They are positioned so that at least one port is always free of liquid. This requirement is met for the zero-g and very low-g condition by virtue of the dielectrophoretic forces, but during maneuvers there will be gravity forces tending to displace the fluid. The use of six ports, as shown, with the ullage given, allows for at least one port free of liquid even when there are 25 liters of LOX in the vessel.

The ingestion of liquid oxygen into the ports is prevented by a system of liquid sensors and solenoid-operated valves. The subminiature valves have a weight of the order of 3 oz. each and require a signal of about 0.3A from a 28V supply to open. These solenoid valves are to be designed with a spring of such stiffness that they open mechanically for pressures over 100 psi (i.e., for safety pressure relief). The method of sensing the LOX, as shown in Figure 27, is novel in this application. Other suggested methods (see Reference 11) include resistance, inductance, and capacitance gauges. However, this method has higher sensitivity and should be more reliable than the others. The principle used here is internal reflection and refraction of light leaving a high refractive index material (glass here), and either being reflected for gas, or refracted for a LOX interface. Thus the photo-sensor detects presence of gas or liquid phase.

The photo-resistive element may now be used in a manner shown in Figure 28 to provide a signal to the solenoid valve. The total weight of the system including the solenoid valve will be approximately 3 ounces, and careful design of the valve could reduce this still further.

Oxygen vapor is transported from the six outlet ports through a manifold or collecting line to a master delivery-flow control. The pilot may set any desired delivery rate by a manual adjustment of the discharge valve area. This is because the temperature at the valve is sensibly constant, and as the pressure drop across the valve is sufficient to cause a sonic flow condition in the valve throat, there will be a vapor delivery based mainly on the area, with small corrections for the manifold pressure variation. The discharge valve area is therefore to be automatically controlled by a diaphragm-servo actuated by manifold pressure feedback. The valve area makes excursions about the manually-set reference level so that the desired constant flow is maintained regardless of fluctuations in tank pressure.

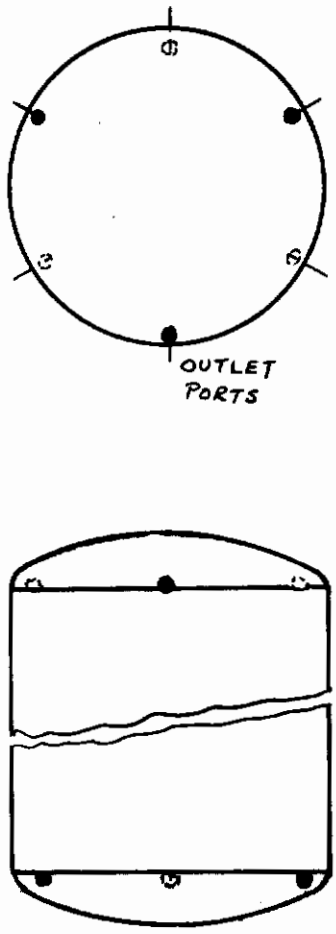

Figure 26: Location of Six Outlet Ports for 30-Liter Vessel Containing 25 Liters of LOX

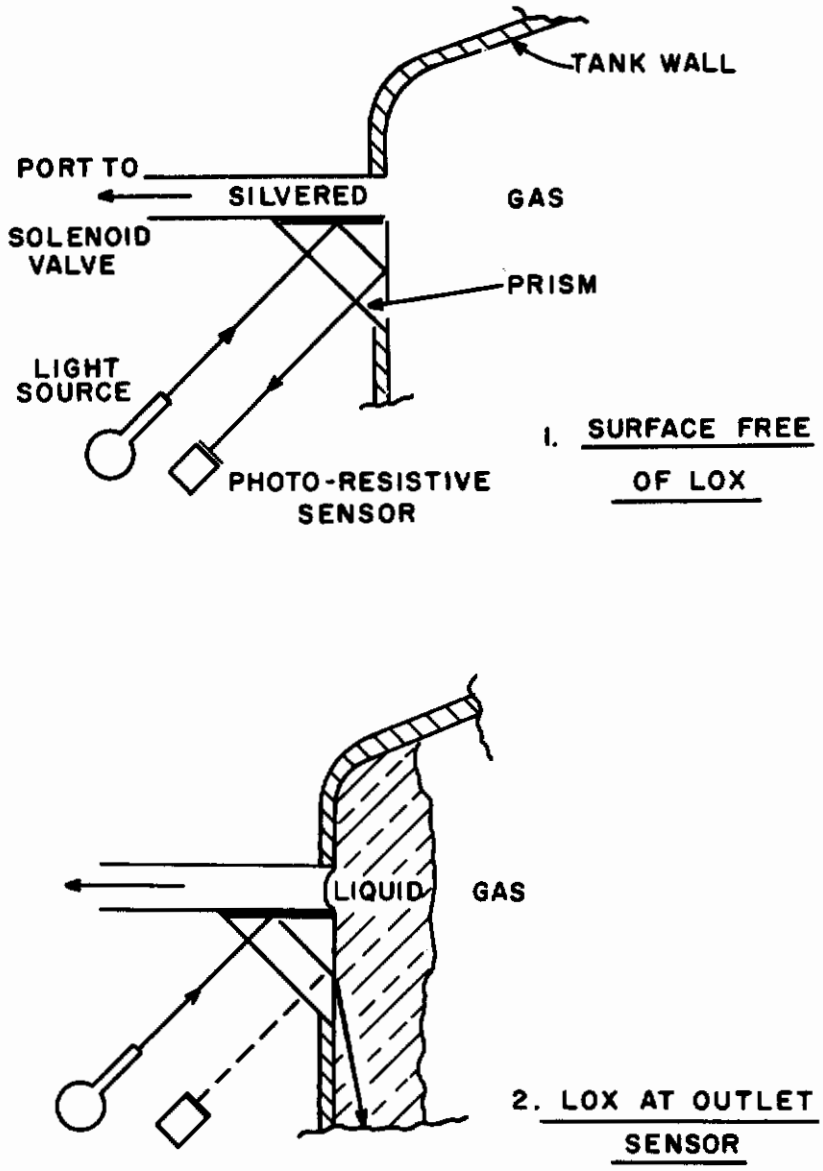

Figure 27: LOX-Light Sensor

Boil-off Rate, Tank Pressure, and Flow Control

The oxygen converter's vapor delivery system serves one purpose: to provide a controlled flow of oxygen gas as selected by the pilot. The minimum specified flow rate of vapor (0.5 liter per minute) is attributed to the boil-off rate due to normal steady heat leakage, Q_L.

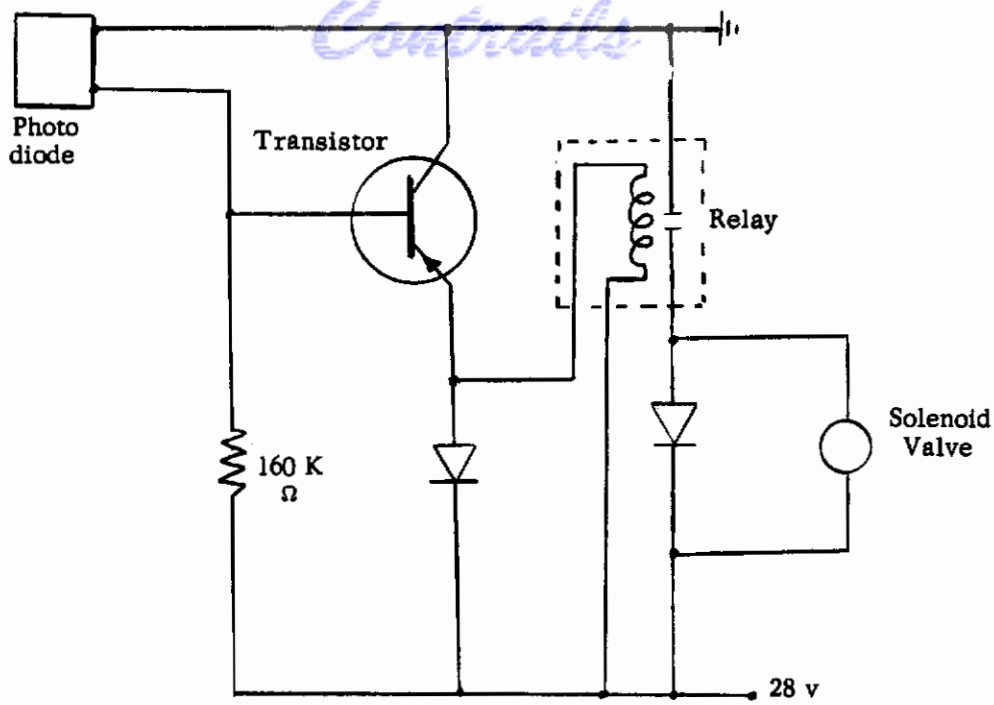

Figure 28: Light Sensor and Solenoid Valve Control Circuit

In order both to provide flow rates greater than the minimum and to maintain the tank pressure between the specified limits (70 psia ± 20 psia), a system composed of an electrical resistance heater, a number of controlled outlet port valves, a manifold, and a controlled flow valve is used. Thus a tank pressure sensor will cause the heater to be actuated when the pressure falls to the minimum, and to be de-energized when the pressure reaches the maximum.

The automatic feedback control system that regulates boil-off rate, tank pressure, and delivery flow rate is discussed in some detail in Appendix E. The problem is left in the standard form of a functional block diagram. In this form, the problem may be solved exactly on an analog computer and optimum values for the design parameters may be chosen.

The Electrical Power Supply

Choice of Frequency

There are three factors which may affect the choice of the supply frequency:

Stability of the liquid-vapor interface

Losses in the liquid dielectric (LOX)

Size and weight of the supply system

Stability analysis of the liquid gas interface has shown that direct current electric fields cannot be used for dielectrophoretic positioning; however, the frequency for stability is not so high as to prohibit the use of normal power frequencies. The dielectric loss in LOX is very small, hence losses do not impose a severe limit on frequency. The frequency for the supply may then be chosen on the basis of the size and weight of the supply, remembering that the volt-amp-rating of the capacitive load increases linearly in the frequency. A frequency of 60 cps is chosen for this design.

Choice of Voltage

The choice of supply voltage is intimately related to both the converter operation and supply size. To ensure both rapid orientation of the LOX and adequate performance under moderate external vibration, a large electric field is preferred. However, unrestricted increase in the field may cause either local or general electric breakdown, i.e., corona

or arcing. The electric field should be as high as safety and stability considerations will allow. The breakdown strength of liquid oxygen is of the order of 1000 kv/cm. For oxygen vapor the value is lower. The pressure and temperature may be taken to affect the breakdown strength of a gas in the same way as they affect its density. That is, the breakdown strength of oxygen vapor at the pressure and temperature of the converter is related to the breakdown strength at standard temperature and pressure according to:

$$E^* = E^*_o \frac{P}{P_o} \frac{T_o}{T} \tag{43}$$

The electrical strength of the oxygen vapor in the converter is,therefore,on the order of 500 kv/cm.

The maximum predicted field is based on a cylindrical geometry but actually is due to an array of rods simulating this geometry. Thus the true maximum electrical field intensity will be somewhat higher in a real converter than predicted by simplified theory. To assure safety from electrical breakdown, a factor of safety is used to account for the simplifying assumptions of the design. Thus, the maximum permissible field strength is held between 50 and 100 kv/cm. The breakdown consideration and the criterion imposed by the stability analysis govern the choice of the operating voltage. For this design, the voltage is 20 kv.

Internal Impedance and Protection

Because of the potential hazard of electrical discharge in LOX - metal regions, it is advisable to have high impedance sources with rapid action fuses. As will be seen in the following section, an inverter and series resonant circuit will be used to step up voltage from 28 v DC to 20 kv AC at the capacitor. Because of the use of a resonance condition, the circuits will be self-protecting, with any breakdown causing an off-resonant condition and consequent drop in voltage.

Type of Supply

Two basic methods are available for production of high voltages from a low voltage source. These are:

a) The use of a transformer

b) The use of a high Q coil to resonate with the inherent capacitance of the system, plus a lower voltage, lower rated transformer.

It has been found during weight optimization studies that method b) has considerable weight advantage over a), for example, a weight reduction of the order of 50% is possible. One additional weight saving involves the inverter-transformer relationship. It may be assumed that a normal inverter of about 10 V A size will consist of transistors feeding into an output transformer. This output transformer may be replaced by the step-up of transformer primary, resulting in about 0.25-lb weight saving.

Rating

The maximum capacitance of the system will be in the order of 1000 $\mu\mu$f. Thus, the rating at 60 cps and 20 kv is:

$$\text{Current} = 20,000\,(2\pi\,60)\,1000\,10^{-12} \text{ amp}$$
$$\approx 7.5 \times 10^{-3} \text{ amp or } 7.5 \text{ ma}$$
$$\text{Rating} = 7.5 \times 20 = 150 \text{ V A}$$

Weight of the System

The system consists of:

1. a 28 V DC to 60 cps inverter
2. a series resonant coil, iron cored with an air gap to give linearity
3. the staging, which may be represented as a capacitor

It is reasonable to assume that the coil may be designed for a Q of 15, and rating of 150 V A at about 20 kv. This means that the losses in the circuit will be 150/15 = 10 watts, and this is the total rating of the inverter. The current of 7.5 ma is therefore supplied, by the inverter, at about $10/7.5 \times 10^{-3}$ = 1330 v. As previously mentioned, the inverter will consist of a power transistor circuit feeding into the primary of this output transformer.

a) Inverter Weight

The inverter consists of transistors, heat sinks and output transformer. A simple feedback system will change the frequency to keep the circuit in resonance at all times. The weight of the transformer will be of the order of 0.3 lb, and the miscellaneous items, exclusive of packaging, will weigh about 0.25 lb. Thus a conservative estimate of 1 lb may be made for the weight of the inverter with such mountings as are needed to incorporate it as shown in the over-all design layout (Figure 23).

b) Resonant Coil Weight

A 150 V A resonant coil will have approximately the weight of a transformer of 75 V A rating. As a guide to possible weight of the transformer, one may use Figure VIII-B-3 of WADD technical report 60-699, Volume VIII. This refers to 400 cps transformers, but values may be converted to 60 cps by assuming that the flux density and current density remain constant. This means a constant ratio of V/f, and a constant current. Thus V I $\propto$ f, and the equivalent 75 V A, 60 cps transformer will be rated at 500 V A, 400 cps. Interpolating on the curves gives a weight of 2.4 lbs. for the transformer.

It may be possible to optimize, use better materials, and achieve better than 2.4 lbs., but this will be used as a conservative figure.

c) Total Electrical Supply Weight

For both inverter and transformer, the total weight will be under 4 lbs.

Level Indicator

The use of a capacitance sensor (or current sensor provided a constant voltage supply is used) will give an indication of the liquid volume present. Appendix F shows the effect of severe misorientation of the fluid due to gravity effects, hang-up, and general sloshing. For example, if the hypothetical tank of Appendix F is half full, the effect of either a lateral or axial g force results in a capacitance midway between the empty and full conditions. The capacitance will be identical in each case because there are, effectively, two "half converters," one full, the other empty. Referring to Appendix F, the "mean" capacitance for a one-half full tank is 90 ± 7 pf/foot. For "perfect" separation the result is 97 pf/ft. For the highly unlikely case in which half the fluid is hung up on the inside of each cell, (i.e., the fluid is uniformly distributed, and then separated exactly opposite to dielectrophoretic principle) the value is 83 pf/foot. For the condition where half the fluid is hung up on the outside of the stage, and the rest is on the inner electrode, the value is 90 pf/foot.

Assuming that the 83 pf/foot value is so unlikely as to be impossible, there is a deviation of possible system capacitances from 90 to 97 pf/foot. The mean expected capacitance for the illustrative example of Appendix F is, therefore, $\frac{90 + 97}{2}$ = 93.5 pf/foot. The expected deviation is ± 3.5 pf/foot or ± 3.7%.

Vessel Design for Minimum Weight

The 25-liter oxygen converter vessel consists of an inner and outer cylindrical tank having spherical-sector end caps, evacuated insulation, and internal and external support members. There are three preferred materials for use in cryogenic tankage, (Reference 13):

1. Stainless-steel, 301, 62% cold worked
2. Aluminum alloy, 6061-T6
3. Titanium alloy, 6Al-4V

The structural design is based on recommendations of safety factors and procedures outlined in References 12 and 13. The inner tank volume is set at 30 liters. This volume allows 5 liters for ullage, which is consistent with the use of six venting ports. Figure 29 defines the components of the vessel and the dimensional nomenclature. Figure 30 gives the tank component weight versus tank length to diameter ratio, L/D. The total vessel weight is seen to increase by a factor of 2 over the range of L/D from 1 to 10.

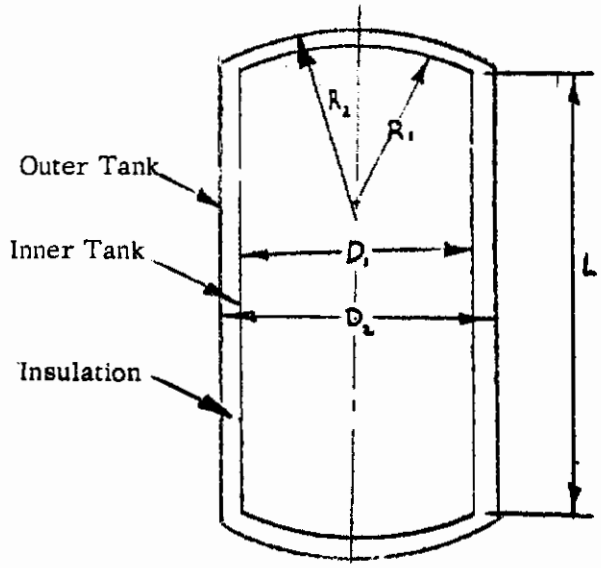

Figure 29: A Sketch Defining the Tankage Parameters

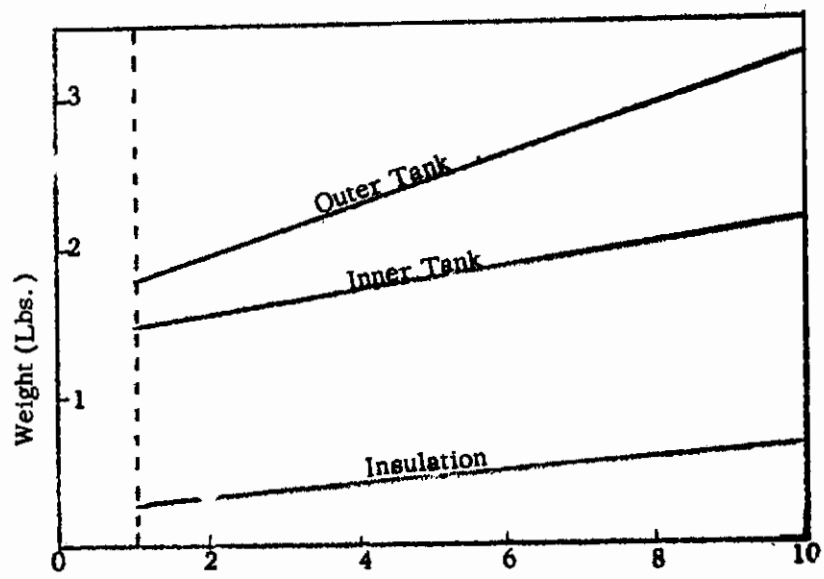

Figure 30: Vessel Component Weights Versus L/D

Inner Tank

The inner tank consists of a cylinder having spherical sector end caps. The tank must withstand an internal pressure of at least 90 psia and also a maximum static head due to the weight of the contents under accelerations as high as 25 g. It will be shown that the minimum weight spherical sector end cap has a radius equal to the diameter of the tank divided by $\sqrt{3.}$ The thickness of a spherical section is

$$\tau = \frac{P_1 R}{2 \sigma_A} \tag{44}$$

where:

σ_A = maximum allowable stress

P_1 = maximum effective internal pressure

= 90 psia + head at 25 g's

The geometry is shown in Figure 31.

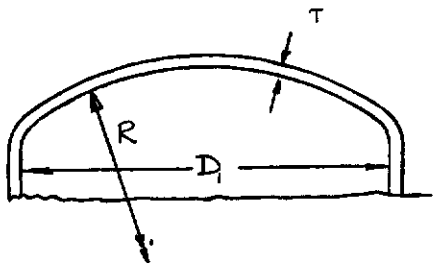

Figure 31: The Geometry of a Spherical Sector End Cap

The area of a spherical sector shell is

$$\text{Area} = 2 \pi R h_2 \tag{45}$$

where:

$$h_2 = R - \sqrt{R^2 - \frac{(D_1{}^2)}{4}} \tag{46}$$

The weight of an end cap is given by:

$$W = \left(\frac{\rho}{\sigma_A}\right)(\pi P_1)\left(R^3 - R^2\sqrt{R^2 - \frac{D_1{}^2}{4}}\right) \tag{47}$$

where ρ is the weight density of end cap material.

By differentiating this equation and setting equal to zero, the minimum weight is found to occur when $R = D_1/\sqrt{3.}$ It is apparent from the cap weight equation that a metal with low ρ/σ_A should be chosen. Stainless steel is chosen for the design both for its low ρ/σ_A and its safety in LOX. Fabrication considerations set a minimum practical thickness of 6 mils. The inner cylinder volume is a constant 30 liters for all values of L/D. The length of a tank having spherical sector caps of radius, $R = D_1/\sqrt{3,}$ is given by:

$$L = \frac{(4)(\text{vol})}{\pi D_1{}^2} - \frac{5 D_1}{9\sqrt{3}} \tag{48}$$

The inner cylinder thickness is given by

$$\tau = \frac{P_1 R_1}{\sigma_A} \tag{49}$$

The weight of the cylinders is proportional to ρ/σ_A of the metal used. As in the end caps, steel is selected to give minimum weight consistent with safety (compatibility with LOX). The weight of the cylinder was calculated on the basis that the walls would never be thinner than 6 mils.

Insulation

The converter specifications require that no more than 3 pounds of LOX be evaporated in 24 hours under stand-by conditions. This boil-off rate limits the allowable steady heat leak to less than 10 Btu/hr. The limiting constraint on maximum steady heat leakage arises out of the specification that the converter deliver a minimum gaseous flow of 0.5 standard liters per minute. This corresponds to a total maximum allowable steady heat leak of the order of 7.2 Btu/hr.

A heat leak of 1.3 Btu/hr, is allotted to the insulation. Various insulations were considered to determine which would give the lowest system weight at the allotted heat leak. NRC-2 evacuated multilayer insulation having a $K\rho$ product of $2.8\ 10^{-5}$ (Btu/hr/ft/^{o}R)-(lb/ft.^{3}) was found to be most satisfactory from minimum weight considerations and was therefore used in this design. The vacuum required is 10^{-4} mm Hg or lower.

Outer Tank

The outer tank is subjected to an external hydrostatic pressure of 15 psia, and therefore the most likely mode of failure is buckling. The design of the outer cylinder and spherical sector end caps is based on a safety factor of two applied to the pressure. Spherical sector end caps were chosen for the outer tank because of their high buckling strength and conformity to the inner tank.

The stress at which a spherical section will buckle is given by:

$$\sigma_{crit} = \frac{K_P \pi^2 E}{12(1 - \nu^2)} \left(\frac{\tau}{d}\right)^2 \tag{50}$$

where

σ_{crit} = critical stress in the spherical shell
K_P = a constant which is a function of the material and end cap geometry
E = Young's modulus
ν = Poisson's ratio (0.3 for most metals)

the other symbols are the same as for the inner cap, except for the subscripts.

Within the Range $1 < L/D \quad 10$, the constant K_P is given by:

$$K_P \approx \frac{0.3\ D_2^2 (1 - \nu_e^2)^{1/2}}{R_2\ \tau_2} \tag{51}$$

The stress in the spherical shell is

$$\sigma = \frac{P_2 R_2}{2\tau} \tag{52}$$

An equation for the thickness of the spherical sector shell may be written:

$$\tau = \sqrt{\frac{20}{\pi^2} (1 - \nu_e^2)^{1/2} (P_2) (SF) \frac{R_2^2}{E}} \qquad (53)$$

where (SF) is a factor of safety.

The expression for the end cap weight may now be written:

$$Wt = 8.95 \rho \sqrt{(1 - \nu_e^2)^{1/2} \frac{(P_2)(SF)}{E}} \left(R_2^3 - R_2^2 \sqrt{R_2^2 - \frac{D_2^2}{4}} \right) \qquad (54)$$

The grouping of terms involving R_2 is the same as for the inner end caps. The weight of the outer end caps is a minimum when $R_2 = D_2/\sqrt{3}$ and when $\rho/\sqrt{E}$ is a minimum. Aluminum has a low value of $\rho/\sqrt{E}$ and is chosen for this design.

Buckling calculations for the outer cylinder indicate that a thickness of 50 mils is required. By using appropriate stiffeners the wall's thickness may be reduced to 15 mils. It is assumed that the stiffeners will weigh no more than 1/3 the weight of the skin; therefore, the weight of the outer cylinder is calculated on the basis of an equivalent tank wall thickness of 20 mils.

Internal Support Members

Between the inner and outer vessel walls there are support members capable of maintaining a constant separation between tanks. These members must support the inner tank and contents against g-loads as high as 25 g_o axial and 10 g_o lateral. The total heat leakage attributed to these members must be kept small. Twenty-five carefully located support buttons are used in this design. There are three equally spaced axial rows each having three buttons. Also there are eight uniformly spaced buttons at each end. The supports, oriented in this way, are subjected to compressive loads only (regardless of the direction of acceleration disturbances). The fabrication of a support button is shown below.

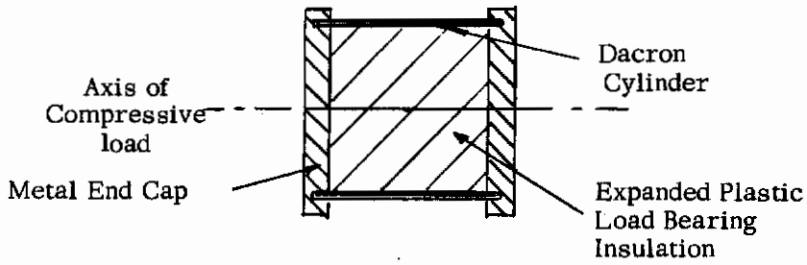

Figure 32: The Fabrication of a Support Button

The button is a capped Dacron cylinder filled with evacuated load bearing insulation. The main heat path is through the Dacron which has a thermal conductivity of 1.05 Btu-in/hr/ft^2/$^\circ$F. The heat leakage due to a single button is 0.15 Btu/hr; the total heat leak due to internal supports is 3.8 Btu/hr. The maximum axial compressive loads to be carried by the supports are 220 lbs. on each end-support under 25 g_o axial loads, and 233 lbs. on each side-support under 10 g_o lateral load. The sealed cylindrical construction of the buttons places the load bearing insulation under hydrostatic stress. Loaded hydrostatically the load bearing insulation will support at least 200 psi. This contributes significantly to the strength of a button. The Dacron outer cylinder will support a buckling force of 85 lbs.; the load bearing insulation core supports another 160 lbs. Each button will thus support 245 lbs., and the weight of the 25 buttons is on the order of 0.5 lbs.

LOX is potentially a very hazardous cryogenic, since it permits so rapid a chemical combination with many materials that propellant-type burning or even detonation may occur. Potential sources of such reactions in the dielectrophoretic converter include impurities in commercial LOX (primarily acetylene), plastic structural or coating materials, and metallic elements such as the electrode rods or the container itself. In addition to the ignition hazard, there is a potential ozone hazard resulting from corona around the electrodes. This is discussed in the following paragraphs.

Arc-Limiting Features

The only novel element in the dielectrophoretic converter is the presence of the high voltage field. Because of this, there is the possibility of an arc resulting from dielectric breakdown in either LOX or vapor.

Two steps are taken to avoid or limit arcing:

(a) The converter is designed so that voltage fields do not even closely approach the voltage breakdown strength of the low temperature gaseous oxygen. In an operational converter, voltage breakdown is checked prior to filling with LOX by filling with oxygen vapor and loading the electrodes to several times the design voltage.

(b) The second step taken to limit the arcing is to limit the intensity and duration of any arc which might occur. The likelihood of ignition is strongly dependent on these factors. Intensity may be limited by including a high electrical resistance in series with the electrodes (Reference 9). Duration is limited to a few milliseconds by including an overload fuse in the power supply primary. Thus the energy content of the spark is limited to the order of millijoules, a large portion of which is absorbed in the oxygen itself rather than at a LOX-metal or LOX-plastic interface. It appears that this represents too small an energy to raise the temperature of the materials in this converter to their ignition point.

Choice of Materials

Under normal circumstances, it can easily be shown that the inherent ignition hazard due to fluorinated hydrocarbons and metals can be made nil if reasonable care is taken in fabrication. In this design, stainless steel is used for the electrode and structural material, Teflon as an anti-wetting coating material for the tank, and alumina ceramic for the webs of the electrode spool. None of these materials in bulk form represents a hazard in LOX (Reference 10).

Ozone Generation

The presence of ozone, generated by corona around the electrodes, represents a potential health hazard. It is not believed that the voltages used in the design (20 kv) are sufficiently high to cause hazardous concentrations of ozone. To confirm this belief, the model converter has been operated with a flow of room temperature oxygen at typical voltages. No odor of ozone was detected.

Acetylene Films

As LOX is evaporated from the converter, the concentration of acetylenic contaminants increases. Eventually the concentration exceeds solubility and fine particles of acetylene "ice" appear. Since these have a different dielectric constant from the LOX, they may be expected to migrate to the electrodes and form a solid film. Assuming that the initial acetylenic contamination is 5 ppm by volume, complete evaporation of 25 liters of LOX would leave a layer 3×10^{-6} mils

thick on each electrode wire of the design of this report. It is evident from Appendix D that even if an arc did occur and somehow managed to ignite this thin layer, there would not be enough energy liberated to ignite the electrode. The reaction therefore could not lead to an explosion. Of course, experimental confirmation of this should be obtained under any continued development program.

Safety Experiments

Some arc-breakdown experiments were performed to demonstrate that arcs may be safely passed through contaminated LOX without ignition occurring. In these tests, small hemispherical electrodes of steel were used in the configuration shown in Figure 20. The test Dewar was filled with LOX having supersaturated concentrations of acetylene. Voltages up to 23 kv were imposed. Many arcs were set off in this apparatus. The tests showed that steel wire, Teflon, and the dissolved or dispersed acetylene represent little hazard under conditions of spark intensity and duration far exceeding those in an actual converter. Ignition was achieved readily, as might be expected, by passing an intense spark directly through such hydrocarbons as polyethylene.

Conclusions

With one possible exception, the dielectrophoretic converter appears to possess adequate safety characteristics for use in an inhabited space vehicle. The one possible exception relates to the behavior of acetylenic hydrocarbon coatings on the electrodes; this should be more fully explored in the model converter.

Both the 25-liter prototype and the flight-test model have been designed according to the best theory currently available. As with any piece of advanced hardware it is not possible to analyze completely or demonstrate solutions to all the novel aspects of the design through paper studies or small-scale laboratory experiments, and it is evident that considerable proof-of-principle and proof-of-reliability demonstrations will be required before the dielectrophoretic oxygen converter becomes an acceptable component of a life support system for space application. Recommendations for further development of the converter are summarized below.

Flight-testing of the converter model is, of course, the most obvious area for continued work. It is anticipated that a series of up to six days of flight testing will be required to confirm operation at zero g, correct any discrepancies between theory and observed performance, and optimize the configuration.

There are two areas which could not be covered under the present program and which should be included in any further program. These are the more accurate computation and mapping of the E-fields around the electrodes, and further testing of a possible hazard due to build-up of organic films on the electrodes. Better knowledge of the E-fields would permit reduced design safety factors in choice of operating voltages and thus would permit design at higher values of effective g. Certain safety tests might be conducted with the flight-test model, following flight tests, by adding organic material to LOX in the tank, evaporating the LOX, and arcing across the elecrodes.

In the future, system studies should be conducted for specific vehicles and cabin layouts to determine exact conditions under which the converter will be used. This will give a better indication of desired tank shape and details of the venting and vapor delivery system. Such studies could indicate that an appreciably different electrode geometry based on different design criteria may be required.

Prior to general hardware development directed at the construction of a converter for use in a vehicle, R & D work is recommended on those components having particularly novel aspects (other than the electrodes). Particular items in this category include the high-voltage power supply and the vapor-delivery system.

The feasibility of utilizing dielectrophoretic forces to separate liquid oxygen from gaseous oxygen has been demonstrated with laboratory experiments and by the preliminary design of a 25-liter oxygen converter. The final verification of the design will be accomplished by flight testing a scale model device.

It is recognized that this design is preliminary. It has been optimized to some extent, but it does not cover the range of all the possible configurations for a prototype converter utilizing the principles demonstrated in this study.

The sub-systems of the dielectrophoretic oxygen converter can be designed for high reliability. The inverter-transformer power supply is recognized to be highly dependable. The electrodes are mechanically reliable through over-design. The design proposed here relies upon dielectrophoretic forces to separate vapor and liquid phases from zero-g_o up to better than $10^{-3}g_o$. When $g > 10^{-3}g_o$, a system of automatic vapor outlets takes over. The proposed system of liquid sensors and solenoid-operated vapor valves contains no elements which are far beyond the present state of the art. Many of the vapor delivery sub-systems have been proven in space apparatus. There is, therefore, every reason to have confidence in the vapor delivery system.

The components of the vapor delivery system are designed to fail safe. The automatic vapor delivery valve which makes excursions about the pilot's initial setting can be manually operated should the need arise. If it fails, the minimum vapor delivery rate, 0.5 liters/min, is assured (by virtue of the steady heat leak) although the maximum delivery rate, 5 liters/min, may be exceeded. The six vapor-delivery ports are so situated that the failure of one at each end of the tank can be tolerated without harm to the pilot.

It is possible to provide for continued operation of the converter even against a total failure of electrical power. In the event of total power failure the mission will of course be aborted but the converter can be designed to function in a manner to prevent suffocation of the pilot. One such scheme is to have all six solenoid-operated outlet valves set to open at an over-pressure of the order of 100 psia allowing both liquid and gaseous oxygen to pass. This would prevent explosion of the converter and would insure breathing oxygen to the pilot as long as the LOX supply held. Further studies along this line may be advisable if the problem of power failure is critical.

All electrodes are teflon-coated so that in the event one breaks and touches another wire it will not cause a dead shorting of the system. The design of the circuit includes a high resistance in series with the converter electrodes so that arc energy is limited to a safe level. The design flexibility of the dielectrophoretic oxygen converter is a point in its favor. A cylindrical 25-liter-sized model may be designed to fit in almost any available cabin space (e.g., it may be designed with L/D from 2 to 8 with almost no increase in weight and no sacrifice of reliability). The only power inputs are electrical (28v DC). The pilot may exercise complete control over vapor delivery rate from 0.5 to 5 liters per minute by setting a valve which may be located remotely from the converter.

The dielectrophoretic oxygen converter is light in weight. The power supply, electrode ensemble, and complete vapor delivery system weigh only 8 lbs. The remaining 6 lbs. is attributed to tankage, insulation, supports, etc., which are not unique to this system. For long range missions in which the ability to recycle a converter becomes important, the dielectrophoretic oxygen converter has a marked advantage over some other schemes. The dielectrophoretic converter may be used over and over again. It may be refilled at any stage of its operation either when empty or not.

REFERENCES

1. Stratton, J. A., Electromagnetic Theory, McGraw-Hill Book Co., Inc., New York, N. Y., 1941.

2. Landau, L. D., and Lifshitz, E. M., Electrodynamics of Continuous Media, Addison-Wesley Publishing Co., Inc., Reading, Mass., 1960.

3. Panofsky, W. K. H., and Phillips, M., Classical Electricity and Magnetism, First Edition, Addison-Wesley Publishing Co., Inc., Reading, Mass., 1955.

4. Debye, P., Polar Molecules, Dover Publications, New York, N. Y., ©1929.

5. Pohl, H. A., "Some Effects of Non-Uniform Fields on Dielectrics," Journal of Applied Physics, Vol. 29, p. 1182, 1958.

6. Rohsenow, W. M., and Choi, H. Y., Heat, Mass and Momentum Transfer, Prentice-Hall, Inc., Englewood Cliffs, New Jersey, 1961.

7. Haberman, W. H., and Morton, R. K., An Experimental Investigation of the Drag and Shape of Air Bubbles Rising in Various Liquids, Report 802 NS715-102, Navy Department, The David W. Taylor Model Basin, Washington, D. C., September, 1963.

8. Peek, F. W., Dielectric Phenomena in High Voltage Engineering, McGraw-Hill Book Co., Inc., New York, N. Y., 1929.

9. Rose, H. E., Pried, T., "Ignition Phenomena in Hydrogen-Air Mixtures", Seventh Symposium (International) on Combustion at London and Oxford, 28 August - 3 September, 1958, London Scientific Publications.

10. Timmerhaus, K. D., ed., Advances in Cryogenic Engineering, Vol. 4, Plenum Press Inc., New York, 1960, p. 27.

11. Arnett, R. W., Warren, K. A., and Mullen, L. O., Optimum Design of Liquid Oxygen Containers, WADC Technical Report 59-62, Aeronautical Systems Division, Wright-Patterson Air Force Base, Ohio, August, 1961.

12. Sacks, A. H., Aerodynamic Forces, Moments, and Stability Derivatives for Slender Bodies of General Cross-Section, National Advisory Committee for Aeronautics, Langley Research Center, Langley Field, Va., November, 1954.

13. Spieth, C. W., et al, Study of Integrated Cryogenic Fueled Power Generating and Environmental Control Systems. Vol. II: Cryogenic Tankage, ASD TR 61-327, Vol. II, Aeronautical Systems Division, Wright-Patterson Air Force Base, Ohio, November, 1961.

14. Seely, F. B., and Smith, J. O., Advanced Mechanics of Materials, Second Edition, John Wiley & Sons, Inc., New York, N.Y., 1952, p. 227.

15. Bynum, D., "How to Calculate Maximum Principal Stress and Maximum Deflection of Perforated Plates", Machine Design, Vol. 35, No. 2, January 17, 1963, p. 179.

16. Morse and Feshbach, Methods of Theoretical Physics, Part 2, pps. 1234, 1235, (1953).

17. Chandrasekhar, S., Hydrodynamic and Hydromagnetic Stability, Clarendon Press, England, 1961.

APPENDIX A

EXACT FIELD SOLUTION FOR THE ELEMENTARY CASE OF A SINGLE INTERMEDIATE STAGE

The field between two cylinders has a potential, V_1, represented by:

$$V_1 = \text{Real part of } \left\{ 2 q_1 \ell n \frac{z}{b} \right\} \tag{55}$$

where:

q_1 = charge on inner electrode,

b = inner radius of outer electrode,

z = complex variable x + jy.

The field due to a "grid" surrounded by an outer cylinder has a potential, V_2, represented by*

$$V_2 = \text{Real part of } \left\{ \frac{2}{n} q_2 \ell n \left(\frac{z^n - a^n}{z^n - (b^2/a)^n} \right) \right\}$$

where:

q_2 = charge on the grid,

a = radius of the grid,

n = number of (equally spaced) grids.

The general potential, V, at any point within the elementary dielectrophoretic cell is the sum of V_1 and V_2.

The electric field or voltage gradient may then be found, preferably in cylindrical coordinates in which:

$$\text{grad} = \bar{u} \frac{\partial v}{\partial r} + \frac{\bar{u}_\theta}{r} \frac{\partial r}{\partial \theta}$$

for the axisymmetric case, where $\bar{u}_r$ and $\bar{u}_\theta$ are the unit vectors. The dielectrophoretic force on a particle is proportional to ∇E^2, i.e., grad $(\bar{E} \cdot \bar{E})$. Thus, it is of interest to map both $\bar{E}$ and ∇E^2 for the elementary geometry. The problem of mapping $\bar{E}$ and $\nabla \bar{E}^2$ is introduced below. It will be shown that a closed-form solution is not practical without the aid of a computer.

It is noted that $\bar{E}$ may be found as follows:

$$\bar{E} = \bar{u}_r \frac{\partial v}{\partial r} + \bar{u}_\theta \frac{1}{r} \frac{\partial v}{\partial \theta} = \nabla v \tag{56}$$

and that ∇E^2 $\left[\text{or } \nabla (\bar{E} \cdot \bar{E})\right]$ may be found from

$$\bar{E} \cdot \bar{E} = \left(\frac{\partial v}{\partial r} \right)^2 + \left(\frac{1}{r} \frac{\partial v}{\partial \theta} \right)^2 \tag{57}$$

* See Reference 16, pages 1234 and 1235.

such that:

$$\nabla \bar{E}\cdot\bar{E} = 2\left[\left(\frac{\partial v}{\partial r}\right) \nabla \left(\frac{\partial v}{\partial r}\right) + \left(\frac{1}{r}\frac{\partial v}{\partial \theta}\right) \nabla\left(\frac{1}{r}\frac{\partial v}{\partial \theta}\right)\right] \tag{58}$$

The problem now reduces to finding the following terms:

$$\frac{\partial v}{\partial r},\ \frac{\partial v}{\partial \theta},\ \nabla\left(\frac{\partial v}{\partial r}\right),\ \text{and}\ \nabla\left(\frac{1}{r}\frac{\partial v}{\partial \theta}\right)$$

and replacing them in Equations (56) and (58).

After much algebra, the expression for $\nabla(\bar{E}\cdot\bar{E})$ may be written in the following form:

$$\nabla(\bar{E}\cdot\bar{E}) = 2\left[\left(\frac{\partial v}{\partial r}\right) \nabla \left(\frac{\partial v}{\partial r}\right) + \left(\frac{1}{r}\frac{\partial v}{\partial \theta}\right) \nabla\left(\frac{1}{r}\frac{\partial v}{\partial \theta}\right) \right] \tag{59}$$

$$\begin{aligned}
\nabla(\bar{E}\cdot\bar{E}) = {} & 2\,\bar{u}_r \Big[(A + BCD^{-1}E^{-1})\,\partial A/\partial r + (ACD^{-1}E^{-1} + BC^2D^{-2}E^{-2})\,\partial B/\partial r \\
& + (ABD^{-1}E^{-1} + B^2CD^{-2}E^{-2})\,\partial C/\partial r - (ABCE^{-1}D^{-2} + B^2C^2D^{-3}E^{-2} + F^2G^2D^{-3}E^{-2})\,\partial D/\partial r \\
& - (ABCD^{-1}E^{-2} + B^2C^2D^{-2}E^{-3} + F^2G^2D^{-2}E^{-3})\,\partial E/\partial r + (FG^2D^{-2}E^{-2})\,\partial F/\partial r \\
& + (F^2GD^{-2}E^{-2})\,\partial G/\partial r \Big] \\
& + 2\,\bar{u}_\theta \Big[(ABD^{-1}E^{-1}r^{-1} + B^2CD^{-2}E^{-2}r^{-1})\,\partial C/\partial \theta \\
& - (ABCE^{-1}D^{-2}r^{-1} + B^2C^2D^{-3}E^{-2}r^{-1} + F^2G^2E^{-2}D^{-3}r^{-1})\,\partial D/\partial \theta \\
& - (ABCD^{-1}E^{-2}r^{-1} + B^2C^2D^{-2}E^{-3}r^{-1} + F^2G^2D^{-2}E^{-3}r^{-1})\,\partial E/\partial \theta \\
& + (FG^2D^{-2}E^{-2}r^{-1})\,\partial F/\partial \theta \Big]
\end{aligned} \tag{60}$$

where the coefficients A, B, C, etc., and their partial derivatives are defined as follows:

$$A = \frac{2}{r} q_1$$

$$\partial A/\partial r = -\frac{2}{r^2} q_1 = -2 q_1 r^{-2}$$

$$B = \frac{2}{r} q_2 (a^{2n} - b^{2n})$$

$$\partial B/\partial r = -2 q_2 r^{-2} (a^{2n} - b^{2n}) = -2 q_2 r^{-2} a^{2n} + 2 q_2 r^{-2} b^{2n}$$

$$C = \left[1 + \left(\frac{b}{a}\right)^{2n} + \left(\frac{r}{a}\right)^{n} \cos n\theta + \left(\frac{b}{a}\right)^{n} \left(\frac{b}{r}\right)^{n} \cos n\theta \right]$$

$$= \left[1 + \left(\frac{b}{a}\right)^{2n} + r^{n} a^{-n} \cos n\theta + r^{-n} \left(\frac{b^2}{a}\right)^{n} \cos n\theta \right]$$

$$\partial c/\partial r = n r^{n-1} a^{-n} \cos n\theta - n r^{-(n+1)} \left(\frac{b^2}{a}\right)^{n} \cos n\theta$$

$$\partial c/\partial \theta = -n r^{n} a^{-n} \sin n\theta - n r^{-n} \left(\frac{b^2}{a}\right)^{n} \sin n\theta$$

$$D = r^{n} - 2 a^{n} \cos n\theta + r^{-n} a^{2n}$$

$$\partial D/\partial r = n r^{n-1} - n r^{-(n+1)} a^{2n}$$

$$\partial D/\partial \theta = 2 n a^{n} \sin n\theta$$

$$E = r^{n} - 2 \left(\frac{b^2}{a}\right)^{n} \cos n\theta + r^{-n} \left(\frac{b^4}{2}\right)^{n}$$

$$\partial E/\partial r = n r^{n-1} - n r^{-(n+1)} \left(\frac{b^4}{a^2}\right)^{n}$$

$$\partial E/\partial \theta = 2 n \left(\frac{b^2}{a}\right)^{n} \sin n\theta$$

$$F = 2 r^{-1} q_2 \sin n\theta$$

$$\partial F/\partial r = -2 r^{-2} q_2 \sin n\theta$$

$$\partial F/\partial \theta = 2 n r^{-1} q_2 \cos n\theta$$

$$G = a^{n} r^{n} + b^{4n} r^{-n} a^{-n} - b^{2n} r^{n} a^{-n} - a^{n} b^{2n} r^{-n}$$

$$\partial G/\partial r = n a^{n} r^{n-1} - n b^{4n} r^{-(n+1)} a^{-n} - n b^{2n} r^{n-1} a^{-n} + n a^{n} b^{2n} r^{-(n+1)}$$

APPENDIX B

COLLECTION TIME IN A LOX CONVERTER

The time to equilibrium of an elemental sphere of LOX in an oxygen vapor matrix in a non-uniform field at zero g orientation may be determined by knowing the location of the bubble at any time. The velocity is found by means of a force balance on the LOX sphere. Recall that

$$F_E = F_{Dielectrophoretic} = F_{Drag} + F_{Inertia} \tag{61}$$

where

$$F_E = \frac{4\pi a^3}{r^3} \epsilon_o \kappa_v \left(\frac{\kappa_L - \kappa_v}{\kappa_L + 2\kappa_v} \right) \frac{V^2}{\left(\ell n \frac{R_0}{R_1} \right)^2} \tag{62}$$

$$F_D = 6\pi u a \frac{dr}{dt} \text{ (assuming Stoke's flow)} \tag{63}$$

$$F_I = (\rho_L) \left(\frac{4}{3} \pi a^3 \right) \frac{d^2 r}{dt^2} \tag{64}$$

Substituting into Equation (61) gives:

$$\frac{4\pi a^3}{r^3} \epsilon_o \kappa_v \left(\frac{\kappa_L - \kappa_v}{\kappa_L + 2\kappa_v} \right) \frac{V^2}{\left(\ell n \frac{R_0}{R_1} \right)^2} = 6\pi u a \frac{dr}{dt} + (\rho_L) \left(\frac{4}{3} \pi a^3 \right) \frac{d^2 r}{dt^2} \tag{65}$$

Equation (65) may be simplified by assuming the following:

1) In the oxygen converter, the "equivalent dielectrophoretic gravity" force on the LOX is not less than 10^{-3} g_o. The minimum force is ~ 1 dyne/cm^3. The average dielectrophoretic force field is considerably higher than that. Therefore, the estimate of the time to equilibrium based on $(F_E)_{minimum}$ = constant = 1 dyne/cm^3 will be pessimistic.

2) The drag force on a sphere of LOX in an oxygen vapor matrix is assumed negligible compared with the inertia force.

Equation (65) then reduces to:

$$(F_E)_{min} = (\rho_L) \left(\frac{4}{3} \pi a^3 \right) \frac{d^2 r}{dt^2} \tag{66}$$

Integrating Equation (66) and assuming that at t = 0, dr/dt = 0, the result is written:

$$t = \frac{(\rho_L) \left(\frac{4}{3} \pi a^3 \right)}{(F_E)_{min}} \frac{dr}{dt} \tag{67}$$

Integrating Equation (67) gives t in terms of r, the radial displacement of the spherical element.

$$t^2 = 2 \left[\frac{(\rho) \left(\frac{4}{3} \pi a^3 \right)}{(F_E)_{min}} \right] \Delta r \tag{68}$$

A sphere initially located at the outer radius of the tank R_0 will take the longest time to be collected to the center. Note that if at $t = 0$, $r = R_0$, then $\Delta R = R_0 - R_1$.

Rewriting Equation (68) in terms of the volume body force, $(F_E)_{min}/vol$, gives

$$t^2 = \frac{2 \rho_L}{\left(\frac{(F_E)_{min}}{vol}\right)} (R_0 - R_1) \tag{69}$$

$(F_E)_{min}/vol$ in the converter has been assumed to be due to an "equivalent dielectrophoretic gravity" of 10^{-3} g_o. It is given by the following equation.

$$\frac{(F_E)_{min}}{vol} = (.001)\ (\rho_L)\ (g_o) \tag{70}$$

where:

ρ_L = density of the liquid ≈ 1 gram/cm^3,

g_o = 980 cm/sec.^{2}.

Thus,

$$t^2 \approx 2(R_0 - R_1) \tag{71}$$

The time for a unit sphere of LOX to be collected from the outer wall to the inner electrode of a converter having R_0 = 8 cm and R_1 = 1 cm is 3.7 seconds. The actual collection time should be lower because of the simplifying assumptions made along the way. The dielectrophoretic force used in determining this time is considerably lower than the true average electrical force.

APPENDIX C

DERIVATION OF THE STABILITY ANALYSIS

LIST OF SYMBOLS

c - arbitrary function of time

e - base of natural logarithms

E - electric field, volt/cm

e_i, e_o - perturbed field ($-\text{grad}\,\delta\,\psi_i$)

F - defined in Equation (96)

f_i - defined in Equation (82)

f_o - defined in Equation (84)

G - defined as $\rho\left(\frac{\partial \epsilon_o k}{\partial \rho}\right)_T$

I_m, κ_m - modified Bessel functions of order m

j - $\sqrt{-1}$

P - hydrostatic pressure, dyne/cm^2

r - radius to point of interest, cm

R^* - radius to fluid interface, cm

R_i - radius of inner electrode, cm

R_o - radius of outer electrode, cm

t - time

T - surface tension, dyne/cm

u - velocity, cm/sec

x - $k R^*$

z - axial coordinate

γ, k, m, p - coefficients of the perturbation of the interface as defined by Equation (78)

Γ - defined as $\frac{\kappa_i - \kappa_o}{\kappa^*}$

δ - denotes a perturbed quantity

ϵ_o - permittivity of free space, $\frac{1}{4\pi}$

θ - angular coordinate

κ - relative permittivity

κ^* - defined by Equation (77)

π - defined as $P - \frac{1}{2} GE^2$

ρ - density, gram/cm^3

σ - conductivity, mho/cm

σ^* - defined by Equation (76)

$\langle\sigma\rangle$, $\langle\kappa\rangle$ - defined in Equations (87) and (88)

Σ - radius of perturbed interface, cm

τ - stress due to surface tension, dyne/cm^2

ϕ - root mean square value of applied voltage, volts rms

Φ - amplitude of applied voltage, volts

ψ - potential, volts

$\overline{\psi}_i$, $\overline{\psi}_o$ - total potential defined in Equation (79)

ω - angular frequency of applied voltage, radian/sec.

Subscripts

i - inner

o - outer

DERIVATION OF THE STABILITY ANALYSIS

INTRODUCTION

The investigation to be outlined here is a study of the conditions under which two fluids held in a cylindrical configuration by electrical forces will be stable. The purpose of the investigation is to:

1) Determine the effects of system dimensions on stability,

2) Determine the effects of fluid properties on stability

so that laboratory observations on small scale-systems may be used with confidence in predicting the performance of larger systems containing different fluids.

The present project is concerned with investigation of the feasibility of utilizing electrostatic forces to orient liquid oxygen and its vapor in a zero gravity oxygen converter. Early in the experimental program of this project, it was observed that steady (DC) electric fields will not perform the required orientation function. On the contrary, experience with laboratory zero gravity simulators indicated that steady fields exert a strong destabilizing influence on dielectric fluids. However, the use of alternating fields did prove successful in orienting the fluids used in the laboratory simulator. The question then arises as to whether the particular laboratory system chosen involves a fortuitous combination of properties and dimensions. In short, would an operational oxygen converter operate in the same manner as the laboratory models? The analysis required to answer this question is outlined in the following sections of this report. The type of analysis is conventional in that it is assumed that the fluid interface is subject to a small perturbation and the resulting linearized equations of motion are inspected to determine whether the motions induced by the disturbance increase in amplitude as time progresses. However, the details of the analysis are unconventional in one important respect. When alternating fields are considered, it is not generally possible to prove that the linearized equations of motion are a valid description of the problem. Linearization in this case has been supported by physical arguments which are verified in the final result. The results indicate that

1) The required electrical potential for stable operation increases as the square root of the product of interfacial tension and system diameter

2) Stable solutions are possible only for a restricted range of fluid properties, and system geometries.

The pertinent conclusion with respect to the oxygen converter is that the voltage required for stable operation of a 25-liter converter is well within the range presently under consideration for the operational design. Consequently, the analysis indicates that no problem will be encountered in translating our laboratory experience to the operational unit.

TECHNICAL DISCUSSION

The first item for consideration is the physical definition of the system to be considered. Here it is important to recognize that the finite conductivity of the fluid must be considered. That is, the free charge which exists at the interface due to the finite conductivity of the fluids is considered since it is due to this charge that the steady field causes the disruption of the interface. In addition, it is necessary to consider the surface tension between the fluids, since this is a classical destabilizing force and its neglect would cause errors which would indicate stability were possible over a greater range than is actually possible. Finally, since the frequencies of the applied fields which stabilize laboratory experiments are low (60 cps), we expect similar frequencies to be adequate for oxygen. Consequently, it is assumed that the applied field is of low enough frequency so that electromagnetic wave propagation into the fluids can be ignored. In the general sense, this restricts us to a consideration of fluids of low conductivity, i.e., dielectric fluids.

The forces to be considered are due to a perturbation of the interface and will have components due to the field in the undisturbed case. The determination of this field is, then, the first order of business.

The Unperturbed Field

We define a system in which the fluids are contained between cylindrical conducting electrodes of radii of R_i and R_o with the outer electrode grounded and the inner electrode voltage given by the real part of $\Phi e^{j\omega t}$. The fluid interface is located at radius R*.

The potentials in the two fluids satisfy Laplace's equation:

$$\nabla^2 \psi_i = 0$$
$$\nabla^2 \psi_o = 0 \tag{72}$$

with the boundary conditions:

$$\psi_i = \Phi e^{j\omega t} \text{ at } r = R_i$$
$$\psi_o = 0 \text{ at } r = R_o \tag{73}$$
$$\psi_i = \psi_o \text{ at } r = R^*$$

$$\sigma_i \frac{\partial \psi_i}{\partial r} + \epsilon_o \kappa_i \frac{\partial^2 \psi_i}{\partial r \partial t} = \sigma_o \frac{\partial \psi_o}{\partial r} + \epsilon_o \kappa_o \frac{\partial^2 \psi_o}{\partial r \partial t} \text{ at } r = R^*$$

where the last boundary condition is continuity of the (complex) current across the interface.

The unperturbed potentials are then given by the real parts of:

$$\psi_i = \left(1 - \frac{\sigma_o + j\omega\epsilon_o\kappa_o}{\sigma^* + j\omega\epsilon_o\kappa^*} \ln \frac{r}{R_i}\right) \Phi e^{j\omega t} \tag{74}$$

$$\psi_o = \left(\frac{\sigma_i + j\omega\epsilon_o\kappa_i}{\sigma^* + j\omega\epsilon_o\epsilon^*} \ln \frac{R_o}{r}\right) \Phi e^{j\omega t} \tag{75}$$

where:

$$\sigma^* \equiv \sigma_i \ln \frac{R_o}{R^*} + \sigma_o \ln \frac{R^*}{R_i} \tag{76}$$

$$\kappa^* \equiv \kappa_i \ln \frac{R_o}{R^*} + \kappa_o \ln \frac{R^*}{R_i} \tag{77}$$

The Perturbed Field

We assume that the surface is disturbed in such a way that the interface at r = R* assumes the shape:

$$\Sigma = R^* + \gamma e^{j(kz + m\Theta) + pt} \tag{78}$$

where γ is a small parameter.

For this case the potentials are given by:

$$\bar{\psi}_i = \psi_i + \delta\psi_i$$

$$\bar{\psi}_o = \psi_o + \delta\psi_o \tag{79}$$

where the $\delta\psi$'s are the components arising from the perturbation of the interface and ψ_i and ψ_o are given by Equations (74) and (75). These potentials are also solutions of Laplace's equation. For this case the boundary conditions are:

$$\delta\psi_i = 0 \text{ at } r = R_i$$

$$\delta\psi_o = 0 \text{ at } r = R_o \tag{80}$$

$$\bar{\psi}_i = \bar{\psi}_o \text{ at } r = \Sigma$$

$$\sigma_i \frac{\partial \bar{\psi}_i}{\partial r} + \epsilon_o \kappa_i \frac{\partial^2 \bar{\psi}_i}{\partial r\, \partial t} = \sigma_o \frac{\partial \bar{\psi}_o}{\partial r} + \epsilon_o \kappa_o \frac{\partial^2 \bar{\psi}_o}{\partial r\, \partial t} \text{ at } r = \Sigma.$$

The solution of Laplace's equation within the region bounded by the surface, Equation (78), and satisfying the first two of the boundary conditions, Equation (80), is given by:

$$\delta\psi_i = \gamma c_i f_i(kr)\, e^{j(kz + m\Theta) + pt} \tag{81}$$

where:

$$f_i(kr) = I_m(kr) - \frac{I_m(kR_i)}{K_m(kR_i)} K_m(kr) \tag{82}$$

where I_m and K_m are the Bessel functions of imaginary argument and order m; and c_i is an arbitrary function of time. Similarly, the potential in the outer fluid is:

$$\delta\psi_o = \gamma c_o f_o(kr)\, e^{j(kz + m\Theta) + pt} \tag{83}$$

where:

$$f_o(kr) = I_m(kr) - \frac{I_m(kR_o)}{K_m(kR_o)} K_m(kr). \tag{84}$$

The algebra required to evaluate c_i and c_o from the final two boundary conditions will not be reproduced here. The result given below is valid to the first order in the small parameter, γ. In addition, since we are interested in solutions of the problem which are stable, we may insist that p be imaginary or zero; that is, the solutions will not yield information regarding the character of an instability once it occurs. The results given below incorporate this assumption and, in addition, the assumption that $\omega >> p$, that is, $\partial/\partial t\, e^{pt} \cos \omega t \approx -\omega e^{pt} \sin \omega t$.* The solutions obtained, therefore, apply to those modes of operation which are stable and close to the mode of neutral stability.

The results for c_i and c_o are:

* It can be shown that, even if γ is considered a periodic function of time, the results obtained in Equations (99) and (100) are unaltered to terms in the first order in ω^{-1}.

$$c_i = \left\{ \frac{(\sigma_i - \sigma_o) + j\omega\epsilon_o(\kappa_i - \kappa_o)}{\sigma^* + j\omega\epsilon_o\kappa^*} \right\} \left\{ \frac{\sigma_o + j\omega\epsilon_o\kappa_o}{\langle\sigma\rangle + j\omega\epsilon_o\langle\kappa\rangle} \right\} \frac{\Phi}{R^*} f_o'(x)\, e^{j\omega t} \tag{85}$$

$$c_o = \left\{ \frac{(\sigma_i - \sigma_o) + j\omega\epsilon_o(\kappa_i - \kappa_o)}{\sigma^* + j\omega\epsilon_o\kappa^*} \right\} \left\{ \frac{\sigma_i + j\omega\epsilon_o\kappa_i}{\langle\sigma\rangle + j\omega\epsilon_o\langle\kappa\rangle} \right\} \frac{\Phi}{R} f_i'(x)\, e^{j\omega t} \tag{86}$$

where $x \equiv kR$ and the prime indicates differentiation with respect to x and Φ is the amplitude of the applied voltage, so that:

$$f_o'(x) = \frac{d}{dx} \left\{ I_m(x) - \frac{I_m(kR_o)}{K_m(kR_o)} K_m(x) \right\}$$

and so on. The quantities $\langle\sigma\rangle$ and $\langle\kappa\rangle$ are given by:

$$\langle\sigma\rangle = \sigma_i f_i'(x) f_o(x) - \sigma_o f_o'(x) f_i(x) \tag{87}$$

$$\langle\kappa\rangle = \kappa_i f_i'(x) f_o(x) - \kappa_o f_o'(x) f_i(x) \tag{88}$$

The perturbed fields are therefore given by Equations (81) and (83) with the c's given by expressions (85) and (86) respectively.

We now have the basic information required for the next step in the solution which is to write a force balance across the fluid interface.

Forces at the Interface

The pressure at the interface is due to hydrostatic pressure, surface tension, and electrical forces. Of these only the last is unfamiliar and is given by:

$$\vec{F}_e = -\frac{\epsilon_o}{2} \left[\kappa + \rho \left(\frac{\partial\kappa}{\partial\rho} \right)_{\substack{\text{const} \\ \text{temp}}} \right] E^2 \tag{89}$$

(see Reference 2) where ρ is the fluid density. Denoting the quantity $\rho \left(\partial\epsilon_o \kappa/\partial\rho \right)_{\substack{\text{const} \\ \text{temp}}}$ by G we have the following stress continuity relation at the interface ($r = \Sigma$):

$$P_i - \frac{\epsilon_o}{2}(G_i + \kappa_i) E_i^2 = P_o - \frac{\epsilon_o}{2}(G_o + \kappa_o) E_o^2 + \tau \tag{90}$$

where τ is the force due to surface tension. This relation must be satisfied at the interface in both the disturbed and undisturbed cases. Consequently, the contributions of the unperturbed components at the surface $r = R^*$ may be factored out of this expression. Note, however, that there remain components in the unperturbed field due to the fact that the interface is displaced a distance, $\Sigma - R^*$.

In order to evaluate the stresses at the interface, the behavior of the hydrostatic pressure must be investigated in the perturbed case. This is accomplished through the equations of motion.

Equations of Motion

In the undisturbed case there is no motion. In the disturbed case there is a motion in which the velocities are proportional to the small parameter, γ. Therefore, the motion within the fluids is described by the linearized relation:

$$\rho \frac{\partial \vec{u}}{\partial t} = - \text{ grad } (P - \frac{1}{2} G E^2). \tag{91}$$

Now, let

$$\Pi \equiv P - \frac{1}{2} G E^2.$$

Then, since the fluids are incompressible

$$\text{div } \vec{u} = 0, \text{ and } \nabla^2 \Pi = 0$$

So here again, we have Laplace's equations to solve, i. e.,

$$\nabla^2 \Pi_i = 0$$

$$\nabla^2 \Pi_o = 0 \tag{92}$$

with the boundary conditions:

$$\text{grad } \Pi_i = 0 \text{ at } r = R_i$$

$$\text{grad } \Pi_o = 0 \text{ at } r = R_o$$

$$- \text{grad } \Pi_i = \rho_i \frac{\partial \vec{u}}{\partial t}$$

$$- \text{grad } \Pi_o = \rho_o \frac{\partial \vec{u}}{\partial t} \text{ at } r = \Sigma \tag{93}$$

where

$$\left(\frac{\partial \vec{u}}{\partial t} \right)_\Sigma = p^2 \gamma e^{j(kz + m\Theta) + pt}$$

is consistent with the displacement of the interface.

This solution follows the same lines as those previously given for the perturbed potentials with the result:

$$\Pi_i = - \frac{\rho_i p^2}{k} F_i \gamma e^{j(kz + m\Theta) + pt} \tag{94}$$

$$\Pi_o = - \frac{\rho_o p^2}{k} F_o \gamma e^{j(kz + m\Theta) + pt} \tag{95}$$

where:

$$F_i = \frac{I_m(x) - \frac{I'_m(kR_i)}{K_m(kR_i)} K_m(x)}{I'_m(x) - \frac{I'_m(kR_i)}{K'_m(kR_i)} K'_m(x)} \tag{96}$$

and F_o is given by the same expression with R_i replaced by R_o.

Now, through Equations (94) and (95) we are able to relate the pressures at the interface to the parameter, p, which is the item of ultimate concern in this analysis. If p^2 is positive, the system is unstable while if p^2 is negative, p is imaginary and the system is stable.

We are now in a position to evaluate all the terms in Equation (90) and obtain the desired solution.

The Solution

From inspection of all the previous results, a general evaluation of Equation (90) will clearly involve an undesirable amount of algebraic manipulation. However, an important simplification results if it is assumed that $\omega >> \sigma/\kappa,\ \sigma^*/\kappa^*,\ \langle\sigma\rangle/\langle\kappa\rangle$.

Now, since the analysis is already restricted to dielectric fluids by the assumption that ω is small (i.e., $< 10^6$ cps), we can examine the order of magnitude of σ/κ for practical dielectric fluids. Characteristically, this quantity is of the order of unity for such fluids. On the other hand, at 60 cps, $\omega = 380$. Apparently, the assumption that $\omega >> \sigma/\kappa\epsilon_o$ is justified and we will proceed on this basis.

We may then summarize the field quantities ignoring terms in ω^{-1}, as:

$$E_i = -\frac{\partial \psi_i}{\partial r} = \frac{\kappa_o}{\kappa^*}\ \frac{\Phi}{r}\ \cos\ \omega t \tag{97}$$

$$E_o = -\frac{\partial \psi_o}{\partial r} = \frac{\kappa_i}{\kappa^*}\ \frac{\Phi}{r}\ \cos\ \omega t \tag{98}$$

$$e_i = -\frac{\partial(\delta\psi_i)}{\partial r}$$

$$= -\frac{\Phi k \gamma}{R}\ f'_o(x)\, f'_i(kr)\ \left(\frac{\kappa_i - \kappa_o}{\kappa^*}\right)\left(\frac{\kappa_o}{\langle\kappa\rangle}\right)\cos\ \omega t\, e^{j(kz + m\Theta) + pt} \tag{99}$$

$$e_o = -\frac{\partial(\delta\psi_i)}{\partial r} = -\frac{\Phi k \gamma}{R^*}\ f'_o(kr)\, f'_i(x)\ \left(\frac{\kappa_i - \kappa_o}{\kappa^*}\right)\left(\frac{\kappa_i}{\langle\kappa\rangle}\right)\cos\ \omega t\, e^{j(kz + m\Theta) + pt} \tag{100}$$

Finally, the surface tension term in Equation (90) is given by (Reference 17):

$$\tau = \frac{1}{R^*} - \frac{\gamma}{R^{*2}}\ (1 - m^2 - x^2)\, e^{j(kz + m\Theta) + pt} \tag{101}$$

Noting that $\omega >> p$, we may take the fluctuating terms at their rms values rather than including the detailed time dependence, insertion of Equations (97) to (101) and (94) and (95) into Equation (90) yields the final result:

$$p^2(\rho_i F_i - \rho_o F_o) = \frac{T x}{R^{*3}}(1 - m^2 - x^2)$$

$$- \frac{\phi^2 x^2}{R^{*4}}\ \epsilon_o f'_o(x)\, f'_i(x)\ \frac{\kappa_i \kappa_o}{\langle\kappa\rangle}\ \left(\frac{\kappa_i - \kappa_o}{\kappa^*}\right)^2 + \frac{\phi^2 x \epsilon_o}{R^{*4}\kappa^{*2}}\ \kappa_i \kappa_o (\kappa_o - \kappa_i) \tag{102}$$

The result given by Equation (102) indicates that the stable region of operation or the region in which the exponent, p, is imaginary is defined by:

$$\frac{T}{R^{*2}}(1 - m^2 - x^2) - \frac{\phi^2 \epsilon_o}{R^{*3} \kappa^{*2}} \kappa_i \kappa_o (\kappa_i - \kappa_o) \left[x \frac{f_o' f_i'}{\langle \kappa \rangle} (\kappa_i - \kappa_o) + 1 \right] < 0 \qquad (103)$$

It is apparent that the state defined by $m = 0$ is the most likely to yield an instability and, hence, is the one to be considered. In order to consider the conditions imposed on the system by the stability analysis, it is convenient to consider Equation (103) in the limits of small and large values of the parameter, x.

Noting that f_i and f_o now involve Bessel functions of zero order ($m = 0$), the following results can be established:

$$\lim_{x \to 0} \left(x \frac{f_o' f_i'}{\langle \kappa \rangle} \right) = - \frac{1}{\kappa^*} \qquad (104)$$

$$\lim_{x \to \infty} \left(x \frac{f_o' f_i'}{\langle \kappa \rangle} \right) = - \frac{x}{\kappa_i + \kappa_o} \qquad (105)$$

If we first consider the approximation at long wavelengths ($x \to 0$), Equation (103) and (104) yield:

$$\frac{T}{R^{*2}} + \frac{\phi^2 \epsilon_o}{R^{*3} \kappa^{*2}} \kappa_i \kappa_o (\kappa_i - \kappa_o) \left[\frac{\kappa_i - \kappa_o}{\kappa^*} - 1 \right] < 0 \qquad (106)$$

or defining:

$$\Gamma \equiv \frac{\kappa_i - \kappa_o}{\kappa^*}$$

this becomes:

$$\frac{\phi^2 \epsilon_o}{T R^*} > \frac{\kappa_i - \kappa_o}{\kappa_i \kappa_o} \left(\frac{1}{\Gamma^2 (1 - \Gamma)} \right) \qquad (107)$$

Equation (107) indicates that, as long as Γ is less than unity, the system will be stable for sufficiently high voltages. Below the stabilizing voltage, the system is subject to a long-wave length instability and surface tension forces will predominate. Examination of Equation (107) indicates that systems with $\Gamma = 0$ or 1 require infinitely large voltages while those with $\Gamma = 2/3$ require the smallest possible voltage level. Consequently, the optimum system design ($\Gamma = 2/3$) requires a voltage given by:

$$\frac{\phi^2 \epsilon_o}{TR^*} > 6.75 \quad \frac{\kappa_i - \kappa_o}{\kappa_i \kappa_o} \tag{108}$$

Considering the short wavelength instabilities ($x \rightarrow \infty$), Equation (103) and (105) yield:

$$\frac{\phi^2 \epsilon_o}{R^{*3} \kappa^{*2}} \kappa_i \kappa_o (\kappa_i - \kappa_o) \left[x \frac{\kappa_i - \kappa_o}{\kappa_i + \kappa_o} - 1 \right] - \frac{T}{R^{*2}} x^2 < 0 \tag{109}$$

which indicates that the system is stable for all:

$$x < \frac{\kappa_i + \kappa_o}{\kappa_i - \kappa_o} \tag{110}$$

For x greater than this value, the stability problem must be considered again. Some algebraic manipulation of Equation (109) indicates that the most important wave number to consider is:

$$x = 2 \frac{\kappa_i + \kappa_o}{\kappa_i - \kappa_o} \tag{111}$$

At this value of x the condition for stability is

$$\frac{\phi^2 \epsilon_o}{TR} < \frac{4}{\Gamma^2} \left(\frac{\kappa_i + \kappa_o}{\kappa_i - \kappa_o} \right)^2 \frac{\kappa_i - \kappa_o}{\kappa_i \kappa_o} \tag{112}$$

Therefore, the results of the stability analysis indicate that there is a lower voltage limit given by Equation (107) and an upper limit given by Equation (112). These limits, for a particular LOX-vapor tank stage are shown in Figure 33. The curves bounding the stable region are both represented by Equation (103). Figure 33 indicates that the minimum voltage level is specified by x = 0 and is given by Equation (107). The maximum voltage level is specified by Equation (112) and the wavelength at which it occurs is given by Equation (111). A more useful representation of the results is shown in Figure 34. Here the stable voltage range is given as a function of the geometric parameter (Γ) for a LOX-vapor system of 6 inch diameter. It is seen that the minimum voltage level is 12 kv while maximum voltage level is of the order of 70 kv. Consequently, stability considerations do not impose a significant restriction on voltage levels in operational tankage of 6 inch diameter.

Since the required voltage increases as the square root of the system diameter a 24 kv power supply would be adequate for tanks up to a diameter of the order of two feet. This is considered an adequate dimension for the 25-liter oxygen converter under consideration in this project.

A more significant restriction occurs due to the fact that Γ ought not to exceed 0.9 (see Figure 34) which means that oxygen systems cannot have stage radius ratios less than 1.6. This indicates that the force levels in the outer stages of the tank will be somewhat lower than other considerations indicate are desirable. Unfortunately, oxygen is a relatively poor working fluid in this respect. Table 10 summarizes the pertinent parameters for other fluids. It is apparent that oxygen systems require more serious consideration of the stability limits than is necessary for other fluids.

Lest this analysis appear to be too casual a treatment of a difficult problem, we would like to point out that we have also considered the problem without resorting to taking rms values of the fluctuating terms. The resulting Mathieu equation can be analyzed from a stability viewpoint. This refinement yields the same stability criteria as presented here and indicates that 60 cps is, indeed, a high frequency in the mechanical sense.

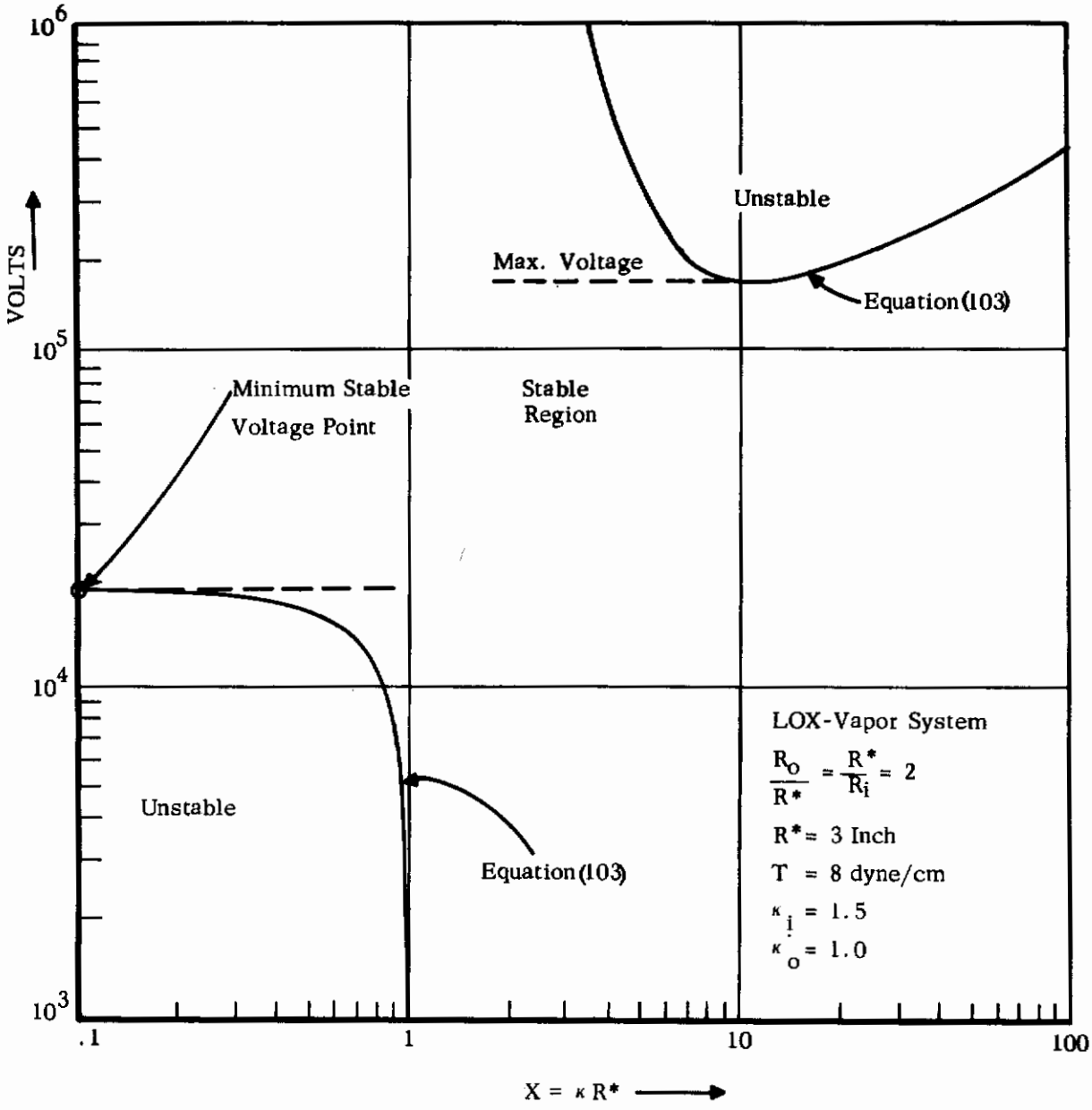

Figure 33. The Voltages-Wave Number Relation for a Particular Geometry Oxygen System

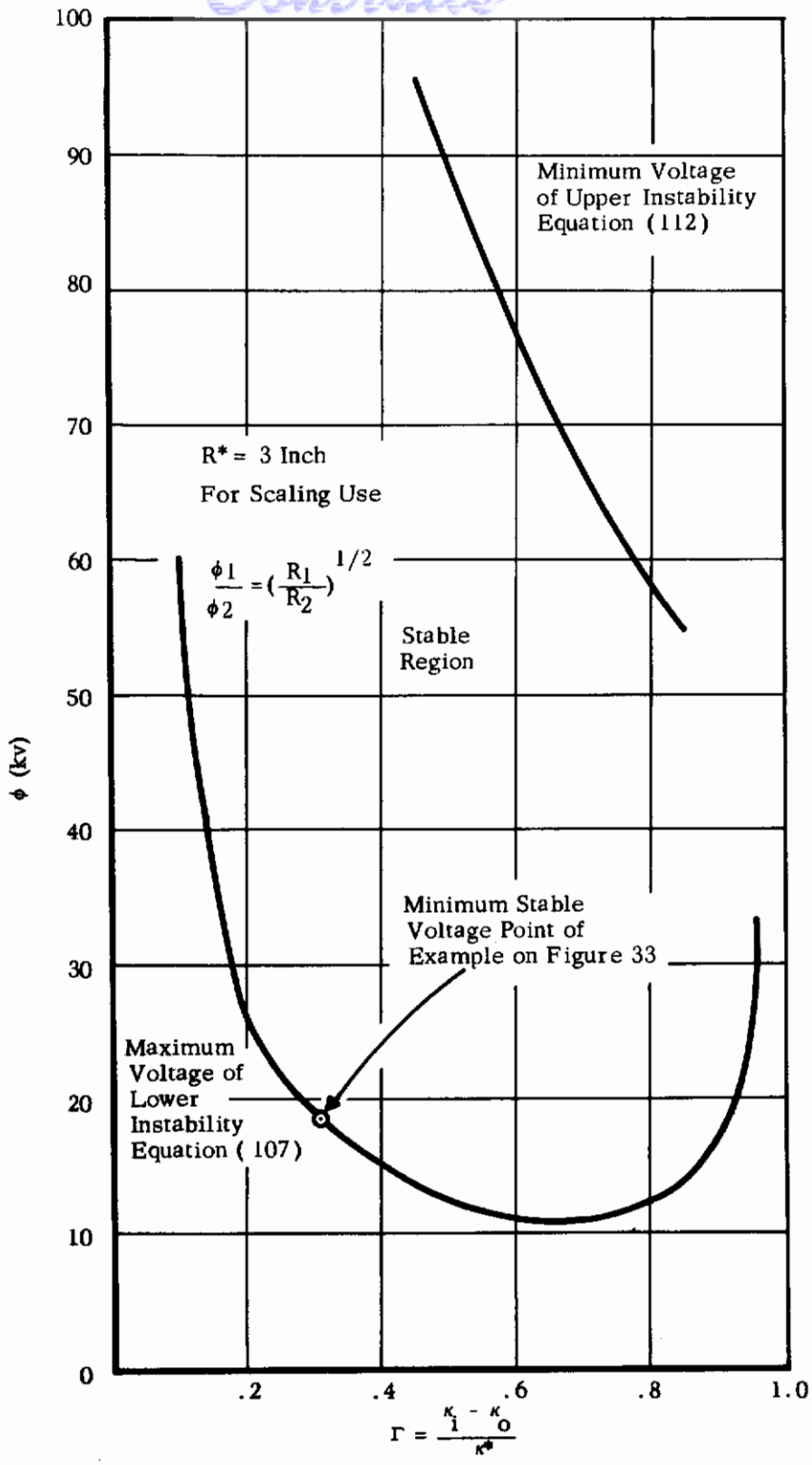

Figure 34. Boundaries of the Stable Region Giving Minimum and Maximum Voltages as a Function Γ for LOX - Vapor Systems

TABLE 10

SAMPLE VALUES OF PARAMETERS DEFINING STABLE OPERATION
Note that ϕ_{max} is Sensitive to the Particular Geometry Assumed

	Simulator	LOX - Vapor at 70 psia	LH_2 - Vapor
T (dyne/cm)	1.3	8	2.9
κ (liquid)	-	1.50	1.25
$(R_o/R_i)_{min}$	1.2	1.6	1.3
$(R_o/R_i)_{opt}$	1.3	2.2	1.45
V_{min}(volts)	2100	12000	5700
V^*_{max}(volts)	2.1×10^4	6.8×10^4	6.0×10^4

* For an interface of 3 - in. radius and $(R_o/R_i)_{opt}$.

APPENDIX D

THE THERMODYNAMICS OF THE ACETYLENE HAZARD

Liquid oxygen commercially available contains hydrocarbon impurities. The impurity present in the greatest amount is acetylene which is present in concentrations from 5 to 20 ppm by weight*. Since acetylene can be oxidized by oxygen and since the oxidation reaction is exothermic, it is important to know:

a) Whether the reaction of acetylene with oxygen will proceed at conditions of operation, and

b) If the reaction proceeds to what extent could its occurrence present a hazard to the equipment?

In order to avoid measuring reaction rates of the system solid acetylene-liquid oxygen to determine whether the reaction will occur at a significant rate, the reaction was assumed to occur and maximum energy liberated by it was calculated.

The reaction which is assumed to take place is that of saturated liquid oxygen at 5 atm (T_{sat} = 108°K) with acetylene to form carbon dioxide and water. The acetylene, carbon dioxide and water are all assumed to be in their natural states of aggregation at the saturation conditions of the liquid oxygen, i.e., solid. Therefore,

$$C_2H_2(s) + 2\text{-}1/2\, O_2(\ell) \rightarrow 2\, O_2(s) + H_2O(s)$$

The reaction to be modelled will be taken to be that which takes place at a constant pressure of 5 atm.

It can be shown that the heat of combustion at constant pressure, Q, is equal to the difference in enthalpy between the combustion products and the reactants. Therefore, if Q is defined per mole of acetylene:

$$Q = (1)\, h_{H_2O\,(s)} + (2)\, h_{CO_2\,(s)} - (1)\, h_{C_2H_2\,(s)} - (2\text{-}1/2)\, h_{O_2\,(\ell)}$$

where h_j is the specific enthalpy of component j at the saturation conditions of the liquid oxygen.

In order to determine the specific enthalpy of all components, it is necessary to first pick a standard reference state. Since enthalpy of formation data is commonly reported at 298°K and 1 atmosphere, it will be convenient to pick this as the standard reference state for the present calculation. Elements at this reference state will have enthalpy values of zero.

The specific enthalpy of any particular component, at the conditions of operation can be calculated as follows:

$$h_{specific} = h_{\left\{\begin{smallmatrix}108^\circ K\\ 5\text{ atm}\end{smallmatrix}\right\}} - h_{elements\ \left\{\begin{smallmatrix}298^\circ K\\ 1\text{ atm}\end{smallmatrix}\right\}}$$

$$= \left(h_{\left\{\begin{smallmatrix}108^\circ K\\ 5\text{ atm}\end{smallmatrix}\right\}} - h_{compound\ \{298^\circ K,\ 1\text{ atm}\}}\right) + \left(h_{compound\ \{298^\circ K,\ 1\text{ atm}\}} - h_{elements\ \{298^\circ K,\ 1\text{ atm}\}}\right)$$

$$= \Delta h_{physical\ \left\{\begin{smallmatrix}108^\circ K\\ 5\text{ atm}\end{smallmatrix}\right\} \rightarrow \left\{\begin{smallmatrix}298^\circ K\\ 1\text{ atm}\end{smallmatrix}\right\}} + \Delta h_{formation\ \{298^\circ K,\ 1\text{ atm}\}}$$

---

* It should be noted that as oxygen gas is withdrawn from the tank, the concentration of the less volatile acetylene in the liquid phase will become greater than 20 ppm.

The $\Delta h_{physical}$ represents change of enthalpy of the component as it goes from its natural state of aggregation at 108°K, 5 atm, to its natural state of aggregation at the standard reference state. It can be obtained either from Mollier charts for the component and/or by calculation of the change in enthalpy with temperature and pressure.

The $\Delta h_{formation}$ represents the enthalpy change occurring when the component j is converted into its elements.

The individual enthalpy values for the four components are summarized in the table below, all in calories per gram mole.

TABLE 11

SUMMARY OF CALCULATED VALUES OF ENTHALPY CHANGE

Component	$\Delta h_{physical}$	$\Delta h_{formation}$	$h_{specific}$
O_2	-2850	0	- 2850
C_2H_2	-9270	+54194	+ 44924
CO_2	-7660	-94052	-101712
H_2O	-4100	-68317	- 72417

The heat of combustion can now be calculated:

$$Q = (1)(-72417) + (2)(-101712) - (1)(44924) - (2\text{-}1/2)(-2850)$$

$$= -312625 \text{ cals/gm mole } C_2H_2$$

Using a molal volume for solid acetylene, $v = 34.2\ cm^3$, the heat of combustion, q, per cm^3 of acetylene is:

$$q = \frac{-312625}{34.2} = -9140 \text{ cals./cc}$$

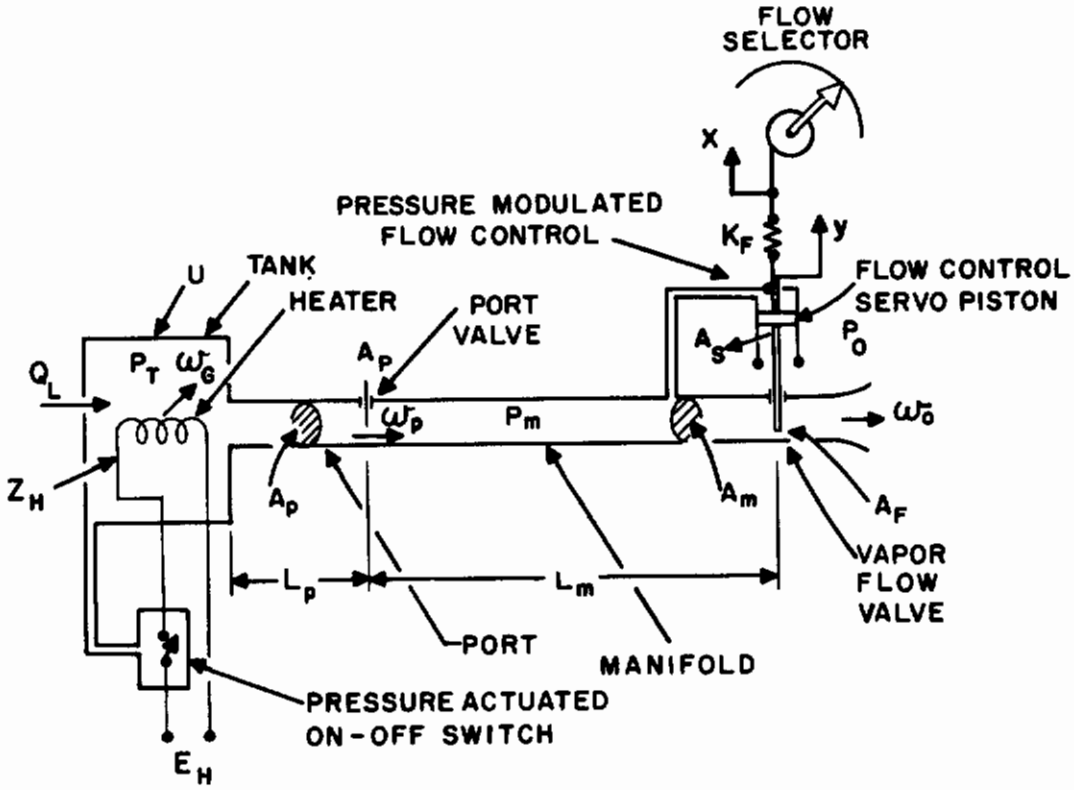

Figure 35: Schematic of Vapor-Delivery Flow-Control System

A_F - area of flow control valve

A_P - area of port valve

A_p, A_m - areas of port and manifold lines

A_S - area of flow control servo

E_H - heater voltage

K_F - spring constant

L_p, L_m - lengths of port and manifold liner

P_m - pressure in manifold

P_o - ambient pressure

P_T - pressure in tank

T_m - temperature in manifold

T_T - temperature in tank

U - volume of tank

w_G - weight rate of formation of gas due to boil-off

w_o - weight rate of delivery flow

Z_H - heater coil resistance

Pilot sets desired flow by moving selector. This causes a change in x. The position of the flow valve, y, is governed by:

$$K_F (x - y) = P_m A_S \tag{113}$$

This assumes the dynamic mass of the servo and vapor flow valve to be negligible. The flow-valve orifice area is proportional to y according to:

$$A_F = K_y \cdot y \tag{114}$$

It is assumed that $P_m - P_o$ is such that there is choked flow through the valve orifice and it is further assumed that the flow is isentropic. Thus, Fliegner's formula holds:

$$\frac{w_o}{A_F} = K_i P_m \tag{115}$$

where

$$K_i \equiv \sqrt{\frac{k}{R}\left(\frac{2}{k+1}\right)^{(k+1)/(k-1)}} \frac{1}{\sqrt{T_o}}$$

k = isentropic exponent.

Now, to maintain constant w_o, the servo must maintain constant $A_F \cdot P_m$. An operational block diagram for the flow-control servo system is shown below.

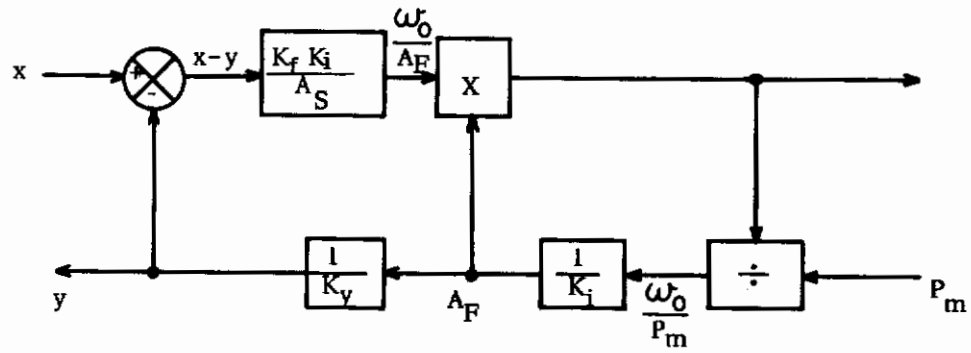

This diagram is useful to the designer wanting to optimize the servo parameters using an analog computer.

Let it be assumed that the manifold line is lossless so that pressure is essentially constant along its length. Assume further, that the manifold volume may be treated as a lumped parameter system.

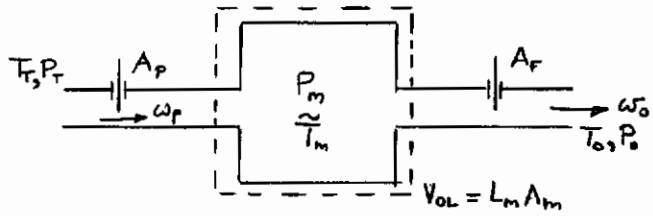

It is assumed that the gas enters the manifold at essentially tank temperature, T_T, and leaves at ambient temperature, T_o. It has therefore been assumed that the gas expands isothermally on passing through the port valve. The manifold temperature, T_m, is assumed to be constant. It will be expressed by an average value, $\tilde{T}_m$, given by:

$$\tilde{T}_m = \frac{T_o - T_T}{2} \tag{116}$$

The unsteady energy equation for the manifold is:

$$w_p C_h T_T - w_o C_h T_o = \frac{\partial}{\partial t}\left(\rho_m L_m A_m C_h \tilde{T}_m\right) \tag{117}$$

If the specific heat is assumed essentially constant over the temperature range T_T to T_o, then Equation (117) may be simplified to:

$$w_p T_T - w_o T_o = L_m A_m \tilde{T}_m \frac{d\rho_m}{dt} \tag{118}$$

The equation of state for the lumped parameter manifold is,

$$\frac{P_m}{\rho_m} = R \tilde{T}_m = \text{constant} = R \frac{T_o - T_T}{2}$$

Thus Equation (118) may be re-stated:

$$w_p T_T - w_o T_o = \frac{L_m A_m \tilde{T}_m}{R \tilde{T}_m} \frac{dP_m}{dt} = \frac{L_m A_m}{R} \frac{dP_m}{dt} \tag{119}$$

An operational block diagram for the manifold is shown below.

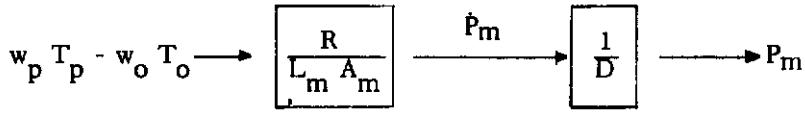

This is now added to the block diagram for the flow control servo.

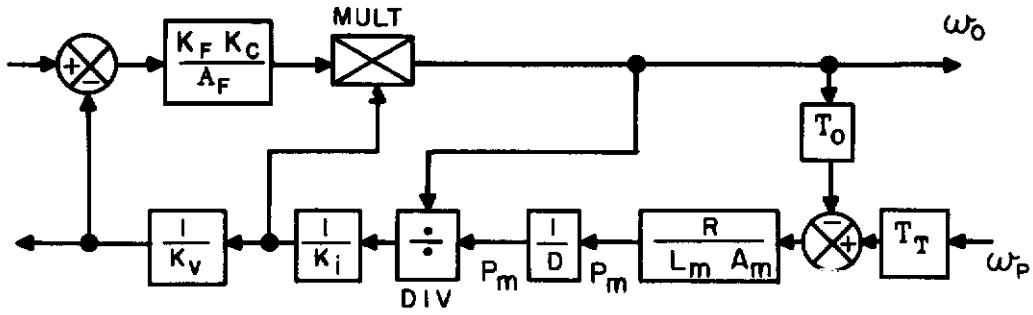

As mentioned previously, the flow through the port valve is assumed isothermal. Thus if it is further assumed that the flow through this valve is choked, Fliegner's relation may be used to relate the flow through the port valve, w_p, to the port area, A_p, and tank pressure P_T.

$$\frac{w_p}{A_p} = K_j P_T$$

where

$$K_j = \sqrt{\frac{k}{r} \left(\frac{2}{k+1}\right)^{k+1/k-1}} \frac{1}{\sqrt{T_T}} \tag{120}$$

The tank pressure, P_T, will be controlled by an electric resistance heater, Z_H, which receives voltage when P_T falls below $P_{T_{min}}$ and is shut off when P_T exceeds $P_{T_{max}}$. The heater is controlled by a simple pressure actuated "on-off" switch.

Consider a system of the heater and the fluid content of the tank. The liquid oxygen is assumed to be saturated so that any heat entering the system is used to vaporize liquid, resulting in a boil-off flow rate of gas, w_G. The first law for this system is

$$Q_L + \frac{E^2}{Z_H} = w_G h_{FG} \tag{121}$$

where

Q_L is the total heat leakage into the system,

E is the voltage across the heater resistance, and

h_{FG} is the heat of vaporization of liquid oxygen.

The unsteady energy equation for the system of the tank and its contents is:

$$w_G C_h T_T - w_p C_h T_T = \frac{\partial}{\partial t} (\rho_T U C_h T_T) \tag{122}$$

If both the tank volume, U, and the tank temperature, T_T, may be assumed invarient, Equation (122) becomes:

$$w_G - w_p = U \frac{d\rho_T}{dt} \tag{123}$$

The equation of state for the vapor in the tank is:

$$\frac{P_T}{\rho_T} = R T_T = \text{constant} \tag{124}$$

Thus Equation (123) becomes:

$$w_G - w_p = \frac{U}{R T_T} \frac{dP_T}{dt} \tag{125}$$

A functional block diagram for the tank and heater system is shown on the following page. The on-off controller is depicted by the ideal representation of its characteristic according to accepted servo-mechanism conventions.

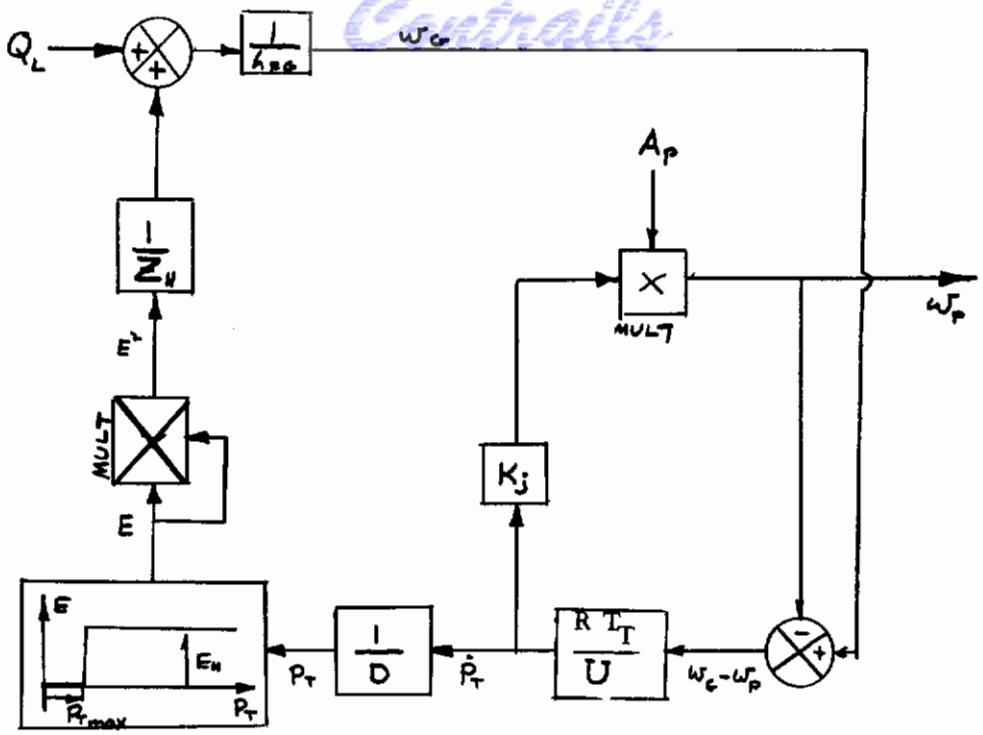

The functional block diagrams for all of the sub-systems are now combined to form a diagram for the entire oxygen converter vapor delivery system. The diagram is useful as the basis of an analog computer program. Such a program is necessary to achieve optimum design of so complex a system. A glance at the diagram will reveal that the system is a second order lag. It is so highly nonlinear, however, that it defies the use of ordinary manual techniques for finding responses.

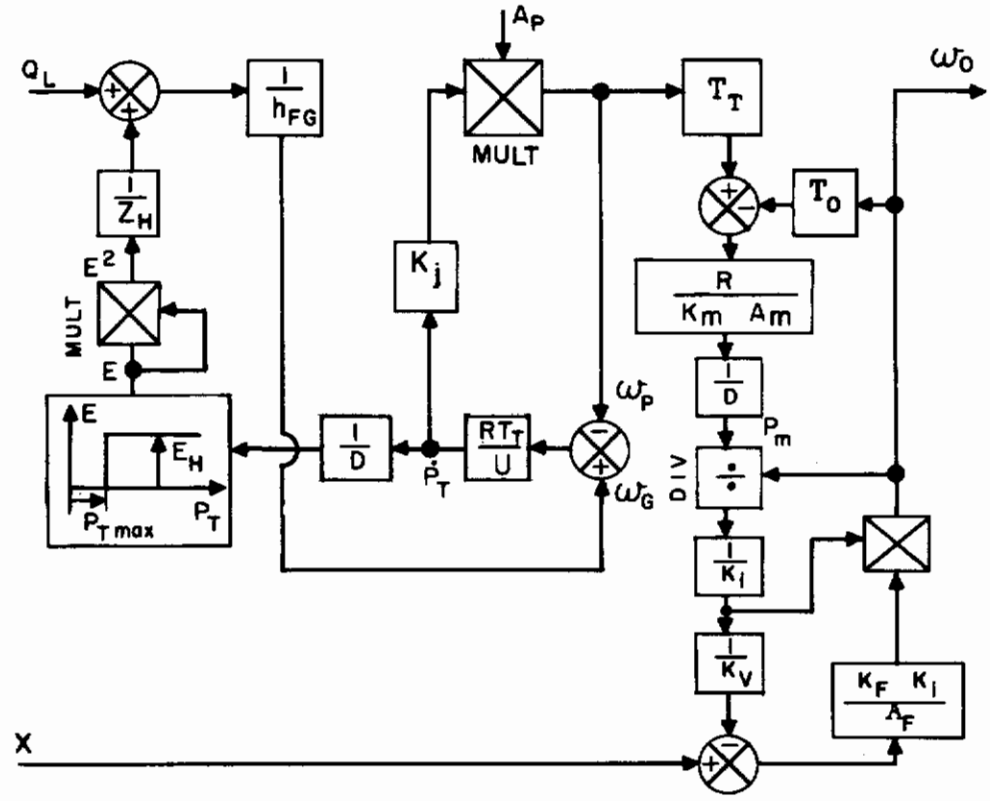

Figure 36. Functional Block Diagram of Vapor Delivery Flow Control System

APPENDIX F

DISCUSSION OF LEVEL INDICATOR ERROR

Illustrative Example:

The level indicator continuously monitors the volume of LOX remaining in the converter by measuring the system's capacitance. The greatest source of error in such a system is due to misorientation of the liquid as might occur:

a) during certain flight maneuvers, launching, re-entry, or

b) as a result of hang-up on stages or on the tank wall.

The purpose of the discussion to follow is to demonstrate that these errors are not so large as to render the level indicator useless.

The five possible extreme variations of fluid orientation (hence system capacitance) are shown in Figure 37 for the simple or elementary converter having one intermediate stage. The system is assumed to be half-filled and the capacitances are calculated and compared.

The system is assumed to have unit length and has the following electrode geometry:

$$R_0 = 5.0 \text{ cm}$$

$$R_1 = 3.1 \text{ cm}$$

$$R_2 = 2.0 \text{ cm}$$

$$R_0/R_1 = R_1/R_2 = 1.6$$

The capacitance per unit length is calculated for Cases I and II according to:

$$C = \frac{7.36\,\epsilon_o}{2}\left(\frac{1}{\frac{1}{\kappa_L}\log\frac{R_0}{R_1}} + \frac{1}{\frac{1}{\kappa_L}\log\frac{R_0}{R_1}}\right)$$

$$+ \frac{7.36\,\epsilon_o}{2}\left(\frac{1}{\frac{1}{\kappa_v}\log\frac{R_0}{R_1}} + \frac{1}{\frac{1}{\kappa_v}\log\frac{R_0}{R_1}}\right)$$

Putting in the numbers,

$$C = \frac{7.36}{2}\left(\frac{1.45}{0.2} + \frac{1.45}{0.2} + \frac{1}{0.2} + \frac{1}{0.2}\right)$$

or,

$$\boxed{C_I = C_{II} = 90 \text{ pf/foot}}$$

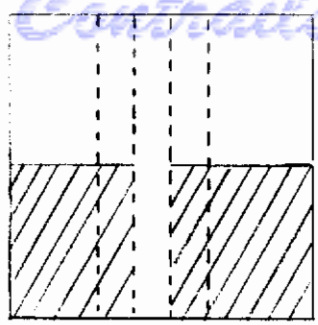

CASE I — Liquid at one end of tank due to large axial g-loads

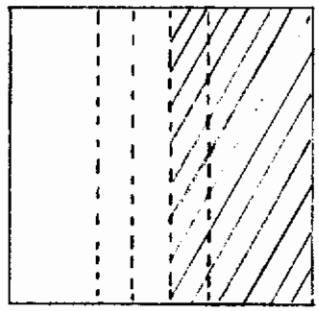

CASE II — Liquid at one side of tank due to large lateral g-loads

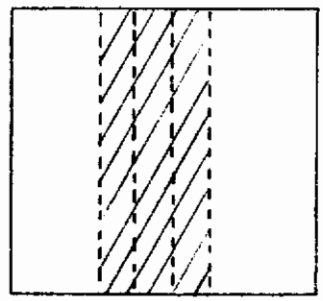

Case III — Liquid theoretically oriented in zero-g

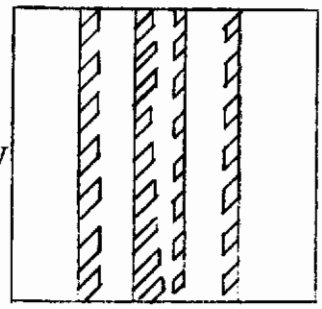

CASE IV — Liquid all hang up on outside of inner electrode and outside of intermediate stage. Zero-g

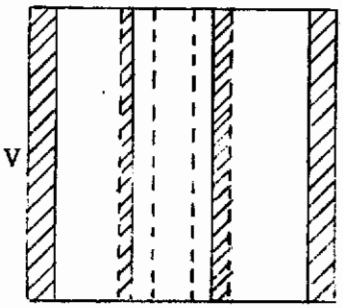

CASE V — Liquid all hang up on tank wall and on inside of intermediate stage. Zero-g

Figure 37. The Five Possible Extreme Variations of Liquid Orientation, Section Views

The capacitance per unit length for Case III is given by

$$C = 7.36 \left(\frac{1}{\frac{1}{\kappa_L} \log \frac{R_1}{R_2}} + \frac{1}{\frac{1}{\kappa_L} \log \frac{R^*}{R_1} + \frac{1}{\kappa_v} \log \frac{R_0}{R^*}} \right)$$

where for this half-filled case, $R^* = 3.8$ cm.

Therefore, the capacitance for Case III is

$$C_{III} = 7.36 \left(\frac{1.45}{\log \frac{3.1}{2.0}} + \frac{1}{\frac{1}{1.45} \log \frac{3.8}{3.1} + \frac{1}{1} \log \frac{5.0}{3.8}} \right)$$

$$= 7.36 (7.65 + 5.5)$$

$$\boxed{C_{III} = 97 \text{ pf/foot}}$$

In Case IV, the capacitance is calculated on the assumption that one-half of the liquid is hung up on the inner electrode and the other half is hung up on the intermediate electrode. The capacitance per unit length is given by

$$C = \frac{7.36}{\frac{1}{\kappa_L} \log \frac{R^*_2}{R_2} + \frac{1}{\kappa_v} \log \frac{R_1}{R^*_2}} + \frac{7.36}{\frac{1}{\kappa_L} \log \frac{R^*_1}{R_1} + \frac{1}{\kappa_v} \log \frac{R_0}{R^*_1}}$$

where: $R^*_1 = 3.9$ cm and $R^*_2 = 2.7$ cm.

Thus, the capacitance for Case IV is:

$$C_{IV} = \frac{7.36}{\frac{1}{1.45} \log \frac{2.7}{2.0} + \frac{1}{1} \log \frac{3.1}{2.7}} + \frac{7.36}{\frac{1}{1.45} \log \frac{3.9}{3.1} + \frac{1}{1} \log \frac{5.0}{3.9}}$$

$$= 7.36 (6.66 + 5.6)$$

$$\boxed{C_{IV} = 90 \text{ pf/foot}}$$

Finally, the capacitance for Case V is calculated on the basis of:

$$C = \frac{7.36}{\frac{1}{\kappa_L} \log \frac{R^*_1}{R_2} + \frac{1}{\kappa_v} \log \frac{R_1}{R^*_1}} + \frac{7.36}{\frac{1}{\kappa_L} \log \frac{R^*_0}{R_1} + \frac{1}{\kappa_v} \log \frac{R_0}{R^*_0}}$$

where: $R_0 = 4.5$ cm and $R^*_1 = 2.1$ cm.

Therefore the capacitance for Case V is:

$$C_V = \frac{7.36}{\frac{1}{1.45}\log\frac{2.1}{2.0} + \frac{1}{1}\log\frac{3.1}{2.1}} + \frac{7.36}{\frac{1}{1.45}\log\frac{4.5}{3.1} + \frac{1}{1}\log\frac{5.0}{4.5}}$$

$$= 7.36\,(4.8 + 6.45)$$

thus,

$$\boxed{C_V = 83 \text{ pf/foot}}$$

The level indicator capacitance, for the half-filled elementary converter is:

$$C = 90 \pm 7 \text{ pf/foot}$$

The error is ± 7.8%.